University of Tennessee Health Science Center
UTHSC Digital Commons

Theses and Dissertations (ETD) College of Graduate Health Sciences

5-2017

The Development of Methods to Account for Physiologic Dynamic Changes and Their Effects on the Pharmacokinetics of Therapeutic Monoclonal Antibodies and other Therapeutics

Josiah Thomas Ryman
University of Tennessee Health Science Center

Follow this and additional works at: https://dc.uthsc.edu/dissertations

 Part of the Other Pharmacy and Pharmaceutical Sciences Commons, and the Pharmaceutics and Drug Design Commons

Recommended Citation
Ryman, Josiah Thomas (http://orcid.org/0000-0002-7692-4432), "The Development of Methods to Account for Physiologic Dynamic Changes and Their Effects on the Pharmacokinetics of Therapeutic Monoclonal Antibodies and other Therapeutics" (2017). *Theses and Dissertations (ETD)*. Paper 444. http://dx.doi.org/10.21007/etd.cghs.2017.0434.

This Dissertation is brought to you for free and open access by the College of Graduate Health Sciences at UTHSC Digital Commons. It has been accepted for inclusion in Theses and Dissertations (ETD) by an authorized administrator of UTHSC Digital Commons. For more information, please contact jwelch30@uthsc.edu.

The Development of Methods to Account for Physiologic Dynamic Changes and Their Effects on the Pharmacokinetics of Therapeutic Monoclonal Antibodies and other Therapeutics

Document Type
Dissertation

Degree Name
Doctor of Philosophy (PhD)

Program
Pharmaceutical Sciences

Track
Pharmacometrics

Research Advisor
Bernd Meibohm, Ph.D.

Committee
Vibha Jawa, Ph.D. Carl Panetta, Ph.D. Frank Park, Ph.D. Charles R. Yates, Ph.D.

ORCID
http://orcid.org/0000-0002-7692-4432

DOI
10.21007/etd.cghs.2017.0434

Comments
One year embargo expires July 2018.

This dissertation is available at UTHSC Digital Commons: https://dc.uthsc.edu/dissertations/444

The Development of Methods to Account for Physiologic Dynamic Changes and Their Effects on the Pharmacokinetics of Therapeutic Monoclonal Antibodies and other Therapeutics

A Dissertation
Presented for
The Graduate Studies Council
The University of Tennessee
Health Science Center

In Partial Fulfillment
Of the Requirements for the Degree
Doctor of Philosophy
From The University of Tennessee

By
Josiah Thomas Ryman
May 2017

Chapter 3 © 2017 by Springer.
All other material © 2017 by Josiah Thomas Ryman.
All rights reserved.

DEDICATION

To my wife and daughter, who are my inspiration and joy, and to my parents for their everlasting love and support.

ACKNOWLEDGEMENTS

I have had many wonderful people helping me all along the way.

First, I would like to express appreciation to my advisor, Dr. Bernd Meibohm, who has been my biggest advocate throughout my time obtaining my PhD. I would also like to thank the other members of my committee, Dr. Frank Park, Dr. Vibha Jawa, Dr. Carl Panetta, and Dr. Charles Ryan Yates for their invaluable suggestions, guidance, and assistance. I would like to especially acknowledge Dr. Vibha Jawa and Amgen Inc. for generously providing me with financial support for most of my research. I must also thank Dr. Lisa Tang for her hard work with the ontogeny data. Much thanks to the Department of Immunology at Amgen Inc. for their assistance in the analysis of all the samples I sent their way.

I also extend a sincere appreciation to all my fellow graduate students, including Dr. Ashit Trivedi, Dr. Chetan Rathi, Dr. Margaret Thomson, Dr. Jordan Toutounchian, Dr. Wararat Limothai and Santosh Wagh for their thoughtful advice and discussions. I will always remember and cherish the memories we have made together while on this journey.

To my parents, Joel and Cynthia, thank you for all of your love and support. You both helped to guide me through life as a child and continue to help and guide me on my journey through life. I want to thank you for always being there for me when things got tough, and for being a voice of reason when choosing my path when life's obstacles presented themselves.

To my daughter, Alexa, you are such a beauty amongst beasts. Every day you show a positive disposition and willingness to approach each day with love and a wonderful energy that is so infectious. You have always looked past my shortcomings and into a future that is wonderful. I promise to provide you with every opportunity to have the future you deserve.

To my wife, Swati, you are a wonderful blessing from the heavens. You came into my life with such a force of love; a love I tried to push away. Yet you stood strong, you were patient with me and showed me love and patience. Thank you for showing me love and patience. I am truly blessed to have a woman that stands strong next to me as we journey through life together.

Support for part of this work was provided by Amgen Inc.

ABSTRACT

Physiologic changes in the body can drastically affect the clearance of a medication, and therefore increase the variability in exposure to the medication. Physiologic changes that can have a profound effect on the exposure of a medication can stem from changes CYP enzymes, transport proteins, binding protein expression, organ function, immune reactivity, and health status to name a few; with the focus of this dissertation on the dynamic changes in the ontogeny of MRP2 (an apical liver transport protein) and the dynamic changes caused by an immune response to a therapeutic monoclonal antibody (mAb). Several approaches can be used to limit or capture the changes in the pharmacokinetics of a medication caused by ontogeny and immune reactivity related dynamic changes. Three approaches were investigated in this dissertation: 1) preventing/limiting immunogenicity's effect on a therapeutic mAb, hence eliminating the increase in clearance and variability, 2) using a pharmacometric PK-ADA modeling approach to model immunology-related dynamic and variable effects on a therapeutic mAb and 3) using a systems pharmacology strategy to model the ontogeny changes in a transport protein (MRP2) and the dynamic effects on its drug substrates.

In the preclinical and clinical setting, anti-drug antibodies (ADA) that develop against therapeutic mAbs can influence patient safety and interfere with product efficacy. Thus, my first focus in this dissertation investigates methods to limit/prevent immunogenicity and therefore help to eliminate a source of variability and clearance that can be seen in preclinical and clinical studies. My first study investigates the use of immune suppressants in mitigating ADA responses to a fully-humanized mAb in preclinical animal studies. Three groups of Sprague Dawley rats (n=18) were treated with low (0.01 mg/kg), moderate (50 mg/kg), or high (300 mg/kg) doses of a mAb. Experimental groups also received either methotrexate or tacrolimus/sirolimus immune suppression. Methotrexate significantly lowered the incidence of anti-variable region antibodies at moderate mAb dose ($P<0.05$), while tacrolimus/sirolimus did likewise at moderate and high doses ($P<0.01$) of mAb. With the exception of low dose mAb plus methotrexate, all immunosuppressed groups displayed more than a 70-fold decrease in ADA magnitude ($P<0.05$). This abrogation in ADA response correlated with higher mAb exposure in the circulation by week 4 for the moderate and high dosed mAb groups. This method provides an approach to mitigate preclinical immunogenicity by the use of immunosuppressant modalities. Such preconditioning can support preclinical drug development of human therapeutics that are antigenic to animals but not necessarily to humans. Similar approaches to reduce immunogenicity will likely play an essential role with advances in novel therapeutics like fully human mAbs, recombinant proteins, fusion proteins as well as bispecific- and drug-conjugated antibodies.

In some cases there may not be a method to reduce/eliminate immunogenicity and the dynamic changes in the elimination of a therapeutic mAb that result. In a preclinical setting, ADA typically influences both multiple dose toxicity studies, as well as preliminary pharmacokinetic (PK) analysis by leading to an increase in clearance of the therapeutic mAb. This increase in clearance caused by ADA can be highly variable due

to each animal's polyclonal immune response to a therapeutic mAb. My second focus aims to account for ADA and its variable effect on a fully human therapeutic mAb. I used data acquired from our previous study that investigated the use of immunosuppressant therapy in mitigating ADA responses to a mAb in a preclinical Sprague Dawley rat study and incorporated much of the data from that study, which included three mAb dosing groups and three immunomodulation therapies. A pharmacometric PK-ADA modeling approach was used to analyze the data. Our model was able to simultaneously capture the pharmacokinetics of the mAb in the presence and absence of ADA, accounting for an immune reaction's highly variable effect on a therapeutic mAb concentration-time profile. The pharmacometric PK-ADA methodology used in this study demonstrates a modeling strategy that can be applied to other therapeutic mAbs to assess the immunogenicity of a therapeutic mAb and the dynamic effect immunogenicity has on the pharmacokinetics. This modeling methodology can further be applied to the simulation of therapeutic mAbs in the presence of varying rates, magnitudes and affinities of ADA reactions, aiding in the development of appropriately powered toxicology studies and an accurate pharmacokinetic evaluation of a human therapeutic mAb in a preclinical setting.

Transport proteins play an important role in determining the disposition of medications in the human body. The expression of transport proteins in the body is not constant throughout childhood development, which affects the pharmacokinetics of a medication that is a substrate of the transport protein. Multidrug resistance protein 2 (MRP2) represents a major hepatic transporter whose expression is dynamic throughout development. MRP2 plays a vital role in the biliary excretion of various organic anions and cations along with glutathione-, glucuronate-, or sulfate-conjugates of several drug substrates. Our third aim is to evaluate the effect the ontogeny of MRP2 has on the pharmacokinetics of ceftriaxone to better understand how a transport protein contributes to the disposition of its substrates throughout childhood development. In order to accomplish our aim, a systems pharmacology modeling approach was used to understand MRP2's contribution to the elimination of ceftriaxone and the effect of ontogeny changes on the pharmacokinetics of ceftriaxone in pediatric patients. Data from *ex vivo* studies, preclinical *in vivo* studies and clinical studies were used to inform our model. Results from the study demonstrate the contribution of MRP2 to the pharmacokinetics of ceftriaxone. Our model was able to capture ceftriaxone's pharmacokinetics, and MRP2's contribution to its clearance, allowing for the prediction of pediatric ceftriaxone concentrations. This modeling strategy can also be used to evaluate ontogeny changes in other biochemical transposition proteins, and the subsequent effect on the pharmacokinetics of other therapeutically used compounds.

In summary, our work has successfully provided approaches to limit/prevent dynamic changes caused by immune reactions to a therapeutic mAb, demonstrate a pharmacometric PK-ADA approach that can capture the PK changes and variability caused by ADA formation on a therapeutic mAb and demonstrate a systems pharmacology model approach which accounts for the ontogeny of a transport protein and the resultant PK effects on its substrate through childhood development. The following chapters describe and discuss these novel approaches.

TABLE OF CONTENTS

CHAPTER 1. PHARMACOKINETICS OF MONOCLONAL ANTIBODIES.....1

Introduction.....1
Structure and Origin.....1
Basic Pharmacokinetic Behavior.....3
Distribution of mAbs.....3
Elimination of mAbs.....6
Routes of Administration.....9
Product-Specific Factors Affecting the Pharmacokinetics of mAbs.....10
Charge.....10
Glycosylation Pattern.....11
Patient-Specific Factors Affecting the Pharmacokinetics of mAbs.....13
Genetic Variants.....13
Inflammatory Status.....14
Time Dependent Changes in Pharmacokinetics.....15
Immunogenicity.....15
Modeling mAb Disposition.....16
Population Variability.....18
Conclusion.....19
The Pharmacokinetics and Pharmacodynamics of Therapeutic Proteins and Their Description and Prediction through Modeling Approaches.....19
The Effect of Immunogenicity on the Pharmacokinetics and Pharmacodynamics of Therapeutic Proteins and Its Description and Prediction by Modeling Approaches.....22

CHAPTER 2. CENTRAL HYPOTHESIS.....25

Specific Aim 1.....25
Specific Aim 2.....25
Specific Aim 3.....26

CHAPTER 3. IMMUNE SUPPRESSION DURING PRECLINICAL DRUG DEVELOPMENT MITIGATES IMMUNOGENICITY MEDIATED IMPACT ON THERAPEUTIC EXPOSURE.....27

Introduction.....27
Methods.....28
Materials.....28
Animals.....28
Immunosuppressive Regimens.....28
Anti-mAb1 Antibody Rat Immunoassay.....30
Pharmacokinetic Assay for Measuring mAb1 Concentration.....30
Statistical Methods.....31
Results.....32
Impact of Immune Suppression on Immunogenicity of mAb1.....32
Incidence of Anti-mAb1 Immune Response.....32
Magnitude and Onset of Anti-mAb1 Immune Response.....32

Impact of Immune Suppression on Exposure of mAb1 36
Immune Suppression on Free Drug Levels 36
Anti-mAb1 Antibodies on Free Drug Levels 36
Discussion 36

CHAPTER 4. MODELING THE EFFECT OF IMMUNOGENICITY OF A HUMAN MONOCLONAL ANTIBODY 43

Introduction 43
Methods 44
Preclinical Study 44
Test System 44
Test Article 44
Study Design 45
Sample Collection and Handling 45
Determination of Serum mAb1 Concentration 45
Determination of ADA to mAb1 47
Model-Based Pharmacokinetic Analysis 47
Analysis Approach and Software 47
Pharmacokinetic Structural Models 48
Pharmacokinetic-ADA Models 48
Interindividual Error Models 49
Covariates 49
Model Comparison, Covariate Selection and Goodness of Fit 50
Simulations 50
Results 51
Discussion 59

CHAPTER 5. MRP2 ONTOGENY AND ITS EFFECTS ON PEDIATRIC CEFTRIAXONE EXPOSURE: A NON-LINEAR MIXED EFFECT MODELING APPROACH 69

Introduction 69
Methods 70
Ontogeny of Relative MRP2 Protein Expression 70
Pharmacokinetics of Ceftriaxone in Normal and Mrp2 Deficient Rats 71
Collection of Ceftriaxone Human Pharmacokinetics in Children and Adults from Literature Sources 71
Model-Based Integrated Data Analysis to Assess the Impact of MRP2 Ontogeny on Pharmacokinetics of Ceftriaxone 76
Modeling Approach 76
Software 76
Pharmacokinetic Structural Models 76
Interindividual and Error Models 78
Covariate Analysis 78
Results 78
Discussion 91

CHAPTER 6. SUMMARY.....98

LIST OF REFERENCES.....102

VITA.....114

LIST OF TABLES

Table 3-1. Maximum ADA S/N and Time of ADA Onset from All Rats in Each Group Were Averaged 35

Table 3-2. The mAb1 Exposures Were Compared Between Anti-Drug Antibody (ADA) Negative and Positive Animals as well as in the Presence or Absence of Immune Suppression 38

Table 3-3. Specificity and Percent Incidence of ADA Against CDR (α-Variable), Fc (α-Framework), or CDR + Fc (α-Both) Epitopes....40

Table 4-1. Treatment Groups 46

Table 4-2. Parameter Estimates....56

Table 5-1. Donor Demographics for Human Pediatric Liver Samples Provided by St. Jude Children's Research Hospital (SJCRH) 72

Table 5-2. Donor Demographics for Human Pediatric Liver Samples Provided by Medical College of Wisconsin (MCW) 73

Table 5-3. Mean ± SD AUC Renal Elimination and Fecal Elimination in WT Versus TR- Rats 80

Table 5-4. Population Pharmacokinetic Model Parameters for the Disposition of Ceftriaxone in Wild-Type and MRP2 Deficient Rats 84

Table 5-5. Pediatric Patient Age Distribution 86

Table 5-6. Population Pharmacokinetic Model Parameters for Ceftriaxone in Humans....88

Table 5-7. Population Pharmacokinetic Model Parameters for the Disposition of Ceftriaxone in Pediatric Patients with an Age Range of (2 Days - 6 Years) 90

LIST OF FIGURES

Figure 1-1. Monoclonal Antibody Structure 2

Figure 1-2. Convective Transport of a mAb....4

Figure 1-3. FcRn Recycling Pathway for IgG Molecules 8

Figure 1-4. Commonly Encountered N-Glycan Structures in the Fc Portion of Monoclonal Antibodies 12

Figure 1-5. Routes of Elimination of a mAb 17

Figure 1-6. Minimal PBPK Model 21

Figure 3-1. Dosing and Experimental Design of mAb1 with and Without Immune Suppressants in Sprague Dawley Rats 29

Figure 3-2. Incidence of Anti-mAb1 Immune Reactivity Following Immune Suppression 33

Figure 3-3. Immune Suppression Regimens Reduce Magnitude and Delay Onset of ADA Response 34

Figure 3-4. Immune Suppression Regimens Alter Drug Exposure 37

Figure 4-1. Mean Observed Concentration-Time Profiles for Each mAb1 Dosing Group....52

Figure 4-2. Mean Observed ADA Magnitudes and Percentage of ADA Positive Individuals in Each Group....53

Figure 4-3. Model Structure 54

Figure 4-4. Population and Individual Model Predictions Versus Observed Concentrations....57

Figure 4-5. Visual Predictive Checks 58

Figure 4-6. Average Observed Versus Predicted ADA Magnitude 60

Figure 4-7. Average ADA S/N in Each Dosing Group 62

Figure 4-8. Magnitude and Affinity of an Immune Reaction....62

Figure 4-9. Methotrexate's Effect on Concentration Time Profiles....64

Figure 4-10. Methotrexate's Effect on AUC 65

Figure 4-11. Methotrexate's Effect Modeled 66

Figure 4-12. Simulation 68

Figure 5-1. Comparison of HPLC Versus Agar Concentration Measurements 75

Figure 5-2. Modeling Strategy Used to Elucidate MRP2 Contribution to Pediatric Ceftriaxone Exposure 77

Figure 5-3. Ceftriaxone Concentration-Time Profiles 79

Figure 5-4. Ceftriaxone 2-Compartment Model 82

Figure 5-5. Hyperbolic Sigmoidal Equation Fitted to the Relative MRP2 Protein Expression in Human Pediatric Liver Samples 85

Figure 5-6. Pediatric Ceftriaxone Visual Predictive Check 89

Figure 5-7. Pediatric Population Predicted Ceftriaxone Concentration Versus Observed Ceftriaxone Concentration for Final Model 89

Figure 5-8. Population Predicted Ceftriaxone Concentration Versus Observed Ceftriaxone Concentration for Pediatric and Adult Populations 93

Figure 5-9. Observed Ceftriaxone Concentration Versus the Model Predicted Ceftriaxone Concentration for Pediatric and Adult Populations 95

Figure 5-10. Pediatric Predictive Model Visual Predictive Check with 59% MRP2 Contribution to Total Clearance 95

Figure 5-11. Estimated Clearance Versus Difference Between Population and Individual Predicted Clearance in Final Model with the Fixed MRP2 Contribution of 59% (Obtained from the Rat Study) 96

Figure 5-12. Estimated Clearance Versus Difference Between Population and Individual Predicted Clearance in Final Model with Estimated MRP2 Contribution 97

LIST OF ABBREVIATIONS

ABC	ATP-binding Cassette
ADA	Anti-Drug Antibodies
ADCC	Antibody Dependent Cellular Cytotoxicity
AIC	Akaike's Information Criterion
AUC	Area Under the Curve
BSV	Between Subject Variability
CDC	Complement Dependent Cytotoxicity
CDR	Complementarity-Determining Region
CRP	C-Reactive Protein
ECL	Electrochemiluminescence
ERT	Enzyme Replacement Therapy
Fab	Antigen Binding Fragment
Fc	Framework
FcRn	Neonatal Framework Receptor
FOCE	First Order Conditional Estimation
HLA	Human Leukocyte Antigen
HPLC	High Performance Liquid Chromatography
IACUC	Institutional Animal Care and Use Committee
IgG	Immunoglobulin G
IL	Interleukin
IM	Intramuscular
IV	Intravenous
IVIG	Intravenous Immunoglobulin
LL	Log Likelihood
LLOQ	Lower Limit Of Quantification
mAb	Monoclonal Antibody
MMF	Mycophenolate Mofetil
MRP	Multidrug Resistant Protein
MTX	Methotrexate
NONMEM	Nonlinear Mixed Effects Modeling
OFV	Objective Function Value
PBPK	Physiologically Based Pharmacokinetic
PD	Pharmacodynamic
pI	Isoelectric Point
PK	Pharmacokinetics
PKPD	Pharmacokinetic Pharmacodynamic
PNRS	Pooled Normal Rat Serum
rhGAA	Recombinant Human α-Glucosidase
RMANOVA	Repeat Measure Analysis of Variance
SC	Subcutaneous
Sir	Sirolimus
S/N	Signal to Noise
Tac	Tacrolimus

TER	Transcapillary Escape Rate
TMDD	Target Mediated Drug Disposition
TNF	Tumor Necrosis Factor
TP	Therapeutic Proteins
TR-	Transporter Deficient
TV	Typical Value
UNISA	Universal Indirect Species Specific Assay
Ve	Excluded Volume
VNTR	Variable Number of Tandem Repeats
VPC	Visual Predictive Check
VSS	Volume of Distribution at Steady State

CHAPTER 1. PHARMACOKINETICS OF MONOCLONAL ANTIBODIES

Introduction

Interest in monoclonal antibodies (mAbs) as medications for therapeutic use has continuously grown over the last 25 years. Increasing research efforts are focusing on developing mAbs against various disease states including multiple cancer indications and chronic inflammatory conditions. At the current time, more than 40 mAbs have been approved by the Food and Drug Administration for marketing in the United States, and several dozens more are currently in clinical development.[1] With this intense focus on mAbs in drug development programs and clinical practice, this tutorial is intended to outline and summarize some of the basic pharmacokinetic properties of this class of medications.

Structure and Origin

All current clinically used therapeutic antibodies are immunoglobulin G (IgG) mAbs and possess the same basic structure (**Figure 1-1**): they are large heterodimeric protein molecules with a molecular weight of approximately 150 kDa and are composed of four polypeptide chains, two identical heavy chains (50 kDa) and two light chains (25 kDa). The heavy and light chains are held together by disulfide bonds to form a Y-shape consisting of constant domains (C_H and C_L) and variable domains (V_H and V_L). The two variable regions and the C_{H1} domains of the heavy chains comprise the antigen binding fragment (Fab) with each variable domain containing the complementarity-determining region, which is highly specific for the target antigen. The C_{H2} and C_{H3} domains of the heavy chain make up the Fc (fragment, crystallizable) region of the antibody and can bind to a variety of cell surface receptors, including the Fcγ receptors and the neonatal Fc receptor (FcRn) on cells, as well as components of the complement system (i.e., complement C1q). The IgG class is divided into four subclasses: IgG1, IgG2, IgG3, and IgG4.[2] Typically, IgG1 and IgG3 are potent triggers of effector mechanisms, whereas IgG2 and IgG4 will induce more subtle responses. However, each of these antibodies remain capable of neutralizing target antigens.[3] Currently marketed mAbs are predominantly IgG1, with a lesser degree of IgG2 and IgG4. The preference for one IgG class over the other is partially determined whether effector functions such as antibody-dependent cellular cytotoxicity (ADCC) or complement-dependent cytotoxicity (CDC) are desired for the mAb activity as well as other structural factors, but also by prior experience and availability of a particular IgG subclass in a company's development portfolio.[4]

Similar to other biologics, mAbs are produced batch-wise in living cells. As such, they are defined by the production process rather than their chemical structure, and batch-to-batch variability in the resulting product is well recognized and needs to be tightly controlled through carefully established and controlled conditions during the cell culturing, product processing and purification steps.[5]

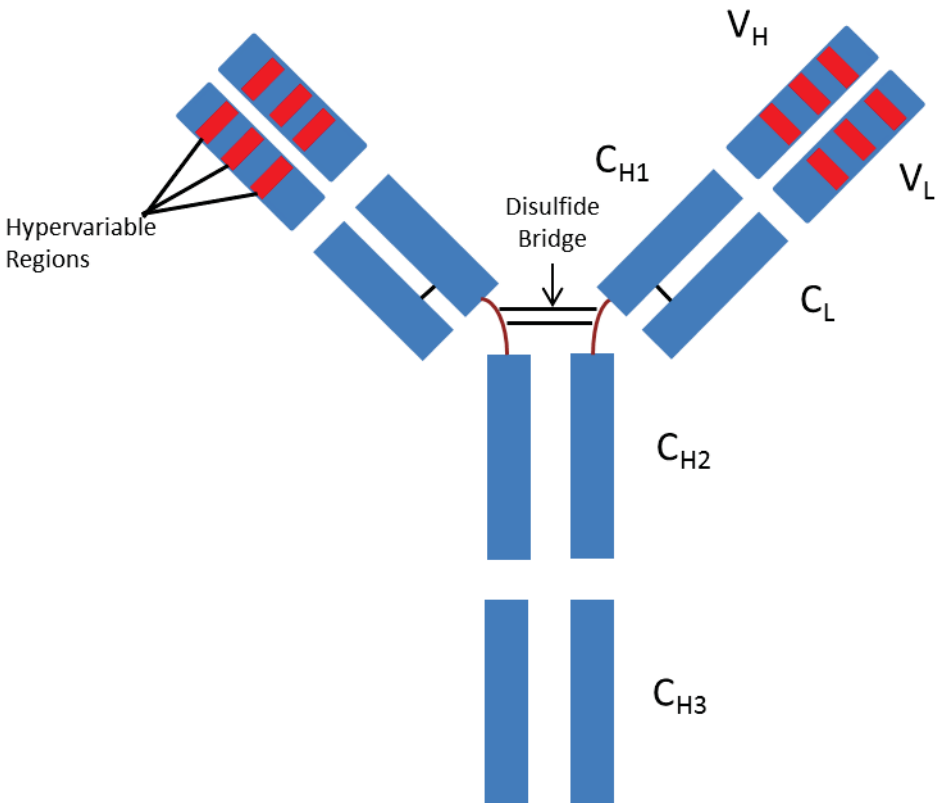

Figure 1-1. Monoclonal Antibody Structure

The production and engineering of therapeutic mAbs was made possible by the groundbreaking hybridoma technology developed by Milstein and Köhler in 1975.[6] Hybridoma technique consists of first injecting a specific antigen into a mouse, and procuring the antigen-specific plasma cells from the mouse's spleen. The isolated plasma cell is then fused with a cancerous immune cell for immortality.[7] This hybrid cell is then cloned to produce many identical daughter clones which continuously produce the monoclonal antibody of interest. Initially, only murine (derived from only mouse) monoclonal antibodies were produced with this technology, for example ibritumomab tiuxetan and tositumomab. As these murine antibodies triggered strong immune reactions in humans, especially on repeated administration, other mAb types were created through additional engineering and recombinant technology. Cetuximab and rituximab are examples of chimeric mAbs. Chimeric mAbs are constructed with V_L and V_H from murine sources and C_{H1}, C_{H2}, and C_{H3} from humans.[8] Further reduction of the murine content led to humanized mAbs, such as trastuzumab and alemtuzumab. Humanized mAbs are predominately derived from the human structure, with only the CDRs made up of murine origin. Ultimately, the production of fully human mAbs was made possible through two technologies, phage display and transgenic mice. The expectation, however, that the reduction and ultimately complete removal of murine components from mAbs would result in better tolerability and less or no immunogenic reactivity did only partially hold true, as immunogenicity of mAb products does seem affected by factors beyond the content of murine structures in the mAb molecule.

Basic Pharmacokinetic Behavior

Distribution of mAbs

The extent of mAb distribution relies upon the rates of extravasation in tissue and distribution in the interstitial space, antibody binding to the tissue components such as cell surfaces, and clearance from the tissue, including intracellular uptake and degradation. For a mAb's extravasation can occur via three basic processes: passive diffusion, convective transport and transcytosis through vascular epithelial cells. Due to the physiochemical properties and large size of mAbs, passive diffusion does not play a significant role in the extravasation process. The main mechanism by which mAbs distribute from the blood into the tissue is through convective transport.[9] Convection is determined by the flux of fluid from the vascular space to the tissue, which is driven by the blood-tissue hydrostatic gradient, as well as by the sieving effect of the paracellular pores in the vascular epithelium.[9-11] The sieving effect is determined by the size, tortuosity and number of the pores, as well as the size, shape and charge of the mAb.[9, 11] The principle behind convection is that the differential between hydrostatic and oncotic (colloid osmotic) pressures, coupled with the sieving effect, contributes to the net driving force for the extravasation of the mAb (**Figure 1-2**). Transcytosis through vascular epithelial cells, mediated via the FcRn receptor, may be another important route of extravasation for mAbs, especially in tissues where extravasation via convection is

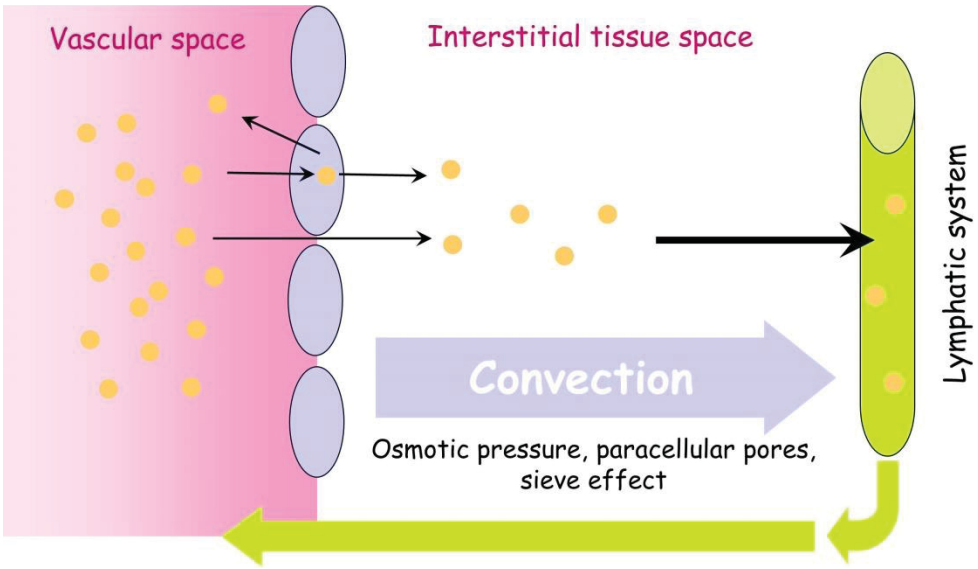

Figure 1-2. Convective Transport of a mAb
Reprinted with permission from Springer. Meibohm, B. (2013). "Pharmacokinetics and Pharmacodynamics of Peptide and Protein Therapeutics." Pharmaceutical Biotechnology: Fundamentals and Applications. D. J. A. Crommelin, R. D. Sindelar and B. Meibohm. New York, NY, Springer New York**:** 101-132.

limited.[12] Several studies have shown a bidirectional transport of IgG from basolateral to apical and apical to basolateral directions.[13-16] This suggests that FcRn mediated transcytosis may also play a role in the distribution of mAbs from the central compartment out into tissue compartments.

After extravasation, antibody distribution through the interstitial space relies upon diffusion, convection and affinity to target antigens within the interstitial space or on cell surfaces in the tissues. In cases where there is no target antigen for the mAb to bind (such as in preclinical mouse studies with a human mAb that is not cross-reactive to the murine analogue of its target antigen) or the target is in the plasma, the distribution of the mAb is expected to be limited. MAbs that have a target in the tissue compartment are expected to potentially have a greater volume of distribution. For endogenous and exogenous antibodies the tissue:blood concentration ratio is in the range of 0.1-0.5, i.e. mAb concentrations are substantially lower in the tissue interstitial fluid than in plasma.[9, 17] For brain tissue, the ratio is even in the range of 0.01 or lower.[18] In cases where the mAb binds with high affinity to extravascular sites with high binding capacity tissue:blood concentration ratios may be much higher.[9, 17, 19, 20] It is worth noting that in cases where the binding capacity of the target is limited, a nonlinear distribution could occur where the volume at steady state decreases with increasing plasma mAb concentrations.[21]

Tissue distribution by large proteins, such as IgG molecules, is further hindered by the extracellular matrix. The interstitial space is filled with extracellular matrix, which has a gel like consistency with a net negative charge and is predominantly comprised of glycosaminoglycans (e.g., hyaluronic acid) and structural proteins such as collagen. There is a mutual exclusion between IgG molecules and the structural proteins of the extracellular matrix. The fraction of the extracellular matrix that is not available for distribution is expressed as the excluded volume (Ve).[22] It is dependent on the molecular weight and charge of the macromolecule and further limits the extravascular distribution for mAbs.[23] The Ve for IgG molecules has been reported as ~50% in muscle and skin tissue.[24, 25]

Distributive antibody removal from the interstitial space is dependent on the rate of antibody convection into the lymph. The process is the same as convection from the blood vessels into the interstitial tissue space, relying on pressure gradients, fluid flow rate (lymph flow rate), and sieving. The movement of the mAbs from the interstitial tissue space into the lymph is met with less resistance compared to extravasation due to the relatively large diameter of the lymph duct pores compared to the paracellular pores in vascular epithelium. Due to the vast differences in efficiency between convection into the interstitial space and out of it, unbound antibody concentrations are much lower in the interstitial space of tissues than in the vascular space. This concentration difference is more pronounced in tissues associated with tight junctions between endothelial cells as compared to tissues with leaky capillaries. As a result, the volume of the central compartment Vc for most mAbs is in the range of 2-3 L, similar to the plasma water, and the overall volume of distribution at steady-state (Vss) is in the range of 8-20 L.[4]

Physiologically based pharmacokinetic models have been used to describe the process of distribution of an antibody through convection as a product of the lymph flow rate (L), which represents the hydrostatic gradient, and an efficiency term (1-σ). The σ is a reflection coefficient and represents the fraction of antibody sieved during the movement of blood through the pore and can have a value between 0 and 1. Reflection coefficients for large molecules, like mAbs, are assumed to be around 0.95 in tissues with continuous capillaries (tissues with tight junctions), such as connective tissue, skin and muscle.[26] The reflection coefficient in fenestrated capillaries and sinusoids (liver, spleen and bone marrow), which have leaky junctions, is in the range of 0.31 and 0.42.[26]

Elimination of mAbs

Antibodies are eliminated by either excretion or catabolism. Unlike small molecules, mAbs are too large to be filtered by the kidneys and are not eliminated in the urine, except in pathologic conditions.[27] If low molecular weight antibody fragments are filtered they are usually reabsorbed and metabolized in the proximal tubule of the nephron.[28] Biliary excretion accounts for a very small amount of the elimination of IgG antibodies. Thus, IgG elimination occurs mostly through intracellular catabolism by lysosomal degradation to amino acids after uptake by either pinocytosis, a unspecific fluid phase endocytosis, or by a receptor-mediated endocytosis process.[29]

Receptor-mediated endocytosis of IgG results from interaction of cell surface receptors with either the Fc domain or one of the Fab binding domains of the antibody. This binding event serves as trigger for the endocytotic internalization of the IgG molecule into a vesicle and subsequent lysosomal degradation. If the binding event is facilitated though interaction of the complementary-determining region of the Fab fragments with the specific target epitope for the mAb, the endocytosis and elimination is called target-mediated drug disposition (TMDD).[30] The rate of elimination of a drug through TMDD is dependent on the expression of the target receptor (which is usually limited), the affinity of mAb for the receptor, the dose of the mAb, the rate of receptor-therapeutic protein internalization, and rate of catabolism within the target cell. It is important to note that the antibodies cleared primarily by TMDD will have dose-dependent nonlinear elimination. Due to the high binding specificity and affinity of the mAb for its target, TMDD is for many mAbs, with a membrane-standing target, a major route of elimination at low doses and concentrations. At higher doses and concentrations, especially therapeutic doses for mAbs intended to block a cell surface receptor, the TMDD elimination pathway is oftentimes saturated due to the limited availability of the target receptors, thereby resulting in a limited or no relevant contribution to overall clearance of the mAb.

Receptor-mediated endocytosis of mAbs can also be facilitated through binding of the Fc domain to Fc-gamma-receptors (FcγR) expressed on many immune cells including, monocytes, macrophages, myeloid progenitor and dendritic cells.[31] Similar to the TMDD process, binding of IgG to FcγR triggers the endocytosis of the complex

and subsequent intracellular catabolism. Binding of immune complexes to FcγR is an important pathway for immune signal processing.[32] Studies with FcγR knockout animals suggest that FcγR mediated elimination plays likely only a minor role (if any) for most mAbs.[33] For those mAbs, however, that form soluble immune complexes, mediate their pharmacology activity through effector functions such as ADCC, and/or have increased binding affinity to FcγR, receptor-mediated endocytosis via FcγR may constitute an additional elimination pathway that contributes to the over elimination of the mAb. This has for example recently been demonstrated for elotuzumab.[34]

Pinocytosis is a relatively unspecific fluid-phase endocytosis by endothelial cells lining the blood vessels. Due to the large surface area of endothelial cells in the body (>1000 m^2) the process efficiently eliminates IgG molecules from the body. Catabolic degradation of IgG following pinocytotic uptake is not limited to a specific organ but occurs throughout the body, particularly in those organs and tissues rich in capillary beds with endothelial cells. Thus, the skin, muscle and gastrointestinal tract are the major elimination organs for IgG molecules that do not undergo receptor-mediated elimination pathways.[35]

Since the intracellular uptake via pinocytosis does not differentiate which proteins in the surrounding of a cell are taken up for degradation, a protective mechanism for IgG molecules is necessary to maintain their concentrations in the plasma. This salvage pathway is provided by the neonatal Fc-receptor (FcRn), also named the Brambell receptor.[36] **Figure 1-3** illustrates the mechanism:[37] IgG is taken up into catabolic cells by fluid-phase endocytosis forming an endosome which includes FcRn. At physiologic pH FcRn has low affinity for IgG, but as the endosome is acidified the affinity of FcRn increases and allows the IgG to attach via a specific binding site in the Fc domain. Once bound, the FcRn-IgG complex will be returned to the cell surface and release the IgG molecule from the binding once physiologic pH has been reached. Proteins in the endosomes that are not bound to FcRn and recycled undergo proteolytic degradation in the lysosome. The FcRn-mediated recycling of IgG molecules, including therapeutic mAbs, protects approximately two thirds of the IgG molecules taken into endosomes from catabolic degradation.[38] As a consequence, the elimination half-life for IgG1, IgG2 and IgG4 is approximately 18-21 days, which is substantially longer than the half-life of other proteins with similar molecular weight.[39] IgG3 molecules that have a substantially lower binding affinity to FcRn exhibit a half-life of 7 days. Besides serving as a salvage pathway, FcRn also facilitates transcytosis of mAbs in a variety of organs and tissues.

The efficiency of the FcRn-mediated recycling was illustrated in FcRn knockout mice, for which IgG clearance increased by tenfold.[40] Similarly, increasing the binding affinity to FcRn through protein engineering could further reduce IgG clearance.[41]. Though efficient, there is a limit to the FcRn recycling capacity. At physiologic IgG concentrations of 12 mg/mL, IgG has a half-life of approximately 21 days. Introducing high concentrations of IgG, either exogenously as in the case of high-dose intravenous immunoglobulin (IVIG) therapy, or endogenously in conditions such as multiple myeloma, there will be an increase in IgG clearance and reduced half-life by saturating

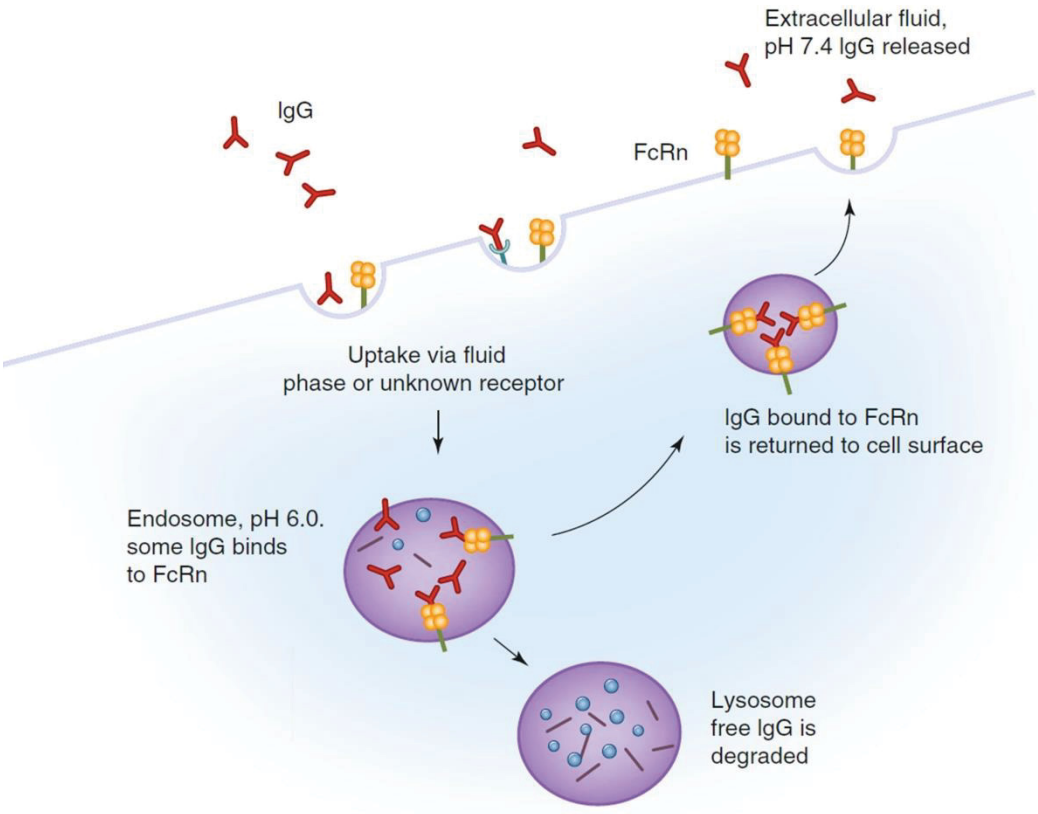

Figure 1-3. FcRn Recycling Pathway for IgG Molecules
Reprinted with permission from Springer. Davis, J. D., et al. (2013). "Monoclonal Antibodies: From Structure to Therapeutic Application." Pharmaceutical Biotechnology: Fundamentals and Applications. D. J. A. Crommelin, R. D. Sindelar and B. Meibohm. New York, NY, Springer New York**:** 143-178.

the FcRn recycling process.[42] Conversely, hypogammaglobulinemia would be expected to decrease the clearance and increase the half-life of therapeutic mAbs. Significant changes in FcRn recycling, however, are not achieved with therapeutic doses of mAbs, because most mAbs are given at dose less than 10 mg/kg, which would increase the overall amount of IgG in the body by only 1-2%.[43]

Routes of Administration

MAbs do not have an appreciable oral bioavailability due to their large size, limited membrane permeability and limited stability towards gastrointestinal protease activity. Therefore, intravenous infusion is the most common route of administration, followed by subcutaneous (SC) and intramuscular (IM) injection. SC is used for a majority of mAbs that are not given through the IV route. SC delivery of mAbs involves an absorption process from the site of injection that relies significantly on the convective transport of the mAb through the interstitial space into the lymphatic system, draining into the systemic circulation.

Similar to the distribution processes for mAbs, uptake of IgG molecules after injection into the interstitial space of subcutaneous tissues is largely driven by convective transport with only minor contribution from distribution processes. Transcytosis of IgG via FcRn contributes also, though only minimally to subcutaneous absorption.[44] In line with other therapeutic mAbs for which the percentage of recovery in lymphatic versus blood vessels is increasing with increasing molecular weight,[45] mAb absorption after SC administration is nearly exclusively facilitated by the lymphatic system rather than the vascular system. Since the flow of lymph fluid in lymphatic vessels is very slow compared to the blood flow in capillary vessels, the resulting absorption process of mAbs into the systemic circulation after SC administration is also slow, with a corresponding slow increase in plasma concentration and delayed time of the maximum concentration (Tmax), ranging for mAbs from 1.7‑13.5 days,[44] with frequent values of Tmax around 6-8 days. A model-based analysis suggests that lymphatic flow rate is the only influential factor to Tmax.[44]

Subcutaneously administered mAbs may undergo presystemic elimination. This is thought to be a combination effect of soluble peptidase activity in the interstitial space, endocytosis and subsequent lysosomal degradation in endothelial cells lining the lymphatic vessels with involvement of the FcRn recycling pathway, as well as interaction with phagocytic immune cells in the lymph nodes, whereby the latter two processes are assumed to be most prominent. The resulting reported bioavailability for SC administered mAbs ranges from 52 to 80%. [4, 44] The underlying degree of presystemic degradation has been suggested to be a function of lymphatic residence time and elimination rate during lymphatic transport.[44]

A variety of factors have been shown to influence SC absorption and bioavailability of mAbs. The site of injection may play a factor in the rate and extent of absorption for mAbs.[46] This is due to the changes in pressure gradient in the interstitial

space at different sites of injection, as well as the amount of lymph movement near the sites of injection, that can also be modulated by activity/motion near the site of injection.[47]

Product-specific factors that affect absorption are charge, size, formulation, and total dose given of the mAb.[48] The net charge of the IgG molecule changes the lymphatic uptake characteristics. Due to the slightly negative charge present in the interstitial space, the highest uptake is seen with negatively charged proteins, with positively charged molecules absorbed slower.[49] The SC bioavailability for rituximab was found to be inversely related to dose level, which might be attributed to saturation of the FcRn-mediated salvage pathway at the absorption site and the corresponding lymphatic vessels draining that area.[48]

Species-specific characteristics which are important for absorption are skin morphology, catabolic capacity at injection site, blood flow at the site of injection, and FcRn receptor affinity.[50] All of these characteristics play a role in the absorption profile in each species, and make it difficult to scale a pharmacokinetic profile from one species to another.[46] For example, FcRn receptor affinity to human IgG varies across species, which needs to be considered in choosing an animal model for pharmacokinetic studies for mAbs. For example, human IgG1 has a ~2.5 fold higher binding affinity to mouse FcRn compared to human FcRn, resulting in a potential overemphasis of FcRn-mediated absorption and disposition processes when human IgG1 mAbs are tested in mice compared to humans.[51]

Subject specific characteristics which can have an effect on absorption are body weight, sex, age, activity level, disease state, respiratory rate, and blood pressure.[52] In humans, hypodermis thickness increases with body weight, decreases with age, and depends on gender, which has the potential of leading to different absorption behavior and variability.[53] The flow of lymph increases for example by 83% during 2 hours of exercise, which may have a substantial impact on the uptake of therapeutic proteins into the systemic circulation.[54] As a consequence of all these factors, there is substantial variability in the rate and extent of absorption between different mAbs and between different individuals for the same mAb.[4, 55]

The outlined concepts have successfully been implemented in recent physiologically-based pharmacokinetic modeling attempts for mAb disposition after SC administration.[56]

Product-Specific Factors Affecting the Pharmacokinetics of mAbs

Charge

Charge is one of the major determinants of how a mAb interacts with the negatively charged components of the cell surface. Changes in charge have been shown

to change the pharmacokinetic behavior of mAbs in serum, interstitial space and tissue.[57] An increase in isoelectric point (pI) by greater than 1 unit through cationic modifications, for example, increased plasma clearance and resulted in a higher distribution into tissue.[58] MAbs with higher pI values had not only faster systemic clearance, but also lower subcutaneous bioavailability compared to antibodies with lower pI.[59] On the other hand, anionic modifications, causing a decrease in pI by 1-2 units, were shown to decrease plasma clearance and tissue accumulation.[60] Though not any small change in pI will have an effect on PK, pI changes above 1 unit in either direction are considered to result in appreciable differences in mAb pharmacokinetics.[61]

Glycosylation Pattern

Some of the pharmacodynamic effects of mAbs rely on immune mediated effector functions including ADCC and CDC. In CDC-mediated effector activity, the binding of compliment C1q to a specific binding site on the Fc domain is critical in the initiation of the compliment cascade, which ultimately leads to lysis of the target cell.[62] In ADCC-mediated effector activity, the Fc portion of the mAb binds to an Fcγ receptor on an effector cell such as a monocyte, macrophage or natural killer cells, while the Fab domains bind to cell surface receptors on the target cell. This leads to the destruction of the target cell by either engulfing the cell through phagocytic activity by the immune cell or release of cytokines leading to cell death.[62] A critical component in a mAb's ability to elicit ADCC or CDC is its affinity to FcγR and C1q, respectively, which is modulated by carbohydrate (glycan) chains at the Asn297 amino acid in the C_{H2} domain of the Fc region (**Figure 1-4**).[63]

The glycan chains attached at the Asn297 amino acid show substantial heterogeneity between and within mAb products. Several defined molecular species of a mAb with different glycan chains may coexist in the same mAb product. The originally marketed form of trastuzumab (Herceptin®), for example, eight different isoforms with different glycan chains are contained at specific relative ratios in the marketed product.[64]

Different glycan chains have been associated with differences in the pharmacodynamics and pharmacokinetics of mAb species. Afucosylation, i.e. the absence of the sugar fucose linked to N-acetylglucosamine (GlcNAc) glycan attached at the Asn297 of the Fc domain, for example, results in dramatically enhanced ADCC due to enhanced Fc-gamma-receptor IIIA (FcγRIIIa) binding affinity without any detectable change in CDC or antigen binding affinity. [65] A combination of only the afucosylated forms of trastuzumab compared to the marketed trastuzumab product that contains fucosylated and non-fucosylated forms not only increased efficacy in an *in vivo* tumor model, but also reduced half-life from 13.1 to 10.1 days, likely due to the accelerated removal of trastuzumab molecules through the ADCC mechanism.[64]

Other glycosylation patterns have also been shown to affect mAb pharmacokinetics: IgG that lacks galactose (G0% glycoforms) of IgG2 and potentially

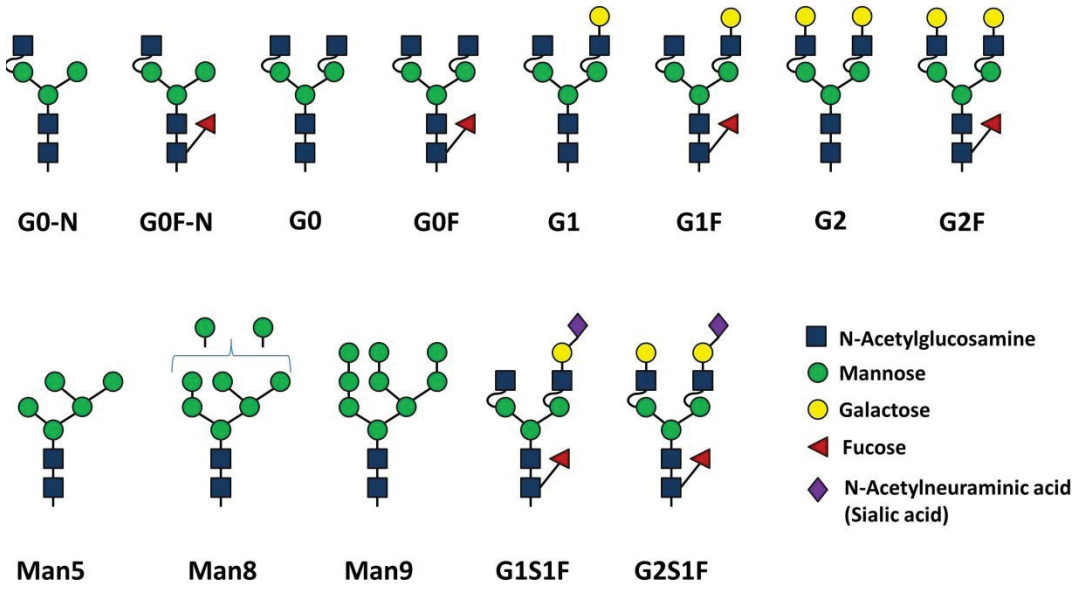

Figure 1-4. Commonly Encountered N-Glycan Structures in the Fc Portion of Monoclonal Antibodies

IgG1 remains 20-40% longer in circulation in mice compared to other glycoforms. A potential explanation is a higher binding affinity of galactosylated forms to FcγRI.[66] PK studies in Cynomolgus monkeys suggest that species of Fc fusion proteins with terminal N-acetylglucosamine are selectively cleared faster than species with other glycan structures.[67] The effect of terminal N-acetylglucosamine could be confirmed in humans.[68] Similarly, a three times faster clearance was noted for the high mannose glycans (Man5; Man8; Man9) compared to regular complex-fucosylated forms (FA2G1, FA2BG2S1), probably facilitated by the mannose receptor.[69] Overall, the alterations of clearance caused by varying glycosylation patterns are still being explored and have not been fully elucidated.[70]

Patient-Specific Factors Affecting the Pharmacokinetics of mAbs

Genetic Variants

The pharmacokinetics of mAbs may be affected by functionally relevant genetic polymorphisms in genes encoding for proteins relevant for their distribution and elimination. The expression of one of the protein components of the heterodimeric neonatal Fc-receptor, FcRn, for example, is affected by a genetic variant in the *FCGRT* gene encoding for it. The promoter region for *FCGRT* exhibits a 37-base pair variable number of tandem repeats (VNTR) polymorphism that affects the level of expression of FcRn. The most common VNTR3/VNTR3 genotype expresses 1.66-fold more FcRn transcript compared to the VNTR3/VNTR2 genotype.[71] As a consequence, patients with inflammatory bowel disease that where heterozygous exhibited 14% lower exposure for infliximab compared to patients homozygous for VNTR3, likely due to reduced salvage of IgG secondary to decreased FcRn expression, resulting in increased clearance and decreased systemic exposure of the mAb. A similar, but substantially more pronounced effect of 24% was observed for adalimumab, which may be explained by the fact that adalimumab is given by the SC route and infliximab by the IV route.[72] Reduced FcRn expression may have affected not only the clearance, buy also the bioavailability of adalimumab by its modulation of presystemic degradation. These observations are supported by studies in patients receiving intravenous immunoglobulin G (IVIG) [73], where the efficacy of treatment is higher in VNTR3 homozygotes.

Similar to FcRn, genetic variants relevant for the pharmacodynamics and potentially also pharmacokinetics of mAbs have also been described for Fcγ receptors, particularly FcγRIIIa. Clinical response for trastuzumab in HER2-overexpressing breast cancer patients was found to be significantly correlated with a genetic polymorphism in the gene encoding for FcγRIIIa resulting in an exchange of valine (V) against phenylalanine (F) at position 158. The amino acid exchange influences the affinity of IgG1 to the Fcγ receptor, resulting in an increased binding affinity and improved mediation of ADCC for the V allele compared to the F allele. Consequently, patients with V/V genotype exhibited higher objective response rates and longer progression-free survival.[74] Similar results were reported for cetuximab in colorectal cancer[75] and

rituximab in B-cell lymphoma.[76] For infliximab, the effect of the FcγRIIIa genotype was suggested to not only be limited to pharmacodynamic efficacy, but also to affect pharmacokinetics, with a reduced clearance for the F/F genotype.[77] These data suggest that Fcγ polymorphisms may affect mAb disposition if ADCC is a major elimination pathway for a specific antibody drug, but may have little or no impact on exposure for those mAbs where ADCC is only a minor or not a relevant clearance pathway.

Inflammatory Status

Proteolytic degradation, as the prime elimination pathway for mAbs, can be affected by a variety of disease states, including cancer, injury and chronic inflammatory conditions. Cancer-associated symptoms, in particular the progressive loss of weight and lean tissue, are manifestations of an ongoing chronic inflammatory response.[78] This elevated inflammatory status results in a 50-70% higher whole body protein turnover rate in cancer patients compared to normal individuals.[79] This affects not only the catabolism of many endogenous proteins, including IgG molecules, but also exogenous proteins such as therapeutically used mAbs. As a consequence, nonspecific proteolytic clearance of mAbs is not constant among patients, but may differ substantially among patient groups with a different indication or disease severity based on the degree of differences in protein turnover secondary to differences in inflammatory status. This has for example been described for the pharmacokinetics of trastuzumab, where systemic exposure in patients with HER2-positive advanced gastric or gastro-esophageal junction cancer was 30-40% lower compared to patients with HER2-positive metastatic breast cancer.[80] Similarly, clearance for infliximab has been reported as on average 0.37-0.41 L/day in Crohn's disease and ulcerative colitis, but only 0.26-0.27 L/day in rheumatoid arthritis and ankylosing spondylitis.[81]

In line with these observations, serum albumin concentrations have frequently been reported as an inversely correlated covariate for mAb clearance, where increased albumin levels are indicative of decreased IgG clearance.[4] Hypoalbuminemia is a well-recognized marker of cachexia and elevated protein turnover secondary to chronic systemic inflammatory conditions, as observed in many cancer indications. The endogenous catabolic rate for albumin is highly correlated with the catabolic turnover of immunoglobulin G.[82] Thus increased protein turnover, as indicated by hypoalbuminemia, results in increased catabolic degradation of IgG molecules, and thus increased clearance and reduced systemic exposure of therapeutically administered mAbs.

Similar to albumin, C-reactive protein (CRP) has also been identified as a predictor for mAb clearance. CRP levels correlate positively with mAb clearance, though CRP is a relatively unspecific indicator of systemic inflammation.[83] This correlation is usually not as strong as for albumin, as CRP is much more variable than serum albumin concentrations and is controlled by a larger variety of factors.

Time Dependent Changes in Pharmacokinetics

Being a function of the systemic inflammatory status, catabolic degradation of mAbs may not necessarily be constant within a specific patient but may change with time. This may become relevant for patients undergoing long-term therapy with mAbs, for example in many cancer indications or chronic inflammatory conditions. The time-dependent change of endogenous protein turnover, and thus mAb clearance, may be produced by either the natural progression of the disease or by the pharmacodynamic and therapeutic effects of the mAb.

If this process is taking place in a mAb therapy in cancer indications, then patients with the most pronounced therapeutic response to therapy should experience the largest reduction in mAb clearance over time. This is due to the reduction of the systemic inflammatory condition, which is in contrast to non-responders where little or no time-dependent change in mAb clearance should occur. Recent observations for nivolumab and pembrolizumab seem to support this notion: patients experiencing partial or complete response under anti-cancer therapy with either of the mAbs exhibited the largest decrease in clearance over time, while patients with progressive disease showed the smallest time-dependent change in clearance.[84]

The time-dependent change in mAb clearance, as a function of response to therapy, poses substantial challenges in a reliable assessment of exposure-response relationships for mAbs, as exposure is in these cases is not an independent variable for predicting response. This is especially the case for posthoc analyses of exposure-response data from studies with only one dose level, as these studies may potentially be biased and misleading.[85]

Immunogenicity

Administration of therapeutic mAbs to patients may trigger an immune response, leading to the formation of anti-drug antibodies (ADA). Immunogenicity is the ability of a particular substance, such as a mAb, to cause an immune response. The immunogenic potential of mAbs is related to a variety of factors, including the fraction of nonhuman sequence in the protein molecule, the route of administration, as well as dose and duration of therapy. Immunogenicity increases as the fraction of nonhuman sequence increases, with fully rodent mAbs being more immunogenic than chimeric mAbs, which are more immunogenic than humanized mAbs, which are generally more immunogenic than ‘fully’ human mAbs.[86] Nevertheless, even mAbs with a structure that is completely analogous to a human IgG molecule may exhibit immunogenicity. The degree of the formation of aggregates and the occurrence of T-cell epitopes have been discussed as potential determinants.[87] Route of administration also affects the probability of an immune response: SC administration oftentimes elicits a higher likelihood compared to intramuscular or IV administration, potentially secondary to aggregate formation at the injection site.[88] The dose of a mAb interestingly may have an inverse relationship to immunogenicity. It has been observed that low doses of a mAb often elicits a greater

immune response compared to a high dose of the same mAb.[89] The mechanistic basis for this observation remains elusive, although it may be speculated that ADA formed by a weak immunogenic response may be consumed by high mAb concentrations in high dose groups, thereby masking the immunogenic effect without major influence on mAb exposure. The duration of therapy also has an effect on immune response. As duration of treatment lengthens the chances to elicit an immune response also increases.[90] The binding affinity of ADA will also mature/increase over time as more mAb is introduced.[91] As binding affinity increases, so will the potential of a decrease in the therapeutic mAb concentration and clinical effect. Predisposition to form an immune response has more recently also been linked to patient genotype, for example certain human leukocyte antigen (HLA) haplotypes.[86]

Immunogenicity resulting in ADA formation is usually a polyclonal response, with multiple ADA species concurrently available and interindividual differences from patient to patient. The formed ADA can either be neutralizing antibodies or non-neutralizing antibodies. Neutralizing ADA obliterate the effect of the mAb by binding to complementarity determining regions, i.e. their active sites. The level of neutralization is dependent on the titer of ADA. Neutralizing antibodies that are at low titers may not show a clinical effect, but at high titers there is a greater potential to see a decrease in clinical efficacy.[88] Non-neutralizing ADA do not interfere with the mAb's antigen binding capacity. Independent of whether ADA are neutralizing or non-neutralizing, ADA formation frequently has an effect on the pharmacokinetics and systemic exposure of the affected mAb, although not all ADA results in a change in the mAb's pharmacokinetic behavior. If there is an effect on pharmacokinetics, it is usually a dramatic increase in the elimination of the affected mAb, resulting in a substantially reduced or no appreciable systemic exposure of the mAb.[92] The mechanistic basis for this increased clearance is the formation of circulating ADA-mAb immune complexes that are large enough to trigger uptake and lysosomal degradation by the reticuloendothelial system, mediated for example via binding of the Fc domain for Fcγ receptor, primarily FcγRIIA on platelets, and subsequent internalization by circulating phagocytes.[93]. Thus, ADA-mAb complex formation constitutes an additional clearance pathway for the affected mAb that may substantially contribute to is disposition and removal from the systemic circulation (**Figure 1-5**).[92]

Modeling mAb Disposition

The pharmacokinetics of most therapeutically used mAbs have been described by compartmental modeling approaches, using the classic two-compartment model with reversible drug transfer between a central and a peripheral compartment. Drug elimination is usually described by a linear, first-order elimination pathway from the central compartment, that may be complemented by a parallel, nonlinear elimination pathway that exhibits Michealis-Menten-style kinetics, with a defined maximum elimination rate (Vmax) and a Michealis-Menten constant (km) defining the concentration at which the elimination pathway is half saturated.[4, 55] The pharmacokinetics of mAbs that undergo TMDD have also been described by

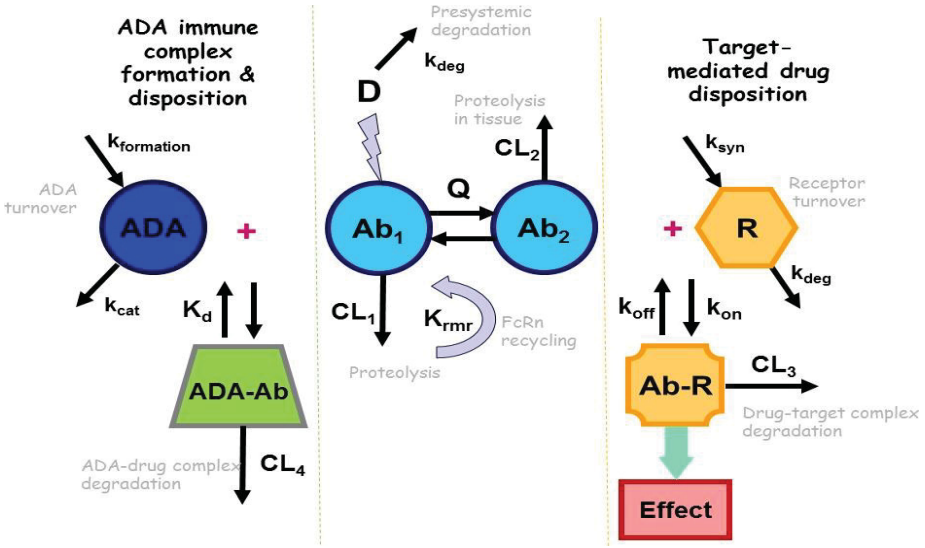

Figure 1-5. Routes of Elimination of a mAb

Multiple clearance pathways affecting the pharmacokinetics of a monoclonal antibody (mAb). Depicted is a typical two-compartment pharmacokinetic model for a mAb with administration of a dose (D) that may undergo pre-systemic degradation (degradation rate constant [k_{deg}]), concentrations of the MAb in the central (Ab_1) and peripheral (Ab_2) compartment, and interdepartmental clearance (Q). The pharmacokinetic model includes two linear clearance pathways representative of unspecific proteolytic degradation, one from the central compartment (CL_1) and one from the peripheral compartment (CL_2), as well as recycling through the neonatal Fc-receptor (FcRn)-mediated salvage pathway (recycling rate constant [K_{rmr}]). Added to these clearance pathways is, on the right-hand side, a target-mediated disposition pathway that constitutes interaction of the MAb with its pharmacologic target receptor, which is in a homeostatic equilibrium of synthesis and degradation (rate constants k_{syn} and k_{deg}). The dynamic equilibrium for the formation of the resulting MAb–receptor complex (Ab–R) is determined through the association rate constant k_{on} and the dissociation rate constant k_{off}. The formation of Ab–R not only elicits the pharmacologic effect but also triggers degradation of the complex. Thus, target binding and subsequent Ab–R degradation constitute an additional clearance pathway for the mAb (CL_3). The left-hand side of the graphic depicts the effect of an immune response to the MAb resulting in anti-drug antibody (ADA) formation. Again, the circulating concentration of the ADA is determined by a homeostatic equilibrium between its formation rate (kformation) and a catabolic turnover process (rate constant [k_{cat}]). The ADA response results in the formation of immune complexes with the drug (ADA–Ab), dependent on the dissociation constant K_d. Dependent on the size and structure of the immune complexes, endogenous elimination pathways through the reticuloendothelial system may be triggered, most likely via Fcγ-mediated endocytosis. Thus, immune complex formation and subsequent degradation may constitute an additional clearance pathway (CL_4) for MAbs (modified from Chirmule at al, [92]; reproduced with permission of Springer)

Reprinted with permission from Springer. Chirmule, N., et al. (2012). "Immunogenicity to Therapeutic Proteins: Impact on PK/PD and Efficacy." AAPS J **14**(2): 296-302.

permutations of the target-mediated drug disposition (TMDD) model. This model includes binding parameters for the mAb-target interaction as well as internalization rate for the mAb-target complex. While the full TMDD model has only been applied in few situations, largely due to the limited availability of concentration data beyond free or total mAb concentration, (e.g. target concentration, mAb-target complex concentrations) as well as the largely different time scales of the kinetic processes involved in the TMDD model (fraction of seconds for complex association rates versus days for elimination rates), simplifications and approximations of the full TMDD model have been widely applied. A comprehensive review on TMDD model variations has recently been reported in this journal.[94]

In order to expand mAb modeling from not only describing plasma pharmacokinetics, but also tissue concentration-time profiles, as well as to facilitate a more mechanistic understanding of the impact of drug disposition processes of mAbs such as TMDD, convective extravasation, FcRn recycling, and proteolytic degradation, physiologically-based pharmacokinetic (PBPK) models have more recently been applied to characterize the complex disposition kinetics of therapeutically used mAbs.[95] A recent example for a full PBPK model includes 16 tissue compartments, each further divided into vascular, endosomal, interstitial and cellular sub-compartments, as well as physiological parameters for four species (mouse, rat, monkey and human), different vascular reflection coefficients for different tissues, use of an association and dissociation constants between mAb and FcRn, degradation rates for FcRn unbound mAb and use of pinocytosis clearance.[96]

Minimal PBPK modeling can be seen as a middle ground between classical compartmental modeling and full PBPK modeling that allows for the incorporation of mechanistic key element in drug disposition without the need for extensive collections of estimated physiologic and theoretical parameters. In a recent minimal PBPK model, the compartmental complexity was reduced to two groups of tissues, the leaky and tight distribution volumes according to their vascular endothelium structure.[26] These kind of reductionist modeling approaches still allow consideration of many mechanistic and conceptual features of mAb drug disposition, but at the same time are not dependent on the assumptions of model parameters that cannot reliably be measured, accessed or estimated.

Population Variability

Although there is substantial heterogeneity in drug disposition and pharmacokinetics of mAbs, particularly if saturable distribution and elimination processes are involved, many of the therapeutically used mAbs exhibit similar pharmacokinetic behavior that is analogous to endogenous IgG molecules. Population estimates of the volumes of distribution in the central (Vc) and peripheral (Vp) compartments are typically small, with median (range) values of 3.1 (2.4–5.5) L and 2.8 (1.3–6.8) L, respectively, reflecting the limited ability of mAbs as large protein molecules to leave the vascular space.[4] The estimated between-subject variability in the Vc was

usually moderate, with a median coefficient of variation of 26%.[4] Much more limited information is available on the between-subject variability in other distribution-related parameters such as the Vp and intercompartmental clearance. The clearance of mAbs with linear elimination characteristics or at concentrations when target-mediated drug disposition processes are saturated typically ranged from 0.2 to 0.5 L/day, which is relatively close to the estimated clearance of endogenous IgG of 0.21L/day. The between-subject variability in clearance was moderate with a median coefficient of variation of 33%, ranging from 20 to 59%.[4] These values, however, may further be modulated by the various product- and patient-specific factors as outlined earlier in this chapter.

Conclusion

MAbs are a unique class of therapeutics that exhibit pharmacokinetic behavior determined and controlled by the specific mechanisms and processes involved in their disposition. Although there are substantial differences in the pharmacokinetics of individual mAbs, their general behavior can still be considered a class property as it is driven by and similar to their endogenous counterpart IgG. The mAb pharmacokinetic properties, however, can be further modulated by the various factors outlined in this chapter.

The Pharmacokinetics and Pharmacodynamics of Therapeutic Proteins and Their Description and Prediction through Modeling Approaches

Pharmacokinetic-pharmacodynamic (PKPD) modeling and simulation is used today as a method of improving decision making in preclinical trials, early stage clinical trials and in late stage clinical trials during drug development. PKPD modeling is recognized as the most rational method for choosing first-in-human dosing, especially in the realm of therapeutic antibodies.

PKPD modeling of therapeutic antibodies is challenging and requires knowledge of mechanisms unique to therapeutic antibodies. Therapeutic antibodies often have a site of action outside of the central compartment. These antibodies will require accurate prediction of not only plasma concentration, but also tissue concentration, since plasma concentration may not accurately predict concentration at the site of action. In order to predict tissue concentrations, knowledge of TMDD, convection, FcRn recycling and proteolysis must be estimated using nontraditional approaches. Nontraditional approaches are required due to therapeutic antibodies' nonlinear plasma pharmacokinetics, which are difficult to model using the traditional allometric scaling methods and mammillary-type compartmental models.[95, 97, 98] It is physiologically based pharmacokinetic (PBPK) models that are gaining recognition as an acceptable and realistic method of estimating drug pharmacokinetics compared to empirical compartmental models.[99]

There have been several PBPK models made for therapeutic proteins, each improving or adding to the next. One of the more recent PBPK models was developed by

Shah and Betts,[96] and comprised a full PBPK model which improved upon the platform PBPK models published previously.[100, 101] The authors added more tissue compartments, four more species, up-to-date physiological parameter estimates, a more mechanistically detailed tissue compartment, different vascular reflection coefficients for different tissues, use of association and dissociation constants between mAb and FcRn, a first-order degradation rate constant for mAb not bound to FcRn, the use of a pinocytosis clearance.[96]

This PBPK model includes 16 tissue compartments. Each of the tissue compartments is further divided into vascular, endosomal, interstitial and cellular sub-compartments.[96] The model structure and equations will stay the same for each of the species considered for this PBPK model (mouse, rat, monkey and human),[96] but he physiological parameters changed for each species. The Shah and Betts model characterizes mAb pharmacokinetics in both the plasma and tissue. By taking into consideration important pharmacokinetic features of mAbs, such as FcRn disposition, target-mediated drug disposition and correlation between the isoelectric value pI and plasma and tissue distribution this model was able to reasonably estimate both plasma and tissue concentrations across the multiple species.[96] Antibody drug conjugates could potentially also be evaluated by the model by adjusting the reflection coefficients.[96] However, it is important to recognize that these PBPK models are not as developed and tested as their counterparts in small molecules. So as more data come out about mechanisms of therapeutic antibody distribution, elimination and absorption, it is important to adapt these models to take into account these newly discovered mechanisms.

Minimal PBPK modeling is another technique that can be used to describe the kinetics of a therapeutic protein when only plasma concentration data is available. Minimal PBPK models provide a simpler way to estimate plasma and tissue drug concentration and may act as a preliminary model to build upon when developing a full PBPK model. In a recent publication, Cao and Balthasar adapted a previously developed full PBPK model to reflect only certain significant PK characteristics of the mAbs evaluated.[26, 102] Their model allows the obtaining of a system average estimate of drug concentrations instead of a tissue specific estimation provided by the full PBPK model. The minimal PBPK model focused on convection mediated by transcapillary escape rate (TER) as the means of mAb distribution into the extravascular space. This assumption was based on several studies that observed convection being the primary means for mAb distributing out into the extravascular space.[9, 10, 103] The minimal PBPK model also made the assumption that endothelial endosomes do not play a significant role in the distribution of this therapeutic antibody.[26] The structure of the minimal PBPK model is shown in **Figure 1-6**.

This minimal PBPK model divides the tissues into two groups, the leaky and tight volumes, according to their vascular endothelium structure.[26] This will help to estimate the concentration of drug in each tissue volume and gives an approximate average total drug in tissues. A major advantage of this approach is that it requires less parameterization, which allows for better parameter identifiability compared to the full PBPK model.

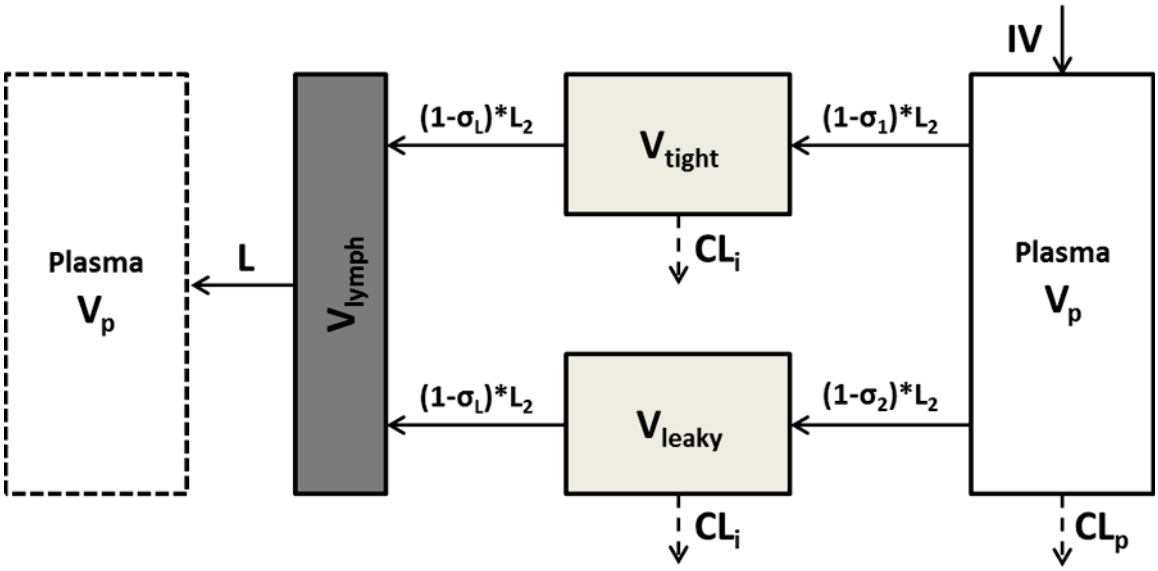

Figure 1-6. Minimal PBPK Model
In this model, drug enters the plasma compartment via intravenous injection. V_p represents the plasma volume. V_{tight} and V_{leaky} are volumes of interstitial fluid in tissues that have continuous and discontinuous or fenestrated capillaries. V_{lymph} is lymph volume, assumed equal to blood volume. The L is total lymph flow equal to the sum of L_1 and L_2, the lymph flow for V_{tight} and V_{leaky}. The σ_1 and σ_2 are vascular reflection coefficients for V_{tight} and V_{leaky}. The σ_L is the lymphatic capillary reflection coefficient. The CL_i and CL_p are mAb clearances from the interstitial fluid and plasma. [26]

The Effect of Immunogenicity on the Pharmacokinetics and Pharmacodynamics of Therapeutic Proteins and Its Description and Prediction by Modeling Approaches

Regardless of the type of modeling approach used, the prediction of immunogenicity's effect on the concentration-effect profile for a therapeutic antibody in the preclinical and clinical setting is difficult. This difficulty in prediction stems from the range of PK and PD responses that can occur, along with the variable effects on the bioanalysis.

The bioanalytical methods used to evaluate the therapeutic antibody concentration are sensitive to ADA formation. ADA can directly interfere with the bioanalytical method in place. This interference of ADA is typically evaluated during the pre-study method development and compensated for, although these pre-study positive controls may not represent the gamut of host-specific polyclonal ADA responses to a therapeutic antibody encountered in clinical studies.[104] There is also the limitation of quantifying the concentration of ADA with our current technologies. In the absence of any ADA standard reagents, assays are limited to semi-quantitative assessments. The semi-quantitative values which are derived can vary depending on the assay used and each individual's variable immune reaction, leading to a value that isn't representative of a consistent *in vivo* response.[104] Therefore, the understanding of ADA's highly variable effect on the PK of a therapeutic protein and the subsequent prediction of ADA's effect from the preclinical studies may have limitations with the currently available bioanalytical technologies.

The mechanism by which each the of the anti-drug antibodies affects the PK of a therapeutic protein is not well understood, and because of the polyclonal nature of the ADA response, a reliable approach to determining ADA affinity has proven difficult. From a PK aspect, ADA formation can cause an increase in the clearance, or a sustaining effect on the concentration of the therapeutic protein.[92] The hypothesis of the mechanism behind ADA's effect on the therapeutic protein's clearance centers on the size of the ADA-protein therapeutic immune complex that is formed, as well as the number of antigenic sites on the therapeutic protein.[92, 105] Larger immune complexes tend to be cleared more readily, increasing the clearance of the therapeutic antibody, while smaller immune complexes may not be recognized by phagocytic cells, and therefore are not cleared by the reticuloendothelial system.[92] The number of antigenic sites hypothesis may be correlated with the size of the immune complexes, as when endogenous ADA are only directed against 1 or 2 sites on the therapeutic protein one may see a half-life similar to that of IgG, but if anti-drug antibodies are directed against three or more sites, the resulting immune complex will be rapidly cleared and the affected therapeutic protein will experience an increase in clearance.

The pharmacodynamic effects of ADAs against a therapeutic protein are also variable. Each of the polyclonal ADA formed can have one of two effects on the therapeutic protein depending on where it binds on the molecule, the ADA titer and its binding affinity: (1) A neutralizing effect on therapeutic proteins activity, or (2) a non-

neutralizing effect on activity.[92] Neutralization of the therapeutic protein's activity usually occurs if the ADA binds to the active site of the molecule, for example the complementarity-determining regions of a monoclonal antibody. If the ADA neutralizes the effect of the therapeutic protein, the level of neutralization is dependent on the titer of ADA. Neutralizing antibodies that are at low titers may not show a clinical effect, but at high titers there is a greater potential to see a decrease in clinical activity of the affected therapeutic protein.[88] The binding affinity of ADA may potentially also mature and increase over time as more therapeutic protein is introduced into the organism.[91] As binding affinity increases, so will the potential of clinically relevant effect on the PK and PD of the therapeutic protein.

Though there is a current lack of knowledge behind the mechanisms of ADA formation and effect on the PK and PD of a therapeutic protein, including mAbs, several modeling approaches have been published that try to help quantitatively assess ADA response.[106-108] The model proposed by Chen et al. may act as a base model.[106] It is useful for situation when therapeutic protein concentrations change due to ADA formation. This PK/ADA model is much similar to a PKPD models. It hypothesizes that as ADA affinity matures, a change in the pharmacokinetic profile will be observed. The affinity maturation of the polyclonal ADA response is driven by cumulative dosing, in a manner similar to the effect of immunizations. This model can generate estimates of maximum ADA response, sensitivity to drug dose, affinity maturation, time lag required to observe ADA response, and elimination rate for the ADA-drug complex.[106] Although the model is used only to evaluate the drug-ADA interaction, it is flexible enough to be added into established TMDD models and/or full or simplified PBPK models. However, the major limitation of this model is that it is only hypothetical until experimental validation, which is currently not possible due to technological limitations. As it stands, this model makes many assumptions about the immune system's potential to react to a therapeutic protein, as well as how the reaction will affect the protein therapeutic's concentration, which both can be highly variable. Therefore, until a better understanding on ADA formation and its effect on a therapeutic protein has been established, this model can be used as a hypothesis generating approach looking at the dynamics of ADA development and its effect on therapeutic protein concentrations.

Another approach to modeling ADA's effect on mAb concentrations was proposed by Edlund el al.[107] The method applied tested the influence of anti-infliximab antibodies on the clearance of infliximab, using the anti-infliximab ADA status or measurements as a covariate. Three mathematical methods were applied to incorporating the ADA covariate into clearance. The first method modeled the ADA-clearance covariate relationship as a fractional change in clearance using anti-infliximab ADA information as a binary covariate on the patient level, with a patient being considered anti-infliximab positive if he/she exhibited equal to or greater than one sample with quantifiable anti-infliximab ADA.[107] The second method modeled the ADA-clearance covariate relationship as a fractional change of clearance using anti-infliximab ADA information as a binary covariate at each sample time point, which gives it a time varying aspect compared to the first method.[107] The third method modeled the ADA-clearance covariate relationship with anti-infliximab ADA concentration included as a

continuous covariate with a linear relationship to clearance.[107] Each method was applied and all three lead to a better fit of the data, with the third covariate method leading to the best fit of the three.

Perez-Ruixo el al. approached modeling ADA's effect on mAb concentrations using two other methods which avoided using ADA as a status variable, whether it be binary or continuous.[108] The novel methods were applied to data and a model which had been previously published on AMG 317.[109] The first method investigated by Perez-Ruixo et al. involved implementing inter-occasion variability on the pharmacokinetic parameters of the model that played a part in clearance and could potentially be impacted by immunogenicity. This method allowed them to generate estimates of the post hoc model parameters that were dynamically estimated overtime according to the pharmacokinetic data observed at various specified occasions.[108] If the parameters changed and were influenced by ADA presence, they could be correlated with immunogenicity status as a time-dependent covariate and studied graphically, allowing for the effect of immunogenicity on AMG 317 pharmacokinetics to be determined.[108] The other approach used by Perex-Ruixo et al. involved developing a population pharmacokinetic model using early data free of ADA interference. This model was then used to predict later drug concentrations. The predicted concentrations were then compared with the observed concentrations, and if a significant difference was seen between the predicted concentrations and the observed concentrations, immunogenicity could be confirmed.[108] Once immunogenicity was confirmed, the magnitude of that difference between the predicted and observed concentrations would quantify ADA's effect.[108]

In conclusion, all of these modeling approaches aid in identifying the effect of immunogenicity on mAb concentration over time. However, it is important to understand that an ADA response and subsequent effect is dependent on different characteristics related to the mAb itself, as well as aspects related to the treatment protocol, and that the data can be imperfect due to limitations in bioanalytical assays. All of these variables need to be taken into account when analyzing and modeling immunogenicity's effect on mAb pharmacokinetics.

CHAPTER 2. CENTRAL HYPOTHESIS

Dynamic changes in biological processes are always present when researching and understanding new medications and pharmacotherapeutic approaches. Currently, preclinical pharmacokinetic and toxicological research with protein therapeutics is hampered by anti-drug antibody (ADA) formation against the therapeutic monoclonal antibodies (mAb), without a methodology to prevent or account for the immunogenicity and its dynamic and variable effect on the mAb pharmacokinetics. There is also a void in our current knowledge on the developmental changes in transport proteins, such as MRP2, and the dynamic changes in the pharmacokinetics of substrate medications due to modulation of transport protein expression. I therefore explored in this dissertation new immunomodulation treatment modalities to limit or prevent immunogenicity and new modeling and simulation based analysis strategies to account for immunogenicity and transport protein ontogeny and their variable and dynamic effect on drug exposure.

Specific Aim 1

Immunogenicity can often alter the levels of therapeutic mAbs in preclinical animal studies performed during early drug development. Fully human and humanized mAbs are frequently antigenic to rodents and nonhuman primates, which may result in reduced systemic exposure of the protein via immune-mediated clearance.[92] High immunogenicity has been addressed in the past by concomitant immunosuppression, such as co-administration of methotrexate with enzyme replacement therapy, and tacrolimus/sirolimus combination treatment for prophylaxis against organ transplant rejection. I hypothesized that the use of such immune suppressants will mitigate an ADA response to a fully-humanized mAb in preclinical animal studies.

In Aim 1 (Chapter 4) I tested this hypothesis by identifying regimens that initiate immune tolerance towards therapeutics that would otherwise be immunogenic in animals. By identifying immunomodulatory treatment modalities, I could provide an approach to mitigate immunogenicity in preclinical species. Such preconditioning can facilitate preclinical drug development of human therapeutics that are antigenic to animals but not necessarily to humans.

Specific Aim 2

ADA formation during a preclinical study typically leads to an increase in clearance of the affected therapeutic mAb. The increase in clearance caused by ADA can be highly variable due to the unique and polyclonal nature of each animal's response to an antigenic therapeutic mAb. Variability in physiologic processes and its dynamic effect on the exposure to the therapeutic can be captured through mathematical modeling and simulation approaches.[110] Therefore, I hypothesized that by using pharmacometric modeling and simulation I would be able to account for the variability seen in mAb

clearance and relate the observed changes in mAb exposure to the time-course and magnitude of the observed ADA formation.

In Aim 2 (Chapter 5), I test this hypothesis by applying a PK-ADA modeling approach to analyze data acquired from the study performed in Aim 1 (Chapter 4). This methodology can aid in the development of appropriately powered toxicology studies, and a better understanding of the dynamic processes related to ADA formation and its impact on the exposure of the affected mAb.

Specific Aim 3

Multidrug resistance protein 2 (MRP2) represents a major hepatic transporter whose expression is dynamic throughout childhood development. MRP2 plays a role in the biliary excretion of various organic anions and cations along with glutathione-, glucuronate-, or sulfate-conjugates of several drug substrates. To date, there has been a lack of studies that have evaluated the ontogeny of MRP2 and the effect it has on the disposition of its drug substrates. My hypothesis was that through a systems pharmacology modeling approach, I can account for the dynamic changes in MRP2 expression during human development from early childhood to adulthood and its effect on the pharmacokinetics of drug substrates by integrating data from *ex vivo* studies, preclinical *in vivo* studies and clinical studies into a mathematical modeling framework.

Therefore, in Aim 3 (Chapter 6) I evaluated the effect the ontogeny of MRP2 has on the pharmacokinetics of ceftriaxone to explore methods to better understand the contribution of a transport protein to the disposition of its substrates throughout childhood development. In order to accomplish my aim, a systems pharmacology modeling approach was used to understand MRP2's contribution to the pharmacokinetics of ceftriaxone, and then to model these changes in the pharmacokinetics of ceftriaxone secondary to the ontogeny of MRP2 expression. This approach was explored to aid in the development of a platform with which to evaluate transporter ontogeny effects on therapeutic drug exposure.

CHAPTER 3. IMMUNE SUPPRESSION DURING PRECLINICAL DRUG DEVELOPMENT MITIGATES IMMUNOGENICITY MEDIATED IMPACT ON THERAPEUTIC EXPOSURE*

Introduction

Immunogenicity can often alter the levels of therapeutic proteins (TP) in preclinical animal studies. Humanized biologics are frequently antigenic to rodents and nonhuman primates, which may result in reduced systemic exposure of the protein via immune-mediated clearance [92]. When complexed with anti-drug antibodies (ADA) or complement, TP are cleared rapidly from circulation by antigen presenting cells via the reticuloendothelial system [111]. ADA in animals may thus hinder more effective determination of dosing regimens in first-in-human drug trials [112, 113]. Numerous guidelines suggest that the few animals that do not develop ADA in response to cross-species biotherapeutics may provide a more accurate picture of drug pharmacokinetics (PK) in subsequent human trials [114-116].

Several approaches have been used during preclinical development to circumvent the impact of ADA. One such strategy includes dosing with high amounts of therapeutic protein so that sufficient amounts of drug remain in circulation despite immune clearance. Alternatively, large numbers of animals per cohort could be utilized with the assumption that a few animals would be ADA-negative or display low ADA magnitudes. Recent approaches include the uses of humanized transgenic mice that have been tolerized to TP (e.g interferon, Factor VIII and human HLA transgenics) [117, 118], and xenograft models designed to mimic a human immune system (e.g. immunodeficient NOD-SCID IL2Rγ-/- or Rag2-/-γc-/- mice) [119]. However, these models are labor intensive to breed, cost prohibitive, and might not comprehensively represent the diversity of HLA alleles present in humans. Therapeutic plasmapheresis, wherein plasma is reinfused after filtering out autoantibodies and antibody-antigen complexes, is yet another technically difficult method of mitigating ADA effects in animals [120].

In the clinic, approaches for minimizing immunogenicity risk have been successfully studied and implemented. For enzyme-replacement therapy (ERT), immunogenicity has been addressed by concomitant immune suppressive regimens such as methotrexate [121, 122]. For non-enzyme based therapeutic proteins like fully human monoclonal antibodies, recombinant proteins with endogenous counterparts, fusion proteins, and novel modalities such as bispecific- and drug-conjugated antibodies, however, the use of immune suppressive regimens has not been evaluated.

*This chapter adapted with permission. Ryman, J., et al., *Immune Suppression During Preclinical Drug Development Mitigates Immunogenicity-Mediated Impact on Therapeutic Exposure.* AAPS J, 2017.

In an effort to reduce the effect of ADA formation in preclinical studies, we focused on identifying regimens that initiate immune tolerance towards therapeutics that would otherwise be immunogenic in animals. The data generated in this study demonstrate that three cycles of methotrexate, as well as weekly doses of tacrolimus plus sirolimus induction, can be effective in reducing anti-drug antibody response after the rats were administered a fully human IgG2 based mAb once weekly for four weeks.

Methods

Materials

A highly purified, investigational fully human, IgG2 monoclonal antibody (referred to as mAb1) without endogenous target in rodents produced by Amgen Inc. (Thousand Oaks, CA) was used as the model TP in this study. The purified stock mAb1 solution (71.8 mg/mL) was stored at -80 °C, protected from light, thawed and stored at 4 °C prior to use. The following immune suppressive agents were purchased commercially as aqueous solutions for injection or oral administration: tacrolimus, a calcineurin inhibitor (Astellas, Deerfield, IL); sirolimus/rapamycin, an mTOR inhibitor (Wyeth Pharmaceuticals Inc., Philadelphia, PA); and methotrexate, an anti-metabolite (APP Pharmaceuticals, LLC, Schaumburg, IL).

Animals

Fifty-four male Sprague Dawley® rats (Strain: Crl: CD(SD)) were obtained (Harlan Laboratories Inc., Indianapolis, IN) at 6 weeks of age. Once the animals were 8 weeks of age and exceeded 300 grams, mAb1 was dosed weekly for 4 weeks. The animals were sacrificed after 4 weeks (low- and moderate mAb1 dosages) or 11 weeks (high mAb1 dosage). All animal experimentation was initiated after prior approval by the Institutional Animal Care and Use Committee (IACUC) of the University of Tennessee Health Science Center and performed in accordance with the USDA Animal Welfare Act: 9 CFR Parts 1, 2, and 3 [123] and the conditions specified in the Guide for Care and Use of Laboratory Animals [124].

Immunosuppressive Regimens

Rats were randomly assigned to one of 3 treatment groups (n=18 per group), which were further divided into 3 mAb1 dosage subgroups (n=6 per subgroup). mAb1 was administered every 7 days for 4 weeks via subcutaneous injection (**Figure 3-1**) at the back of the neck with injection sites being rotated between three locations: left, center, and right. Methotrexate (Mtx) was administered as an intraperitoneal injection and tacrolimus (Tac) as a subcutaneous injection at a site separate from mAb1. Sirolimus (Sir) was administered through oral gavage. Animals in the control group received mAb1

Group	mAb1 dose (mg/kg)	Route/ frequency	No. of animals	Immunosuppression
Control	0.01 50 300	Subcutaneous/ once weekly	6 6 6	None
Tacrolimus/ Sirolimus	0.01 50 300	Subcutaneous/ once weekly	6 6 6	Sirolimus (6 mg/kg) dosed once with first mAb1 dose Tacrolimus (2 mg/kg) co-administered with each subsequent mAb1 dose
Methotrexate	0.01 50 300	Subcutaneous/ once weekly	6 6 6	Three dose methotrexate (5 mg/kg) cycles, co-administered with first mAb1 dose, and 24 and 48 h thereafter

Figure 3-1. Dosing and Experimental Design of mAb1 with and Without Immune Suppressants in Sprague Dawley Rats

The experimental plan for dosing of mAb1 alone (control group), mAb1 with tacrolimus and sirolimus (tacrolimus/sirolimus group), and mAb1 with methotrexate (methotrexate group) across 4 weeks is provided. Each group had 18 animals per group that were subdivided into three subgroups with different mAb1 doses (0.01, 50 and 300 mg/kg with 6 animals per dose group). Immune suppression dosing regimens are also provided.

alone at low (0.01 mg/kg), moderate (50 mg/kg), or high (300 mg/kg) dosages without immune suppression. The first immune suppression group, mAb1+Tac/Sir, was treated likewise with mAb1 plus sirolimus (6 mg/kg) at day 1 and tacrolimus (2 mg/kg) on days 8, 15, and 22. The treatment regimens were derived from previously tested protocols [125, 126]. In the second immune suppression group, mAb1+Mtx, animals received three intraperitoneal injections of methotrexate upon 0, 24, and 48 hours post initial mAb1 treatment. This regimen for preconditioning of animals with methotrexate was selected for its proven success in inducing antigen specific tolerance in enzyme replacement therapies [122]. Weekly serum samples were obtained from all study animals via tail vein for ADA and PK analyses. In addition, PK samples were taken pre-dose in addition to 0.5, 2, 8, 24, 72, 120, and 168 hours post-dose in the first and fourth weeks. All serum samples were stored at -60 °C to -80 °C until analysis.

Anti-mAb1 Antibody Rat Immunoassay

The ADA assessments were performed using the universal indirect species-specific assay (UNISA) as described previously [104, 115, 127]. Briefly, a bare standard-bind MSD 6000 plate was coated overnight with mAb1 for sample ADA capture, then blocked, and washed. Serum samples were diluted 1:200 in 5 × KPL buffer that was untreated (screening test) or contained excess antibodies (confirmatory test). The diluted serum samples were then added to the MSD plate for an extended incubation. Following that incubation, a ruthenylated rabbit anti-rat IgG (whole molecule) (Sigma-Aldrich, St Louis, MO) was added. The plates were read using the SECTOR® Imager 6000 plate reader (Meso Scale Discovery® (MSD), Gaithersburg, MD), and the response measured as electrochemiluminescence (ECL) units. Pooled normal rat serum (PNRS) at 0, 100, or 500 ng/mL of anti-human IgG chimeric antibody were analyzed on every plate as quality controls. For the screening assay, sample results were expressed as a ratio of the sample ECL to the negative control ECL (PNCS) as a signal to noise ratio (S/N). Analysis of specificity to variable and framework regions of mAb1 was performed by competitive inhibition of the screening assay signal with excess mAb1 or an irrelevant antibody with the same framework but different CDR as mAb1. For the specificity and competitive binding analysis, the ratio of the treated S/N compared to the untreated S/N was expressed as a percent depletion. No acid dissociation was performed for this assay format. Samples were considered ADA-positive in screening if S/N>1.5 and signal depleted more than 20% in either confirmatory test. The sensitivity of the assay is 64 ng/mL of anti-human IgG chimeric antibody. The assay is able to tolerate 20 µg/mL of excess therapeutic in the presence of 500 ng/mL of antihuman IgG chimeric antibody.

Pharmacokinetic Assay for Measuring mAb1 Concentration

An ECL based method to detect unbound mAb1 (not complexed with ADA) was used as described previously [104]. Briefly, standard streptavidin-coated plates (Meso Scale Discovery® “MSD”; Gaithersburg, MD) were passively coated with the biotin-labeled murine idiotypic monoclonal antibody against the CDR region of mAb1 (clone 1,

Lot 2579060 # 2, Amgen Inc., Thousand Oaks, CA). The standard and quality controls were made by spiking the mAb1 into 100% SD rat serum and diluted 1:30 in an assay buffer (1× PBS with 0.5 M NaCl and 0.5% Tween 20) prior to loading into the wells. A ruthenium-labeled murine monoclonal antibody against the CDR region of mAb1 antibody (clone 2, Lot 2566770 # 3, Amgen, Inc.CA) was used to detect the captured mAb1. Both capture and detection antibodies were characterized as anti-idiotype specific with ability to neutralize mAb1. Following another wash step, a tripropylamine read buffer (MSD®, Gaithersburg, MD) was added to the plate. The plate was then read using the SECTOR® Imager 6000 Instrument (MSD, Gaithersburg, MD) equipped with Discovery Workbench software (v3.0.18). The final readout was measured and reported in ECL units. The range of this analytical method was 0.03–10 µg/mL.

Statistical Methods

ADA responses to the variable (CDR), framework (Fc), or variable + framework portions of the TP, as well as pharmacokinetics were evaluated in the following analyses:

- Fisher's exact test was implemented at each dose to evaluate if the treatment of animals with immune suppression regimens significantly reduces the incidence of ADA when compared to mAb1 alone treated animals.
- To assess the dose dependency of the time profile of ADA response S/N ratios, a Repeated Measure Analysis of Variance (RMANOVA) model was implemented on natural log transformed S/N ratios for each suppression regimen with dose group, week and interaction between dose group and week as fixed effects, and subject as random effect.
- To assess if immunosuppression can significantly reduce the magnitude and onset of ADA a mixed effect model with compound (mAb1, mAb1+Tac/Sir, or mAb1+Mtx), dose, and interaction between compound and dose as fixed effects was implemented on natural log transformed ADA parameters (S/N at each time point, maximum S/N, and time of first ADA). A final model assuming variance heterogeneity and with the smallest corrected Akaike information criterion (AICC) was selected for statistical analysis.
- To assess if the immunosuppression can significantly increase mAb1 exposure, a mixed effect model with suppression regimen, dose, and interaction between suppression regimen and dose as fixed effects was implemented on natural log transformed PK parameters (AUC (mg/mL*hrs), AUC Week 1, AUC Week 4, and Cmax).

Results

Impact of Immune Suppression on Immunogenicity of mAb1

The following sections cover the impact of immune suppression on immunogenicity of mAb1 dosed in a rat model.

Incidence of Anti-mAb1 Immune Response

ADA incidence increased stepwise with mAb1 dosage, while immune suppression curtailed this effect (**Figure 3-2**). UNISA, a modified ELISA method (described above), was utilized to compare serum levels of ADA. Treatment with mAb1 alone resulted in 50%, 83%, and 100% incidence in low, moderate, and high dosages, respectively. At least half of these anti-drug antibodies were specific to the variable, complimentarity determining region (CDR), of mAb1. Tacrolimus/sirolimus eliminated all ADA at moderate (50 mg/kg) mAb1 dose ($P<0.01$). This treatment also reduced incidence by 33% (not significant) and 66% ($P<0.05$) in low- and high doses of mAb1. Methotrexate lowered ADA incidence less effectively than tacrolimus/sirolimus: 50% in moderate- and high dose groups. Surprisingly, 17% more animals receiving methotrexate with 0.01 mg/kg mAb1 developed anti-drug antibodies. In the high dose cohorts, immune suppression also caused a shift in ADA epitope from CDR to framework, fragment crystallizable (Fc), portions of mAb1.

Magnitude and Onset of Anti-mAb1 Immune Response

Both modes of immune suppression, tacrolimus/sirolimus and methotrexate, lowered the magnitude as well as delayed the onset of anti-mAb1 antibodies (**Figure 3-3**). The magnitude of immune response was measured in serum as a signal:noise (S/N = ratio of post-dose:pre-dose ECL) utilizing UNISA. Control animals that tested positive for ADA did so within one week (168 hours) of mAb1 treatment (**Figures 3-3a - 3-3c**). When averaged with ADA-negative rats in their groups, onsets were 336 hours for low- and moderate doses of mAb1 and 504 hours for high dose mAb1. Tacrolimus/sirolimus significantly lowered ADA magnitude within all dosed groups by week 3 (504 hours) after commencing mAb1 treatment ($P<0.05$). Furthermore, Tac/Sir groups showed more than 70-fold lower maximum S/N for low and high mAb1 doses ($P<0.01$) (**Table 3-1**). Methotrexate outperformed tacrolimus/sirolimus in mitigating magnitude and delaying ADA onset ($P<0.01$) when co-administered with 300 mg/kg mAb1 (**Figure 3-3c, Table 3-1**).

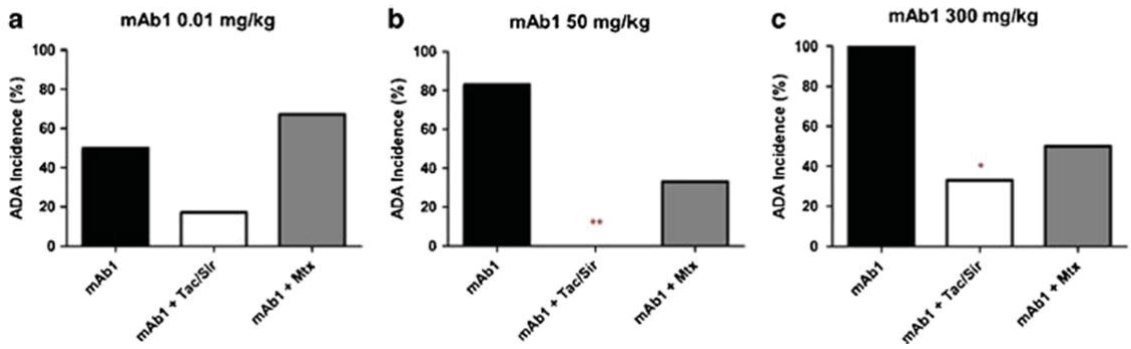

Figure 3-2. Incidence of Anti-mAb1 Immune Reactivity Following Immune Suppression

Serum from rats (n=6 per group) dosed with mAb1 alone, tacrolimus + sirolimus (Tac/Sir) co-treatment, or methotrexate (Mtx) co-treatment, was analyzed for ADA response via universal indirect species-specific assay (UNISA). ADA were assessed for specificity against CDR (α-variable), Fc (α-framework), or CDR + Fc (α-both) epitopes of mAb1 and percent incidence shown. Fisher's exact test utilized to calculate significance of immune suppression vs. mAb1 alone (shown in parentheses where applicable). *$p<0.05$, **$p<0.01$

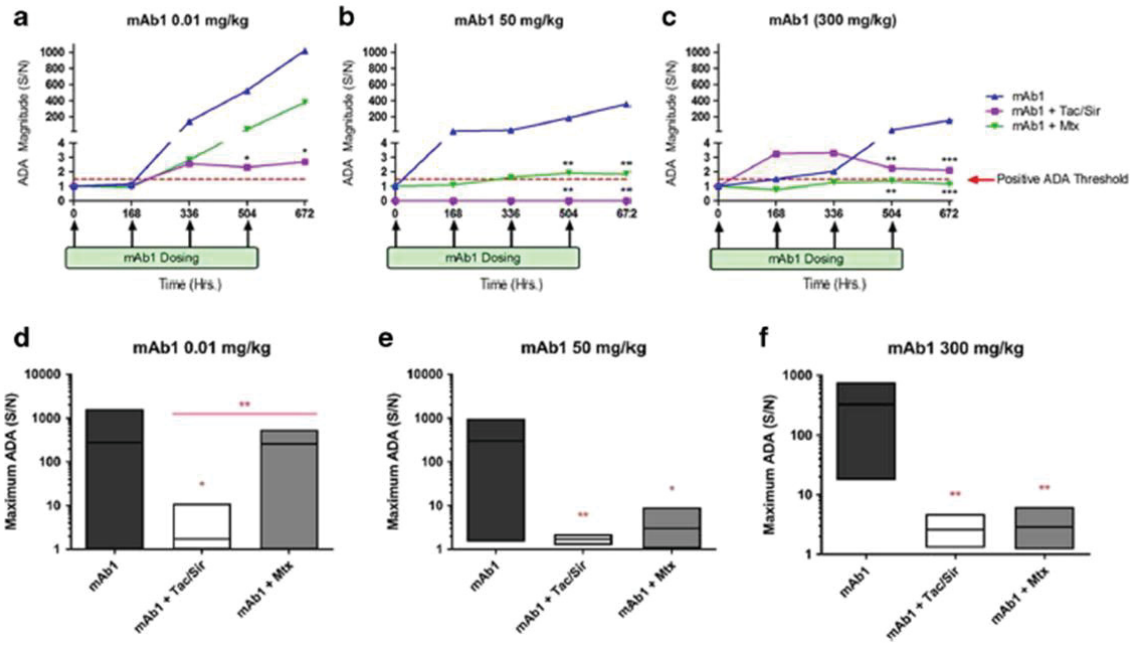

Figure 3-3. Immune Suppression Regimens Reduce Magnitude and Delay Onset of ADA Response

Universal indirect species-specific assay (UNISA) was utilized to detect ADA. Signal to noise (S/N) was calculated as the ratio of post-dose:pre-dose electrochemiluminescence. Positive ADA threshold was set to S/N>1.5 (red dashed line). Average ADA magnitudes among ADA-positive animals in each group is plotted against time (A-C). Maximum ADA S/N (D-F, table) and time of ADA onset (table) from all rats in each group were averaged. Repeated measure ANOVA (RMANOVA) as mixed model implemented on natural log transformed S/N was used to determine statistical significance (shown in parentheses where applicable). *P<0.05, **P<0.01, *** P<0.0001

Table 3-1. Maximum ADA S/N and Time of ADA Onset from All Rats in Each Group Were Averaged

mAb1 Dose (mg/kg)	Treatment	ADA Max		ADA Onset	
		Avg. S/N (Probt)	CV (%)	Avg. Hour (Probt)	CV (%)
0.01	mAb1	510.6	129	504	37
	mAb1 + Tac/Sir	3.2 (0.0171)	121	672	0
	mAb1 + Mtx	253.3	94	476	35
50	mAb1	298.6	134	392	52
	mAb1 + Tac/Sir	1.7 (0.0048)	22	N/A[a]	N/A[b]
	mAb1 + Mtx	3.0 (0.0121)	100	588 (0.0054)	24
300	mAb1	323.9	97	504	21
	mAb1 + Tac/Sir	2.6 (0.0019)	49	1568[c] (<0.0001)	31
	mAb1 + Mtx	2.9 (0.0037)	77	1400[c] (<0.0001)	33

Repeated measure ANOVA (RMANOVA) as mixed model implemented on natural log-transformed S/N was used to determine statistical significance (shown in parentheses where applicable).
a No sample positive for DNA
b ≤1 sample positive for ADA
c Time points not depicted on graph

Impact of Immune Suppression on Exposure of mAb1

The following sections cover the impact of immune suppression on the exposure of mAb1 dosed in a rat model.

Immune Suppression on Free Drug Levels

Although both forms of immune suppression initially depressed the quantity of free mAb1 in circulation, they boosted drug levels by week 4 (**Figure 3-4a-f**). The concentration of mAb1 was plotted against time and the mean area under the concentration curve (AUC) determined for each group. By the end of week 1, tacrolimus/sirolimus significantly lowered AUC by 67% ($P<0.001$) and 40% ($P<0.05$) in low- and moderate dose groups. Methotrexate likewise reduced week 1 AUC by 49% and 52% at low- and high mAb1 dosages, respectively ($P<0.01$). Tacrolimus/sirolimus immune suppression boosted free drug above mAb1 controls by 3- and 10-fold at the two highest treatments at week 4 ($P<0.01$). Methotrexate also increased mAb1 exposure by 3- and 6-fold at moderate- and high dosages at the latter time point ($P<0.05$).

Anti-mAb1 Antibodies on Free Drug Levels

Control groups exhibited a drastic decrease in circulating drug when test subjects developed ADA to mAb1, whereas this effect was tempered with immune suppression regimens. By week 4, ADA-positive rats showed 5-fold and 7-fold lower AUC in low- and moderate-dose control groups (**Figures 3-4b, 3-4d**). In contrast, the highest discrepancy based on ADA status in experimental subgroups at 4 weeks was 22% with low dose mAb1+tacrolimus/sirolimus (**Figure 3-4b**) and 43% with moderate dose mAb1+methotrexate (**Figure 3-4d**). Though statistical analyses did not show significant differences based on the development of ADA (**Table 3-2**), general trends suggest that immune suppression could allow for better approximation of free drug levels if therapeutics are prone to immunogenicity.

Discussion

Preclinical studies of human therapeutic proteins in rodents and nonhuman primates are often associated with high immunogenicity. We evaluated two regimens of immune suppression, methotrexate and tacrolimus plus sirolimus induction, with the goal of identifying a means to study drug pharmacokinetics without anti-drug antibody interference. These treatments were selected because of their clinical pervasiveness in enzyme replacement therapies, graft-versus-host prophylaxis, and autoimmune disease management to mitigate ADA responses. Inducing immunological tolerance can aid in pharmaceutical development of biologics and viral vectors, further improving patient

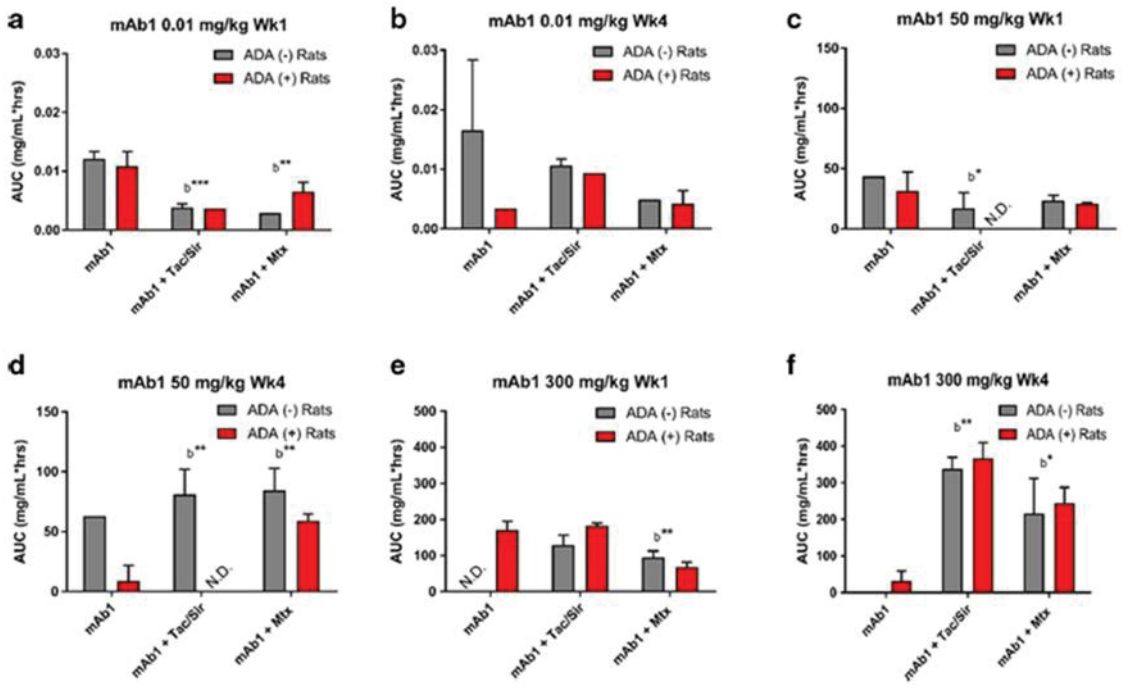

Figure 3-4. Immune Suppression Regimens Alter Drug Exposure
Area under the concentration curve (AUC) was calculated as free mAb1 concentration determined from ELISA plotted against time (mg/mL*hrs) for each treatment. The mAb1 exposures were compared between anti-drug antibody (ADA) negative and positive animals (a) as well as in the presence or absence of immune suppression (b). Statistical significance was determined by one way ANOVA of natural log transformed PK parameters. *P<0.05; **P<0.01, ***P<0.001

Table 3-2. The mAb1 Exposures Were Compared Between Anti-Drug Antibody (ADA) Negative and Positive Animals as well as in the Presence or Absence of Immune Suppression

mAb1 Dose (mg/kg)	Treatment	Week 1		Week 4	
		[a]ADA Pos vs. Neg (Probt)	[b]Ttx vs. mAb1 (Probt)	[a]ADA Pos vs. Neg (Probt)	[b]Ttx vs. mAb1 (Probt)
0.01	mAb1	0.4301		0.3370	
	mAb1 + Tac/Sir	0.8715	<0.0001	0.3487	0.6274
	mAb1 + Mtx	0.0699	0.0021	0.9299	0.6529
50	mAb1	0.5580		0.3419	
	mAb1 + Tac/Sir	N/A	0.0159	N/A	0.0011
	mAb1 + Mtx	0.5236	0.1918	0.1107	0.0013
300	mAb1	N/A		N/A	
	mAb1 + Tac/Sir	0.0972	0.4335	0.3929	0.0092
	mAb1 + Mtx	0.1015	0.0009	0.5760	0.0178

Statistical significance was determined by one way ANOVA of natural log transformed PK parameters
N/A not applicable
[a] Anti-drug antibody (ADA) negative and positive animals
[b] Presence or absence of immune suppression

outcomes. Our data demonstrate that these treatments can successfully lower antibody responses in animals to humanized therapeutics and boost amounts of drug in circulation. Combination tacrolimus/sirolimus better reduced ADA incidence and magnitude although methotrexate proved more efficacious with the highest dosage of mAb1. Tacrolimus/sirolimus treatment more than halved ADA incidence across dosages and consistently outperformed methotrexate in this regard (**Figure 3-2**). Maximum ADA signal:noise also fell with tacrolimus/sirolimus to less than 1% that of control (**Table 3-1**). Methotrexate similarly elicited at least a 50% drop in ADA incidence in the higher dosed groups. Despite higher incidence with 300 mg/kg mAb1+methotrexate relative to combination immunosuppressant therapy (**Figure 3-2c**), the ADA magnitudes were below those of the matched tacrolimus/sirolimus cohort (**Figure 3-3**). In addition, methotrexate further delayed the average onset of antibody response by 112 hours relative to tacrolimus/sirolimus with high dose mAb1 (**Table 3-1**).

Noteworthy, is that methotrexate treatment showed an enhanced incidence of ADA in the lowest dose group (67%) compared to control (50%). This additional response was CDR specific (**Table 3-3**) and had a similar magnitude to that observed in the mAb1 alone group (**Figure 3-3d**). One reason for a less effective immune suppression by methotrexate at this dosage could be the difference in frequency of immune suppressant administration. While methotrexate was administered three times (0, 24, and 48 hours) after the first mAb1 dose, tacrolimus was administered weekly (with sirolimus only on day 1). A methotrexate regimen identical to that used in this study was found to sustain ADA responses up to 4 months post ERT infusion of recombinant human acid α-glucosidase (rhGAA) of mice with Pompe disease [128]. Tolerance was extended to 8 months with a 3 week, low dose methotrexate regimen [129]. Both studies dosed rhGAA at 20 mg/kg and described expansion of regulatory B cells that proved crucial in suppressing anti-rhGAA antibodies. It is therefore possible that insufficient mAb1 was present in circulation in the 0.01 mg/kg dosed group to induce methotrexate-mediated tolerance. When higher doses of mAb1+methotrexate were used, ADA magnitudes fell throughout the time course extending up to 8 weeks after initial drug treatment (**Figures 3-3b, 3-3c**). To this end, utilizing additional cycles of methotrexate along with higher doses of TP may further mitigate anti-drug immune responses.

Additionally, the different mechanisms of action employed by the immune suppressants used in this study could also have contributed to their varying efficacies. Tacrolimus is a macrolide lactone that exerts its immunosuppressive properties by reducing interleukin-2 (IL-2) production by T-cells. Similarly, sirolimus (rapamycin) is a bacteria-derived macrolide that prevents activation of T cells and B cells by inhibiting their response to IL-2. In contrast, methotrexate suppresses the clonal expansion of T effector cells that eventually drive antigen specific memory [130]. Thus, repeated tacrolimus/sirolimus administration may have prevented primary immune responses to mAb1 with each weekly dose. The sole methotrexate regimen, however, could have only temporarily enabled mAb1 tolerance and delayed the onset of secondary antibody responses with even greater magnitudes (**Figures 3-3a, 3-3b**).

Table 3-3. Specificity and Percent Incidence of ADA Against CDR (α-Variable), Fc (α-Framework), or CDR + Fc (α-Both) Epitopes

mAb1 (mg/kg)	Treatment	α Variable	α Framework	α Both	Total	P Value
0.01	mAb1	17%	0%	33%	50%	
	mAb1 + Tac/Sir	0%	0%	17%	17%	0.27273
	mAb1 + Mtx	33%	0%	33%	67%	0.87879
50	mAb1	83%	0%	0%	83%	
	mAb1 + Tac/Sir	**0% (0.00758)	0%	0%	**0%	0.00758
	mAb1 + Mtx	*17% (0.04004)	0%	17%	33%	0.12121
300	mAb1	83%	0%	17%	100%	
	mAb1 + Tac/Sir	**0% (0.00758)	17%	17%	*33%	0.0303
	mAb1 + Mtx	33%	17%	0%	50%	0.09091

Fishers exact test utilized to calculate significance of immune suppression vs. mAb1 alone (shown in parentheses where applicable)
*$p<0.05$; **$p<0.01$

Immune modulation was found to alter the level of free drug circulating in animals. Drug concentrations declined in ADA-positive control animals relative to their ADA-negative counterparts by week 4 (**Figures 3-4b, 3-4d**). These differences disappeared in the groups treated with immunosuppressant regimens, which also displayed significantly lower ADA magnitudes. Animals in the higher dosed groups treated with immune-altering effects exhibited elevated levels of free drug at week 4 as well. Taken together, these observations suggest that lower ADA magnitudes correlate with improved retention of an otherwise immunogenic monoclonal antibody therapeutic. Ongoing animal and clinical studies continue to optimize drug-immunosuppressant combinations for specific medical indications. Cyclosporin A with azathioprine has been utilized to reduce humoral immunity against recombinant iduronidase for Mucopolysaccharidosis I [131]. Methotrexate, both alone [121, 128] and when combined with rituximab ± gammaglobulins [122] can boost the effectiveness of rhGAA enzyme replacement therapy for Pompe disease. Similarly, methotrexate-thymoglobulin [129] and mycophenolate mofetil (MMF) [132] therapies prolonged allograft survival in transplant mice and patients, respectively. Lysostaphin, a powerful antibiotic against Staphlylococcus aureus that also promotes ADA responses, can be made more effective at clearing infection with deletion of T cells specific to the drug in murine models [133, 134]. Finally, immune suppression continues to play an essential role in cancer. Patients with mesothelioma who received the active drug, SS1P, together with pentostatin/cyclophosphamide immunosuppression tolerated more treatment [135].

Given the expansion of immune suppression applications, additional studies will be essential to streamlining its use in preclinical drug development. A broader selection of immunosuppressant techniques, such as those noted above, could further aid in selection of an optimal regimen. Beyond examining ADA, it will also be important to examine the transition of B cell, T cell, and antigen-presenting-cell phenotypes following co-dosing with immune modulators. Transcriptomic, cell marker, and cytokine analyses will contribute valuable data to our understanding how immune processes are subverted in animals when challenged with humanized therapeutics. Preliminary ELISpot experiments in which rat splenocytes were incubated with mAb1 along with methotrexate or tacrolimus/sirolimus showed no mAb1-specific T cell activation in both immune suppressed groups (unpublished observation). Instead, it is anticipated that regulatory markers IL-10, TGF-b, and Foxp3 will be most upregulated.

Concerns regarding preconditioning with immune suppressants include the fact that co-therapy can change the overall toxicology profile and alter drug efficacy. For the current study, animals displayed only minor symptoms of immunosuppressant toxicity in that some seemed transiently lethargic, dehydrated, and lost weight immediately after the 3 methotrexate administrations. This frailty seemed to resolve within one week after methotrexate administration ceased. To address this issue, one solution is to retain an immunosuppressive regimen alone arm in the study that will help understand any organ/tissue toxicities caused by such agents. However, the combined effect and interaction of the co-therapy agents with the therapeutic protein will be a challenge to tease out. As the regimens used in this study were short lived, the boost in circulating drug evidences a greater benefit than risk in mitigating immunogenicity. The authors

recommend that such immunosuppressive regimens be tailored to minimize side effects in test subjects and maximize parallel conditions anticipated in human trials.

CHAPTER 4. MODELING THE EFFECT OF IMMUNOGENICITY OF A HUMAN MONOCLONAL ANTIBODY

Introduction

The number of therapeutic proteins approved or under development for human use has markedly increased this decade.[1] Many of the approved products are IgG1 or IgG2 recombinant monoclonal antibody based biotherapeutics that have been engineered to be close to endogenous human mAbs. Fully human biotherapeutics such as monoclonal antibodies are designed to be less immunogenic in humans, but are often immunogenic when administered to preclinical animal models during drug development, and are associated with the formation of anti-drug antibodies (ADA) in those species. ADA formation may not only neutralize the pharmacologic activity of the therapeutic protein, and hence impact its efficacy, but may also modulate its pharmacokinetics and thus systemic exposure by forming immune complexes and modulating its clearance.[92] Clearance of a protein therapeutic through an immune response has been well documented, with the primary result being enhanced clearance of the immune complex.[92, 104, 136] The mechanism of clearance by ADA is either through phagocytosis of the immune complex by the reticuloendothelial system or through the complement system, which will opsonize the immune complex and deposit it on an erythrocyte which will carry it to the liver or spleen to be phagocytosed by macrophages.[137, 138] If the immune complex is cleared via the reticuloendothelial system, the Fcγ receptors on the Kupffer cells and sinusoidal endothelial cells in the liver, monocytes and macrophages in the spleen and platelets will recognize the constant domain on the monoclonal antibody and clear the immune complex.[139-142] The clearance of the ADA therapeutic protein complex can be highly variable though. Variability in clearance of an immune complex is mainly due to the polyclonal nature of an immune response. Each ADA has a different affinity to the biotherapeutic's antigenic site, which leads to variable rates of binding to the biotherapeutic, with a higher affinity ADA reaction leading to larger immune complexes and a faster clearance once an immune reaction occurs against the therapeutic protein. An example of the clearance variability caused by variable interaction of ADA with the therapeutic protein has been exemplified for interleukin-6, where small immune complexes with only one of two ADAs had a sustaining effect in the systemic circulation, while interaction with three or more ADA resulted in larger immune complexes with increased clearance of the drug-ADA complex.[105, 143]

The highly variable effect of ADA formation on the exposure to a therapeutic protein may cause problems in toxicity studies in preclinical species, as well as the preclinical pharmacokinetic assessment of the protein therapeutic. Toxicity studies require that a certain systemic exposure is met in animals over time, in order to observe any toxic effects. If formation of ADA occurs and leads to an increase in clearance of the therapeutic protein, the targeted systemic concentrations will likely not be achieved in many of the studied animals. Without meeting the target concentration in many of the animals, the toxicity study will not be powered appropriately to detect the presence or

absence of any relevant toxicity with adequate statistical significance. The variable increase in clearance of the therapeutic protein secondary to ADA formation and the resulting variability in concentration-time profiles will also complicate a reliable pharmacokinetic assessment of the therapeutic protein. Model-based analyses provide a potential pathway to overcome these limitations by simultaneously analyzing ADA positive and ADA negative animals and thereby adequately characterizing the impact of ADA on the pharmacokinetic profile of a therapeutic protein in a preclinical animal model.[92]

Therefore, the objective of this study was to characterize the impact of ADA formation on the pharmacokinetic profile of a fully human mAb in rodents using a model-based analysis approach. The analysis was based on data from a previous study performed by our group.[89] In this study, the pharmacokinetics and immunogenicity of a fully human monoclonal antibody were investigated in the presence or absence of two immunomodulation strategies at different mAb dose levels, within a naïve rat model. Data from each of the studied nine groups was used to inform our PK/ADA model allowing it to estimate the fully human mAb's PK parameters, and to characterize and quantify the effect immunogenicity has on the mAb's pharmacokinetics. The results of this analysis are reported in this manuscript.

Methods

Preclinical Study

The preclinical study used as basis for the model-based analysis approach has previously been reported elsewhere in detail.[89] In brief, the following are the key features of the study:

Test System

Male Sprague Dawley rats (Strain: Crl: CD) were sourced from Harlan (Indianapolis, IN) at 6 weeks of age, weighing 250–300 g. Three animals were housed in each cage during the study with free access to standard food and water and were maintained on a 12/12-hour light/dark cycle. Animals were allowed to acclimate for 1 week before study initiation. This study was conducted in accordance with an approved protocol by the Institutional Animal Use and Care Committee at the University of Tennessee Health Science Center (Memphis, TN).

Test Article

The therapeutic protein used in this study as a model drug was a fully human IgG2 monoclonal antibody (mAb1), supplied by Amgen Inc. (Thousand Oaks, CA). The

concentration of the original solution was 71.8 mg/mL, which was diluted to the desired concentration for dosing, if necessary prepared just prior to dosing in a sterile container. If dilution was necessary, which was the case for the groups administered 0.01 mg/kg of mAb1, the original solution was diluted with 0.9% saline solution to the desired concentration of 0.01 mg/mL in order to allow for more accurate dosing. MAb1 does not have an endogenous target in rodents.

Study Design

Animals were divided into nine groups (*n* =3-6 each) according to the dose of therapeutic protein and immunosuppressive regimen (**Table 4-1**). The therapeutic protein was dosed to all rats subcutaneously at the back of the neck, rotating between 3 injection sites: left, center and right. Animals were given four weekly subcutaneous administrations of either 0.01 mg/kg, 50 mg/kg or 300 mg/kg of mAb1. At each dose level, two groups received immunosuppression with either tacrolimus (2mg/kg) (Astellas, Deerfield, IL) and sirolimus (6 mg/kg) (Wyeth Pharmaceuticals Inc., Philadelphia, PA), or methotrexate (5 mg/kg) (APP Pharmaceuticals, LLC, Schaumburg, IL). Tacrolimus was given subcutaneously at the lower back, by the hind leg, with each dose of the therapeutic protein. Sirolimus was given through oral gavage with only the first dose of mAb1. Methotrexate was given through intraperitoneal injection in a three dose cycle, shown to be efficacious in another study, [129] starting with the first dose of mAb1, then on the second day of the study and third day of the study.

Sample Collection and Handling

Serial blood samples (0.3 mL) were obtained from the tail vein under isoflurane anesthesia and placed into nonheparinized microhematocrit tubes (Thermo Fisher Scientific, Pittsburgh, PA). Samples were obtained weekly for ADA and pharmacokinetic analysis, as well as pre-dose and 0.5, 2, 8, 24, 72, 120, and 168 h post-dose in the first and fourth week for pharmacokinetic analysis. Blood was allowed to clot at room temperature for 30–45 minutes, and serum was separated by centrifugation at 2000 *g* for 20 minutes at 4°C. Serum was divided into aliquots and stored at -60 - −80°C until analysis.

Determination of Serum mAb1 Concentration

A sandwich enzyme-linked immunosorbent assay was used to quantify mAb1 concentrations in rat serum samples. Standard streptavidin-coated 96-well microplates (Meso Scale Discovery® “MSD”, Gaithersburg, MD) were passively coated with the biotin-labeled murine idiotypic monoclonal antibody against the CDR region of mAb1 (Clone 1, lot 2579060 # 2, Amgen Inc., Thousand Oaks, CA). Standards and quality controls were made by spiking mAb1 into Sprague Dawley rat serum and dilution 1:30 in

Table 4-1. Treatment Groups

mAb1 Dose	Immunosuppressant Treatment	Group (n)
Low Dose (0.01 mg/kg)	None	1 (3)
	Tacrolimus & Sirolimus	2 (6)
	Methotrexate	3 (3)
Moderate Dose (50 mg/kg)	None	4 (4)
	Tacrolimus & Sirolimus	5 (5)
	Methotrexate	6 (6)
High Dose (300 mg/kg)	None	7 (4)
	Tacrolimus & Sirolimus	8 (6)
	Methotrexate	9 (4)

an assay buffer (1X PBS with 0.5M NaCl and 0.5% Tween 20) prior to loading into the wells. A ruthenium-labeled murine monoclonal antibody against the CDR region of mAb1 (Clone 2, lot 2566770 # 3, Amgen Inc., Thousand Oaks, CA) was added for detection of captured mAb1. Following another wash step, a tripropylamine read buffer (MSD®, Gaithersburg, MD) was added to the plate. The plate was then read using a SECTOR Imager 6000 instrument (MSD®, Gaithersburg, MD) equipped with Discovery Workbench software (v3.0.18). The resulting electrochemiluminescence (ECL) was measured and reported in ECL units. The range of this analytical method was 0.03–10 µg/mL.

Determination of ADA to mAb1

A Universal Indirect Species-specific Assay (UNISA) was used to measure the relative amount of ADA in the rat serum samples, as described previously.[104, 127, 144] A bare standard-bind MSD 6000 plate was coated overnight with mAb1 for sample ADA capture, then blocked, and washed. Serum samples were diluted 1:200 in 5× KPL buffer that was untreated (screening test) or contained excess antibodies (confirmatory test). The diluted serum samples were then added to the MSD plate for an extended incubation. Following that incubation, a ruthenylated rabbit anti-rat IgG (whole molecule) (Sigma-Aldrich, St Louis, MO) was added. The plates were read using the SECTOR® Imager 6000 plate reader (Meso Scale Discovery® (MSD), Gaithersburg, MD), and the response measured as electrochemiluminescence (ECL) units. Pooled normal rat serum at 0, 100, or 500 ng/mL of antihuman IgG chimeric antibody were analyzed on every plate as quality controls. For the screening assay, ECL signal of the rat serum prior to therapeutic protein dosing was compared to ECL signal after the therapeutic protein's dosing using **Equation 4-1** forming a signal-to-noise ratio (S/N), used as the measurement for ADA in each sample. A signal-to-noise ratio of greater than 1.5 was set as a positive ADA measurement.

$$\frac{S}{N} = \frac{Predose\ ECL\ signal}{postdose\ ECL\ signal} \qquad \textbf{Eq. 4-1}$$

No acid dissociation was performed for this assay format. The sensitivity of the assay is 64 ng/mL of anti-human IgG chimeric antibody. The assay is able to tolerate 20 µg/mL of excess therapeutic in the presence of 500 ng/mL of antihuman IgG chimeric antibody.

Model-Based Pharmacokinetic Analysis

Analysis Approach and Software

The serum concentration–time profile of mAb1 for the study population was evaluated by nonlinear mixed effects modeling (NONMEM, version VII, ICON plc, Dublin). The first-order conditional estimation (FOCE) method was used for all

parameter estimations. During model evaluation Pirana (Pirana, version 2.9.2, Pirana Software & Consulting BV, http://www.pirana-software.com), Perl speaks NONMEM (PSN, version 4.2.0, http://psn.sourceforge.net) and R (R, version 3.0.1, The R Foundation for Statistical Computing) were used.

Pharmacokinetic Structural Models

The pharmacokinetic of mAb1 concentrations were described using compartmental pharmacokinetic modelling. One- and two-compartment models with first-order absorption, distribution and elimination constants were tested. Estimated pharmacokinetic parameters were absorption rate constant, apparent volumes of distribution and clearances. These values were apparent because mAb1 was administered extravascularly by subcutaneous injection. Competing structural models were compared using Akaike's information criterion (AIC), defined as follows: AIC = −2LL + 2p, where −2LL is the twice the negative log-likelihood and p is the number of model parameters to estimate.

Pharmacokinetic-ADA Models

ADA was incorporated into the pharmacokinetic structural model similar to a pharmacodynamics effect being incorporated into a classic PK/PD model.[145] Different alternative approaches were explored to integrate ADA formation into the pharmacokinetic model, but several general assumptions were followed during model development process, similar to what has been suggested by others.[146]

1. No ADA is formed during the first dosing interval (7 days). This assumption is made because it has been reported that the lag period for ADA to rise during the primary immune response varies anywhere from 7 days to several weeks.[147]
2. After the first dose, ADA has the potential to be produced at any time with an estimated rate constant of K_{ada}, and once produced its appearance in the systemic circulation is delayed through a set of lag compartments.
3. From the lag compartments, ADA enters the central compartment with an overall time delay of T_{lag}. This time delay is represented by the parameter k_t. k_t is the transfer rate constant of ADA between delay compartments and can be transformed into T_{lag} through **Equation 4-2**.
4. PK parameters of free mAb1 are estimated from the animals that do not have an immune reaction, and thus are independent of ADA production.
5. mAb1 will be bound by ADA with a molar rate of $K_{complex}$ and will be irreversibly eliminated from the central compartment.

$$k_t = n/t_{lag} \qquad \textbf{Eq. 4-2}$$

Interindividual Error Models

The interindividual variability in pharmacokinetic parameters was described using an exponential model in **Equation 4-3**, as follows:

$$\theta_i = \theta_{TV} \times e^{\eta_i} \quad \textbf{Eq. 4-3}$$

where θ_i is the estimated individual parameter, θ_{TV} is the typical value of the parameter and η_i is the random effect for the i^{th} patient. The values of η_i were assumed to be normally distributed, with a mean of zero and variance ω^2. Correlations between random effects were tested. Additive, proportional and mixed additive–proportional residual error models were tested.

Covariates

Several covariates were tested in our model and two were found to be significant covariates, as indicated by a drop in objective function value (OFV) of 3.84 or greater and a drop in BSV of greater than 10%. The two covariates were weight and dose level. Weight was used as a continuous covariate centered on the mean weight of all the animals in the study. The structure of the covariate model is shown in **Equation 4-4**:

$$\theta_i = \theta_{TV} \times \frac{Wt_i}{Wt_{mean}}^{\theta_c} \quad \textbf{Eq. 4-4}$$

where Wt_i is the weight of the individual animal, Wt_{mean} is the mean weight of the animals in the study and θ_c is the allometric scaling exponent. Dose level was used as a binary covariate for relative bioavailability in the highest dose group (300 mg/kg). At the highest dose level, the relative bioavailability appeared to decrease compared to both the 0.01 mg/kg dose group and 50 mg/kg dose group. A potential explanation for this observation is a potential saturation of the neonatal Fc receptor (FcRn). FcRn typically is not saturated at doses given to human patients, but at extremely high doses such as the 300 mg/kg given to study animals, the total (endogenous and exogenous) IgG concentration in serum was approximately doubled in this group, which may lead to an increase in the elimination of the mAb1 due to partial saturation of the FcRn salvage pathway. This same effect is also seen in patients with multiple myeloma who have highly elevated IgG levels.[43] Therefore, dose was used as a categorical covariate for bioavailability, and implemented as follows in **Equation 4-5**:

$$F = \theta_F \times \theta_{Dose}^{FcRn} \quad \textbf{Eq. 4-5}$$

where the parameter estimate for the dose effect (θ_{Dose}) was raised to the high dose effect (FcRn) which was either 0 or 1 depending on if the dosing group was 0.01 and 50 mg/kg or 300 mg/kg respectively.

Model Comparison, Covariate Selection and Goodness of Fit

Model development was guided by the standard diagnostic plots and plausibility of the parameter estimates. Interindividual, residual and covariate models were compared using −2LL and AIC. The model with the lowest significant −2LL value, assessed by a likelihood ratio χ^2 test, and the lowest AIC, was selected. The individual influence of each covariate on each pharmacokinetic parameter, if biologically plausible, was tested using the likelihood ratio test with $\alpha = 0.05$ (change in OFV≥3.84). The number of selected covariates was low, so no stepwise forward/backward covariate selection was needed. The covariates were kept in the final model if their influence was significant for $\alpha = 0.01$ (change in OFV≥10.83), and resulted in a reduction in between-subject variability of 10% or more.

The precision and stability of the model parameters was investigated by a stratified bootstrap analysis and a visual predictive check (VPC). Specifically, 500 replicate data sets were generated through random sampling with replacement using individuals as sampling units. Stratification during the random sampling process was implemented to ensure that the bootstrap datasets adequately represented the original data with respect to the different doses administered, as well as immunomodulation strategies. The 90% confidence interval was constructed by observing the 5^{th} and 95^{th} percentiles of the parameter distributions resulting from the bootstrap runs. To ensure that the model accurately represents the observed data, a VPC was performed. The final model was used to simulate 2000 replicates, and a 95% prediction confidence interval was constructed from the simulated concentration time profiles and compared with the observed data. We stratified the VPC according to dose and whether the animal was ADA positive and ADA negative.

Simulations

To demonstrate the influence of ADA formation on the pharmacokinetic profile in a study population, studies with different percentages of animals with ADA formation were simulated 2000 times. The simulated study populations represented a percentage of ADA formation between 0% and 100%. By simulating the effect ADA formation can have on the concentration-time profiles of a biotherapeutic in a study population, the model facilitates to visualize and quantify the effect ADA will have on the therapeutic protein's overall exposure in the animals and predict the range of concentration-time profiles in a study population treated with a therapeutic protein in the presence and absence of an immune reaction. This will allow for a power analysis to be performed that will provide information for determining the minimum number of animals required to meet an average exposure over time as prerequisite for a successful toxicology study.

Results

The current study provides a model-based analysis on the time-dependent formation of ADA and its impact on the systemic exposure of a biotherapeutic. The analysis was based on data from a previously performed study by our group,[89] in which different immunosuppressive regimens were explored with regard to their effect to modulate ADA formation after administration of a human monoclonal antibody, mAb1, to rats. Overall, 41 animals were used to inform the PK/ADA model, some of which were ADA positive and some ADA negative. The observed mAb1 average concentration-time profiles from this study are shown for each mAb1 dosing group in **Figure 4-1**. The corresponding observed relative ADA measurements for each dose level and treatment group are shown along with the percentage of ADA formation in each group in **Figure 4-2**.

The PK/ADA model that best described the mAb1 concentrations over time is illustrated in **Figure 4-3**. The pharmacokinetics were best described using a two-compartment model with first-order absorption process, with an inter-compartmental clearance Q and clearance from the central compartment CL. The modeling of the ADA response was based on the observed relative ADA measurements, as well as the change in clearance not explained by the clearance CL predicted by the PK portion of the model. As defined in the modeling assumptions, the potential for ADA generation starts with the second dose. If ADA develops, the amount of ADA produced, represented by the ADA molar formation rate (K_{ada} parameter estimate), is informed by the relative amount of ADA measured in the animals which were ADA positive. To account for the time delay to develop an immune response, the ADA molar formation rate is introduced into a series of delay compartments, and subsequently enters the central compartment, with a total time delay T_{lag}. The number of the delay compartments n can be flexible, but as n increases it will result in a better resolution and better approximation of a true (switch-like) delay.[146] The value of n was chosen to be 5 in our model, which is supported by previous reports.[146, 148] The transfer rate constant k_t between the ADA depot and all the delay compartments is derived from T_{lag} (**Equation 4-2**). Once the ADA reached the central compartment, the ADA-mediated drug elimination rate in the PK/ADA model was estimated through the $k_{complex}$ parameter. The $k_{complex}$ parameter represents the ADA binding to mAb1 and irreversible elimination of the formed immune complex from the circulation, and was dependent on the deviation in clearance not explained by the clearance parameter CL in the PK portion of the model.

Consequently, the developed PK/ADA model is characterized by the following set of equations (**Equation 4-6** through **Equation 4-11**):

$$\frac{dADA_1}{dt} = k_{ADA} - k_t \times A_1 \qquad \textbf{Eq. 4-6}$$

$$\frac{dADA_i}{dt} = k_t \times (A_{i-1} - A_i) \;\; i = 2, 3, 4 \; and \; 5 \qquad \textbf{Eq. 4-7}$$

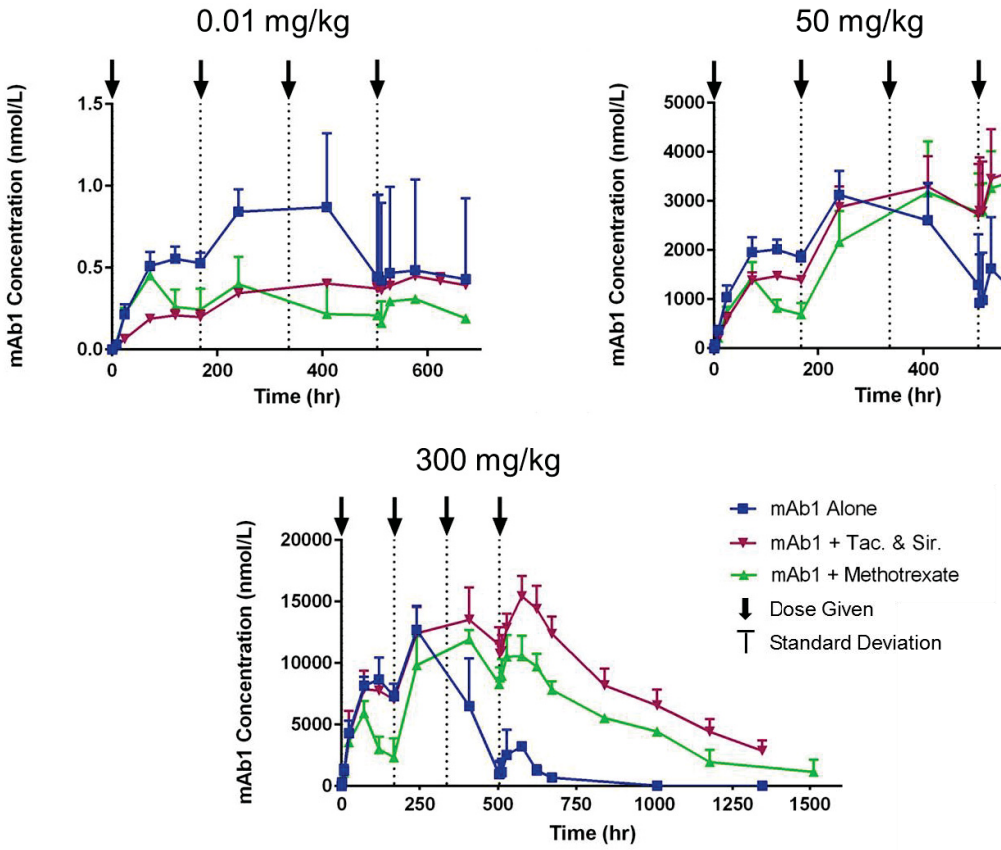

Figure 4-1. Mean Observed Concentration-Time Profiles for Each mAb1 Dosing Group

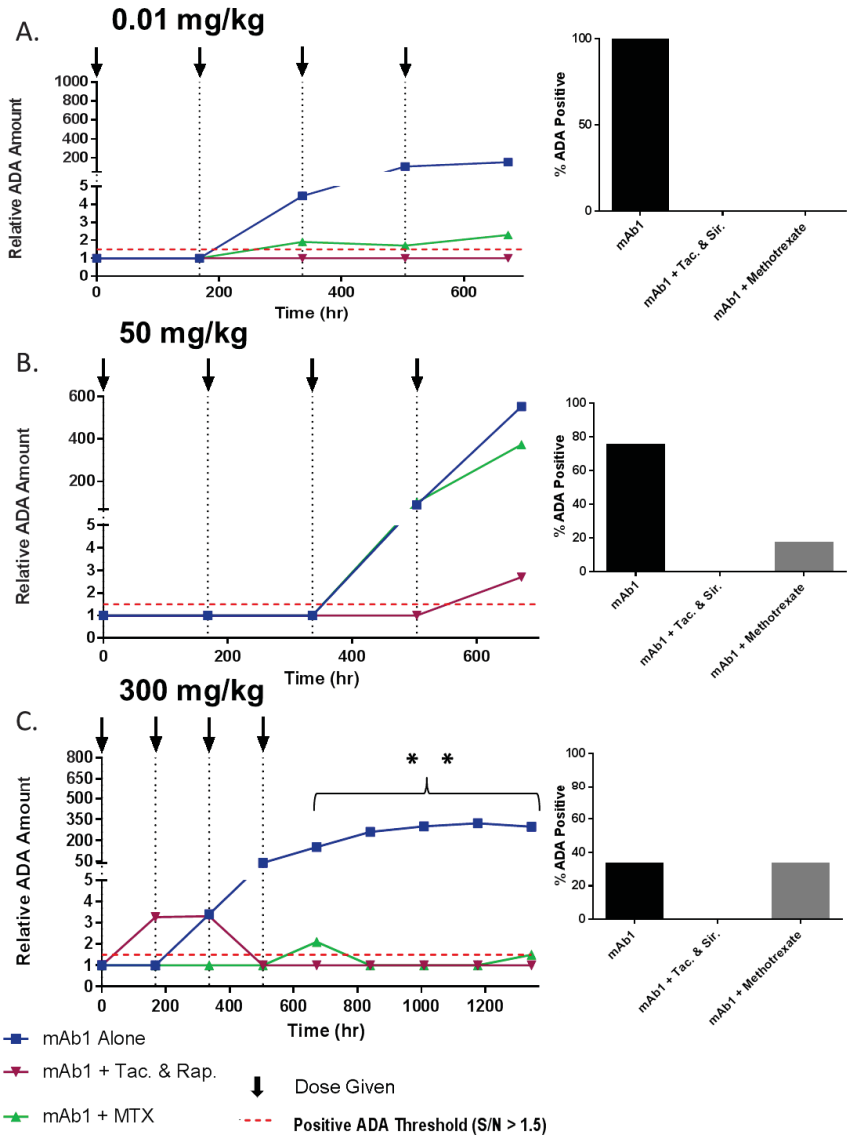

Figure 4-2. Mean Observed ADA Magnitudes and Percentage of ADA Positive Individuals in Each Group

A. Observed relative ADA magnitudes for 0.01 mg/kg mAb1 dose group. Bar graph represents the percent of animals in each group that tested positive for an immune reaction at any time during the study.
B. Observed relative ADA magnitudes for 50 mg/kg mAb1 dose group.
C. Observed relative ADA magnitudes for 300 mg/kg mAb1 dose group. **This group had a washout period where ADA sample measurements were drawn weekly, which stretched from 672 hrs to 1344 hrs.

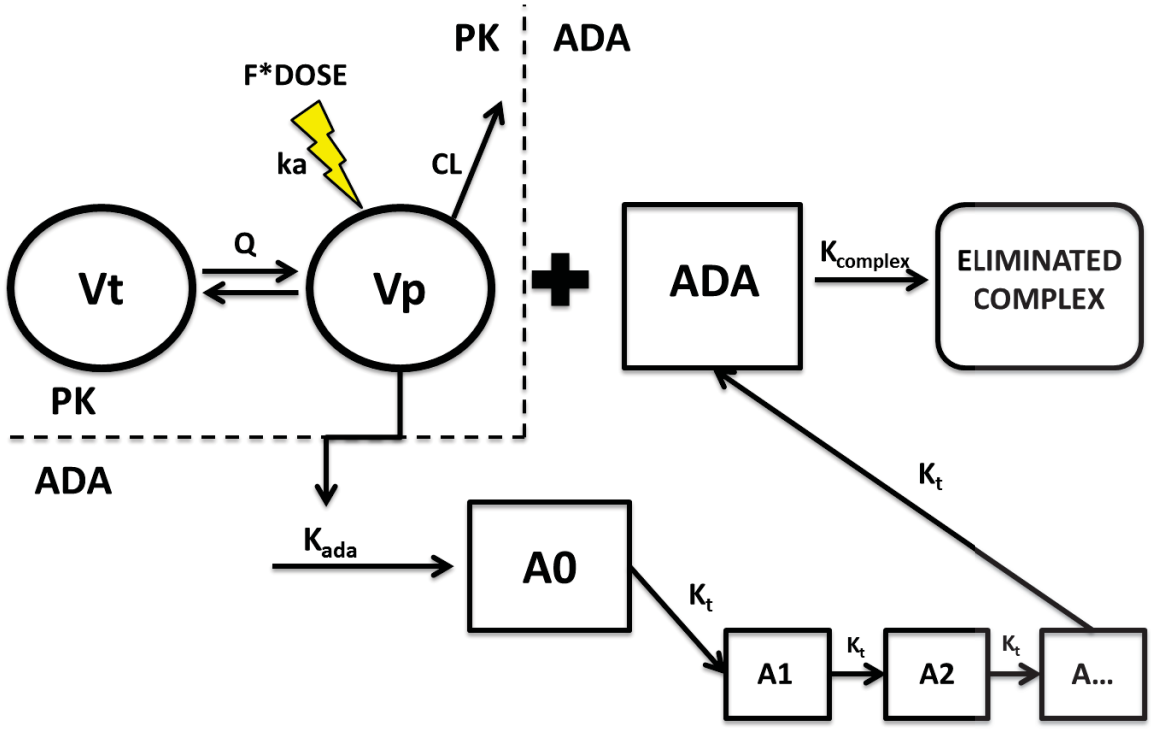

Figure 4-3. Model Structure
Structural PK/ADA model for immunogenicity assessment. With repeated dosing of the therapeutic protein (TP) an immune reaction may form against the TP. If ADA develops, ADA molar rate injections, represented by the K_{ada} parameter estimate, are introduced into a series of delay compartments, and subsequently enter the central compartment, with a total time delay T_{lag}. Once the ADA reaches the central compartment, the ADA-mediated drug clearance is estimated by $k_{complex}$. $K_{complex}$ represents the ADA binding to and irreversibly clearing the mAb1 from the circulation.

$$\frac{dADA_p}{dt} = k_t \times A_5 - K_{complex} \times ADA_p \times \frac{A_p}{V_p} \quad \textbf{Eq. 4-8}$$

$$\frac{dA_d}{dt} = -ka \times F_{rel} \times A_d \qquad \text{with } A_d \text{ at time 0 = Dose} \quad \textbf{Eq. 4-9}$$

$$\frac{dA_p}{dt} = ka \times F_{rel} \times A_d - Q \times \frac{A_p}{V_p} + Q \times \frac{A_t}{V_t} - CL \times \frac{A_p}{V_p} - K_{complex} \times ADA_p \times \frac{A_p}{V_p} \quad \textbf{Eq. 4-10}$$

$$\frac{dA_t}{dt} = Q \times \frac{A_p}{V_p} - Q \times \frac{A_t}{V_t} \quad \textbf{Eq. 4-11}$$

K_{ADA} is the molar rate of ADA moving into the ADA delay compartments. A_1, A_2 … A_i are the amounts of ADA in the delay compartments, and ADA_p is the amount of free ADA in the serum. A_d is the amount of mAb at the subcutaneous absorption site, A_p is the amount of free mAb1 in the central compartment, and A_T is the amount of free mAb1 in the tissue. Dose is the input dose for mAb1. The parameter k_t is the transfer rate constant of ADA between delay compartments. $K_{complex}$ is the second order association rate constant for the mAb1-ADA immune complex formation, representative of the ADA binding to mAb1 and elimination the ADA–drug complex. The parameter Q is the intercompartmental clearance of drug between serum and tissue. V_p and V_t are the volume of the central compartment and peripheral compartment, respectively. Ka is the first-order rate constant at which mAb1 is absorbed from the subcutaneous injection site into the central compartment. CL is the parameter that is representative of the clearance of the mAb1 in animals which do not form ADA. F_{rel} represents the relative bioavailability between each of the dose levels. All the amounts used in these equations are in molar units. The parameter estimates of the PK/ADA model, their precision and their between-animal variability are summarized in **Table 4-2**.

The diagnostic goodness-of-fit plots of predicted vs. observed measurements as presented in **Figure 4-4** for the final model suggest that the PK/ADA model described the data adequately. All model based parameters were estimated with satisfactory accuracy (**Table 4-2**). The visual predictive check plots in **Figure 4-5** indicate that there was no obvious model misspecification (**Figure 4-5**). The precision of the model parameters were investigated by a stratified bootstrap analysis. 500 replicate data sets were generated through random sampling with replacement using individuals in the original data set as sampling units. Not surprisingly, a large interindividual variability in ADA parameters was observed. This was notably the case for $K_{complex}$ and K_{ada}, for which between subjects variability was 129% and 74%, respectively. This high variability can be rationalized by the fact that each individual's immune system's reaction to mAb1, or any antigen, will be different. This variability in each animal's immune reaction is reflected in our model, as the mAb1-ADA complex elimination lead to an increase in clearance between 2 to 500 fold compared to the clearance in individuals who did not form ADA. This increase in elimination was driven by the magnitude of ADA formation in a linear fashion, so with an increase in ADA (quantified as S/N) there was a constant increase in immune complex-mediated clearance. In summary, we could successfully develop a structural

Table 4-2. Parameter Estimates

Parameter	Estimate	SE	BSV (%)	Bootstrap CI
		Pharmacokinetic Parameters		
CL (mL/day)	3.89	0.213	62.0	3.60-4.30
Vc (mL)	19.3	3.34	--	9.76-20.7
Vp (mL)	43.7	8.89	--	27.1-56.4
Dose Effect on F	0.801	0.0768	--	0.738-0.863
Q (mL/day)	4.10	1.39	--	2.98-7.54
Ka (day^{-1})	0.229	0.0276	65.0	0.208-0.298
		ADA Parameters		
K_{ada} (nmol/day)	77.0	7.01	74.0	66.2-89.3
T_{lag} (day)	14.6	3.12	71.0	7.79-21.5
$K_{complex}$ (mL/(nmol*day))	0.530	0.00122	129.0	0.480-0.533

Allometric scaling coefficients
θ_c=0.75 (CL)
θ_c=1.00 (V1 and V2)

A.

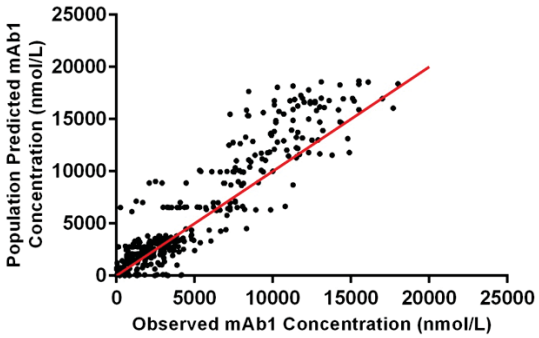

B.

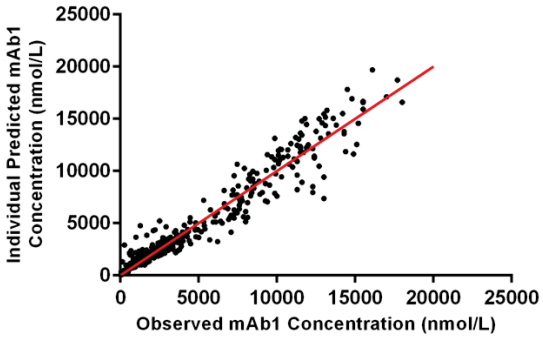

Figure 4-4. Population and Individual Model Predictions Versus Observed Concentrations

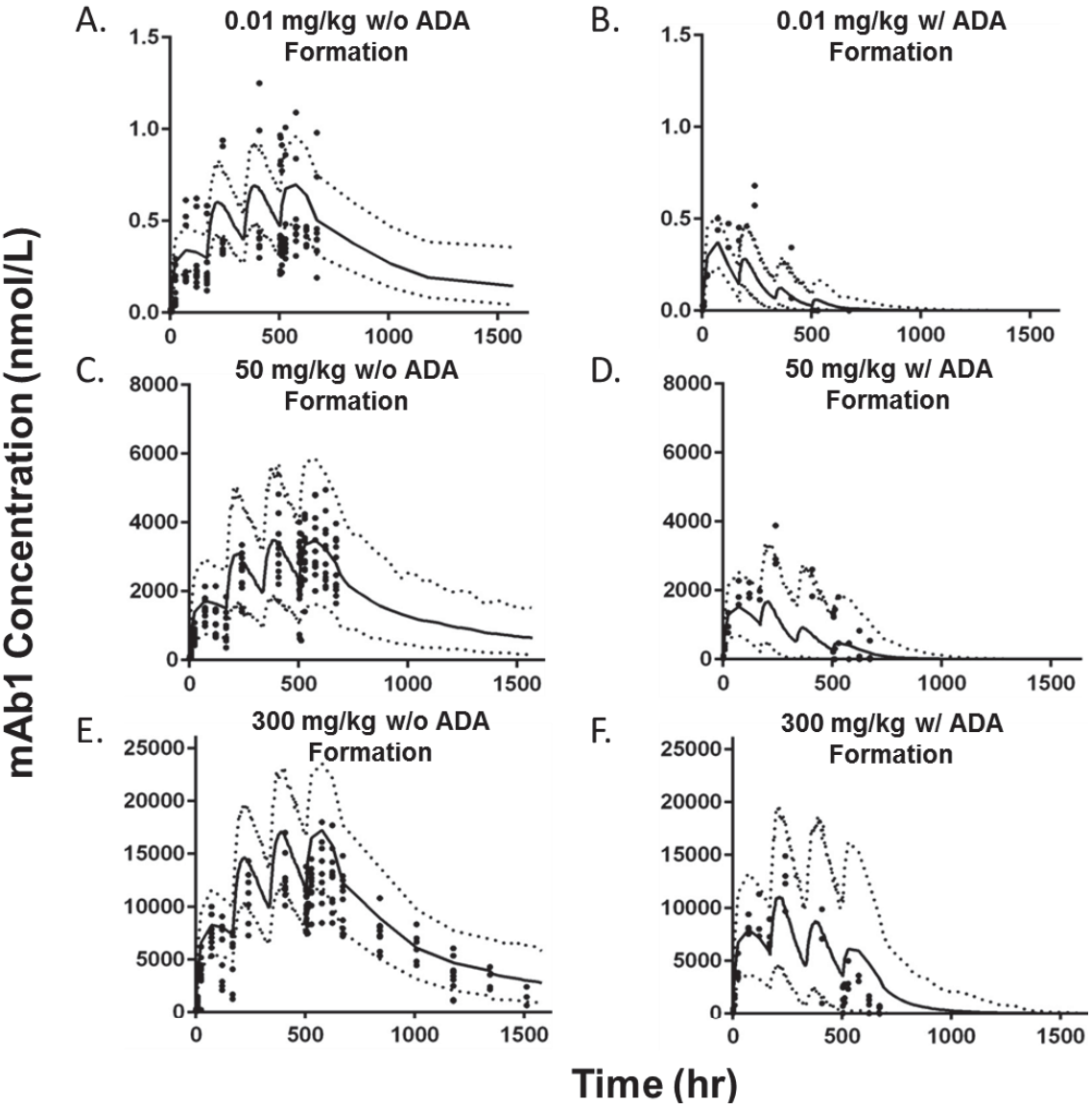

Figure 4-5. Visual Predictive Checks

Visual predictive checks were stratified into 6 groups related to dosing group and ADA status.

A. 0.01 mg/kg mAb1 dose group without immune reaction
B. 0.01 mg/kg mAb1 dose group with 100% immune reaction
C. 50 mg/kg mAb1 dose group without immune reaction
D. 50 mg/kg mAb1 dose group with 100% immune reaction
E. 300 mg/kg mAb1 dose group without immune reaction
F. 300 mg/kg mAb1 dose group with 100% immune reaction

PK/ADA model that adequately described the concentration-time profiles of mAb1 profiles in the presents and absence of ADA formation.

Discussion

We used pharmacokinetic modelling to investigate the effect ADA formation has on the concentration time profile and variability in systemic exposure for a human mAb in rodents. Similar models have been proposed by Chirmule *et al.*, Perez Ruixo *et al.* and Chen et al. to evaluate the effect of immunogenicity on therapeutic protein pharmacokinetics.[92, 108, 146] Our PK/ADA model, as an extension to the above three models, is based on the assumption that the disposition of the therapeutic protein is affected by ADA-mediated clearance. It simultaneously captures the therapeutic protein's pharmacokinetics as well as the ADA response, and permits the simulation of ADA production in preclinical species based on multiple dose studies.

Serum concentration-time data for mAb1 and ADA responses were obtained from Sprague-Dawley rats given four consecutive doses of three different dose levels of mAb1, under three different immunomodulation strategies. The mAb1 pharmacokinetic parameters were estimated based on data obtained from the animals without an immune reaction to mAb1. The mAb1 profile was best described using a two-compartment model with first-order elimination rate, which is a common structural model used for many monoclonal antibodies.[4] We described mAb1 absorption kinetics using a first-order absorption rate (ka), with a mean estimate of 0.229 day^{-1}. This value is close to what has been reported in other studies in humans, for example for omalizumab (~0.45 day^{-1}) and efalizumab (~0.25 day^{-1}).[149-151] The mAb1 central volume of distribution (V1) in our study is 0.0544 L/kg (allometric scale comparison), a value which is typically seen for other monoclonal antibodies, as they are mostly confined to the vascular space and well perfused organs. The value of clearance (CL) estimated in the present study, is 3.89 mL/day, a value similar the clearance of trastuzumab, another monoclonal antibody, in rats which was reported as 2.42 mL/day.[152] CL had a BSV of 62% which is high, but within what has been seen in other studies.[4] Intercompartmental clearance (Q) was estimated at 4.10 mL/day with a BSV that was not identifiable due to insufficient data.

The magnitude and timing of the ADA responses can be directly visualized by the observed data and model-estimated ADA–time profiles of ADA (**Figure 4-2**). The magnitudes of the ADA effect are described in the model by the parameters K_{ada} and $K_{complex}$, while the timing of the ADA response is described by T_{lag}. K_{ada} represents the molar rate of ADA moving into the lag compartments, and eventually into the central compartment, for each individual. The parameter estimate for K_{ada} was dependent on the measured ADA level (S/N) in ADA-positive animals. K_{ada} continued to increase as the measured ADA S/N ratio increased over time. This parameter proved to be effective in estimating the amount of ADA moving into the central compartment, as seen in the individual animals that had an ADA formation reaction (**Figure 4-6**). Within these animals, the model adequately captured the overall level of ADA that increased over time, with the repeated drug dosing. This is consistent with the observed increase in

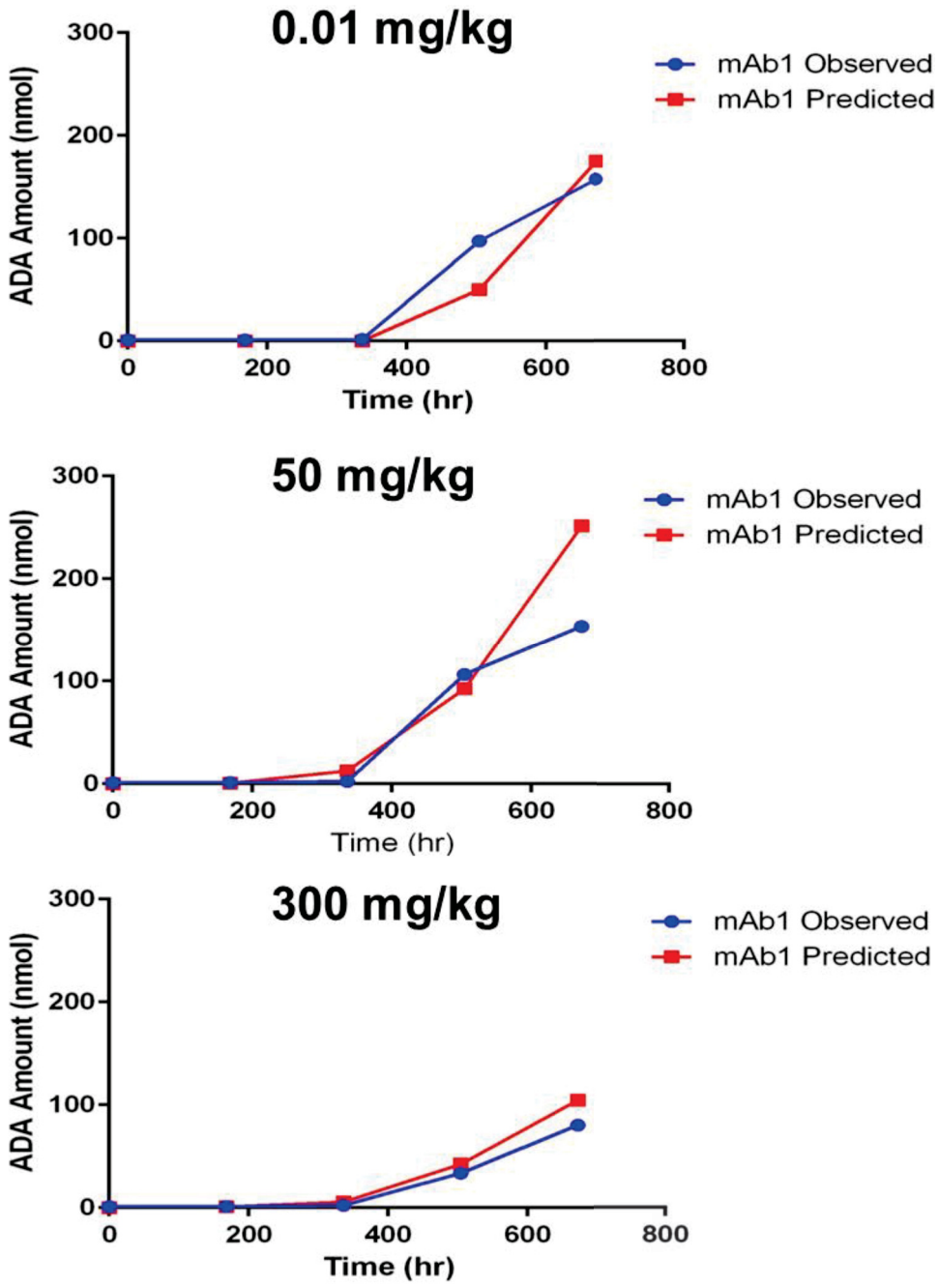

Figure 4-6. Average Observed Versus Predicted ADA Magnitude
Average observed ADA magnitude over time vs. average model predicted ADA magnitude over time for each dose level, in the animals that tested positive for ADA

drug elimination throughout the study in ADA positive animals. The choice of using measured ADA S/N ratios rather than another method, like cumulative drug dose as used other modeling approaches [146, 153], is supported by the fact that across multiple doses (0.01, 50 and 300 mg/kg) the measured relative ADA in the animals which formed an immune reaction was not consistent within each dose level. Another reason we had to forgo using cumulative dose and inform our model with measured relative ADA is seen in **Figure 4-7**, which shows the relative magnitudes of ADA formation across the three dose levels. **Figure 4-7** shows an inverse relationship between dose and ADA magnitude, with the lowest dose of 0.01 mg/kg having the greatest magnitude of ADA response, followed by the 50 mg/kg dose and lastly the highest dose (300 mg/kg), a phenomenon that has also been reported in numerous other studies.[154, 155] In **Figure 4-7**, the magnitude of ADA formation can be seen, and though cumulative dose appears to be correlated with an increase in ADA S/N ratio within each individual mAb1 dose level, the fact that there is an inverse relationship between magnitude of ADA formation and dose across multiple dose groups, along with the large amount of variability in the measured ADA S/N ratios (as indicated by the large standard deviations) strongly suggests that using the measured ADA S/N ratios along with the change in clearance to predict ADA formation is a more suitable approach for our study rather than simply using cumulative dose.

$K_{complex}$ is a measurement of the mAb1-ADA complex binding and subsequent elimination.The $k_{complex}$ parameter was informed by the increase in clearance not explained by clearance in an ADA negative individual and is the rate at which the ADA binds to the mAb1 and eliminates it; representing a second order elimination pathway for mAb1 in our model and study. $K_{complex}$ only works in one direction of binding and eliminating the mAb1, without a rate of unbinding of the mAb1, as seen in other models, like Chen's model, where affinity maturation was estimated through another parameter (k_{off}), which estimates the rate at which the therapeutic protein dissociates from the ADA.[146] Estimating the affinity maturation of each individual's immune response would be ideal, but due to our sparse sampling of ADA we lacked the data necessary to describe the affinity maturation of the immune response. Even though affinity maturation could not be captured, the affinity of the ADA for the mAb1 in each individual was captured by $k_{complex}$. As could be expected, each individual's immune response was different and lead to much variability in $k_{complex}$, as reflected by the large BSV (129%). This variability was caused by the differences in ADA affinity for the mAb1, which is depicted in **Figure 4-8**, where similar ADA magnitudes have been formed against mAb1, but one has a greater effect on the pharmacokinetics of the mAb1. This difference in affinity between each individual made it difficult to link a consistent ADA magnitude to a subsequent effect on the pharmacokinetics of mAb1, which lead us to use the method of informing the parameter $k_{complex}$ with the additional clearance not explained by CL in the ADA negative animals, a method which was successfully applied.

The timing of the initiation of ADA response is represented in the model by T_{lag} , the time delay between the first administration of a dose and occurrence of ADA. The estimated T_{lag} for the three mAb1 doses was approximately 14 days. This is in line with the expectations, as it has been observed that the primary immune response matures

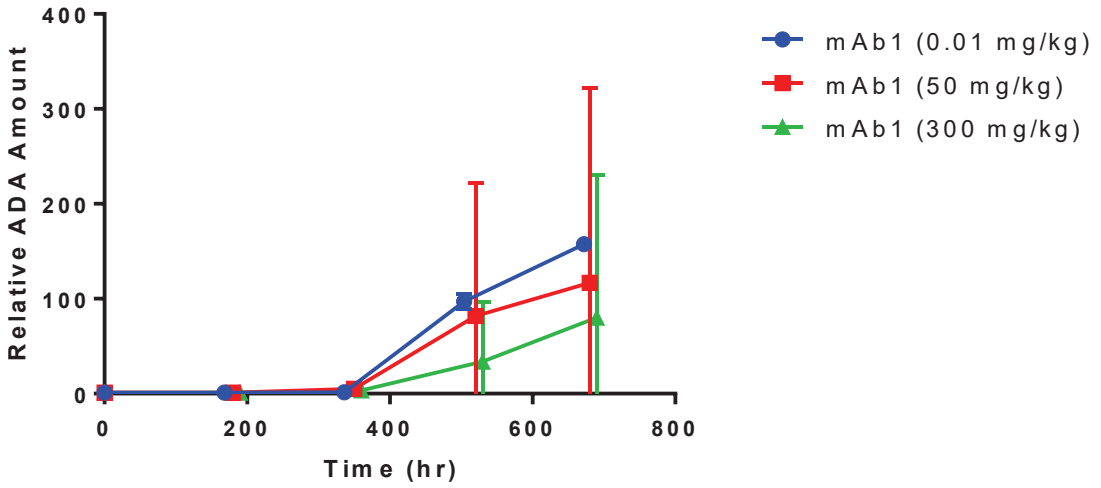

Figure 4-7. Average ADA S/N in Each Dosing Group
Average ADA formation in the non-immunomodulated subgroup for each dosing group. These averages didn't include animals which were ADA negative.

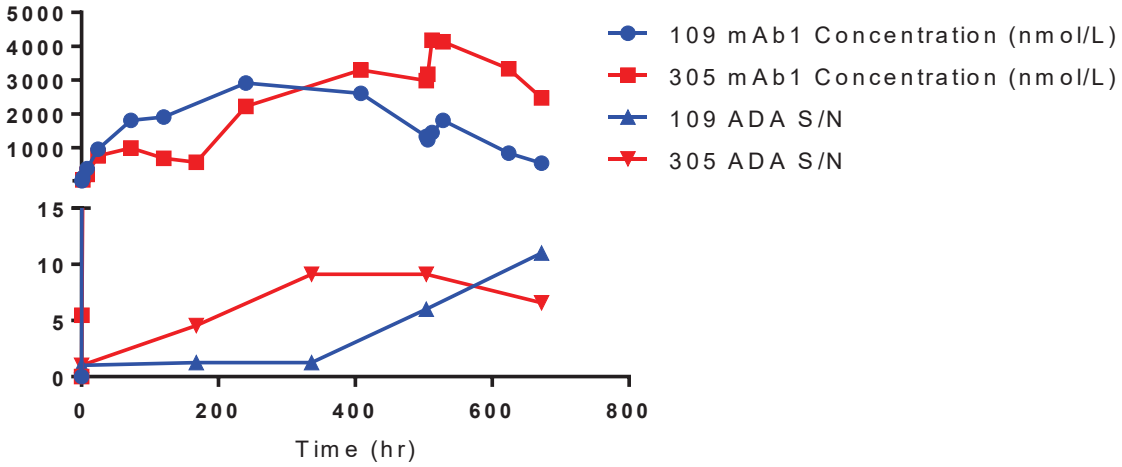

Figure 4-8. Magnitude and Affinity of an Immune Reaction
Both individuals shown here have received the same dose of mAb1 (50 mg/kg). Displayed are the observed data. This is a good example of the disconnect between ADA magnitude and affinity/clearance.

within around 10 days after the first antigen challenge, as immune cells need this time to become activated and differentiate to produce antibodies.[156] Thus, our estimate of T_{lag} appears to be consistent with previously reported experimental observations. The delayed ADA response can also be directly observed in **Figure 4-2**, where ADA concentration rises significantly after two weeks of therapy.

During our study and model building it became apparent that predicting ADA and its effects is not possible with limited covariates. In our study there was a difference in not only ADA response but also affinity between each individual, which made it difficult to link a consistent ADA cause and subsequent effect to the pharmacokinetics of mAb1. Therefore simply measuring ADA S/N or mAb1 concentrations will not allow one to predict the other. These vast differences in both ADA magnitude of response and affinity required us to use measured ADA S/N in concert with measured mAb1 concentrations to inform the parameters K_{ada} and $K_{complex}$, both of which allowed us to model the effect ADA has on the pharmacokinetics of the mAb1 in our PK/ADA model. Without the measured mAb1 concentration and the ADA S/N magnitude we would not have been able to accurately model the pharmacokinetics of mAb1 and the effect of ADA on the PK, let alone predict and simulate what dose will cause what magnitude of reaction, what ADA magnitude will cause a certain clearance or what clearance is caused by a certain magnitude of ADA reaction. More research into what is predictive of an organisms potential to elicit an immune response in the presence of a potential antigen is required before a prediction of immunogenicity can be made for therapeutic proteins.

An interesting phenomenon observed while developing the PK/ADA model was a decreased systemic exposure and consistent overestimation of the concentration-time profiles for mAb1 in rats treated with methotrexate in the medium and high mAb1 dose groups (**Figures 4-9** and **4-10**). It has been demonstrated previously that Fcγ receptor expression was down regulated in the presence of methotrexate.[157] This interaction could potentially be occurring in our study, and could potentially also affect the neonatal Fc receptor (FcRn), which could lead to a downregulation of FcRn, eliminating a key recycling mechanism for IgGs, causing an increase in the clearance of mAb1. To further explore, if this interaction could help explain our models discrepancy with our observed data we built methotrexate into the model as a categorical covariate on clearance (CL), and implemented as follows in **Equation 4-12**:

$$CL = \theta_{CL} \times (\theta_{MTX})^{ITX} \qquad \textbf{Eq. 4-12}$$

where the parameter estimate for the methotrexate effect on clearance was raised to the ITX interaction switch which was either 1 or 0 depending on whether the animal received methotrexate or not, respectively. With the experimental methotrexate covariate built into the model, we were able to explain more of the discrepancy between the animals treated with methotrexate and those that were not as seen in **Figure 4-11**. We did not add this interaction as a covariate into our final model, as there is not a study to justify its addition, but the interaction could certainly be explored in the future.

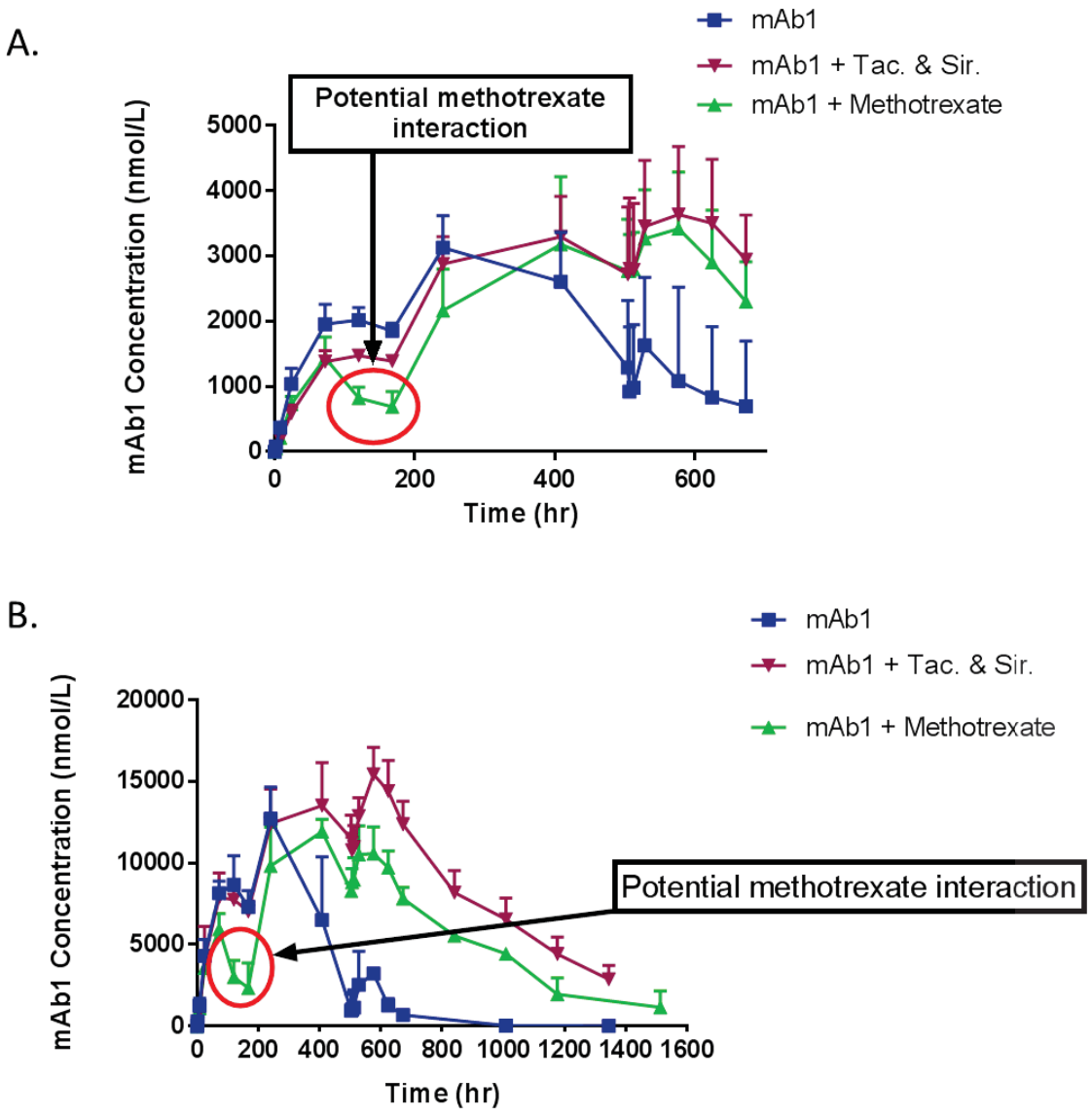

Figure 4-9. Methotrexate's Effect on Concentration Time Profiles
Potential methotrexate interaction indicated by the circle.
A. 50 mg/kg mAb1 dosing group
B. 300 mg/kg mAb1 dosing group

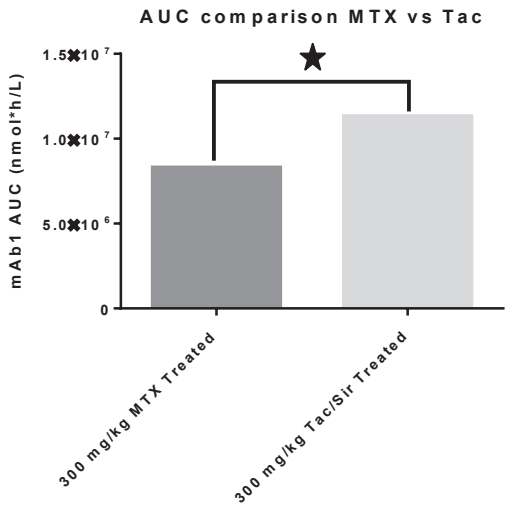

Figure 4-10. Methotrexate's Effect on AUC
Figure shows the statistically significant change in AUC between the tacrolimus/sirolimus treated group and the methotrexate (MTX) treated group. A decrease in AUC is indicative of an increase in clearance. This increase in clearance may potentially be due to methotrexates effect on FcRn recycling in these animals.

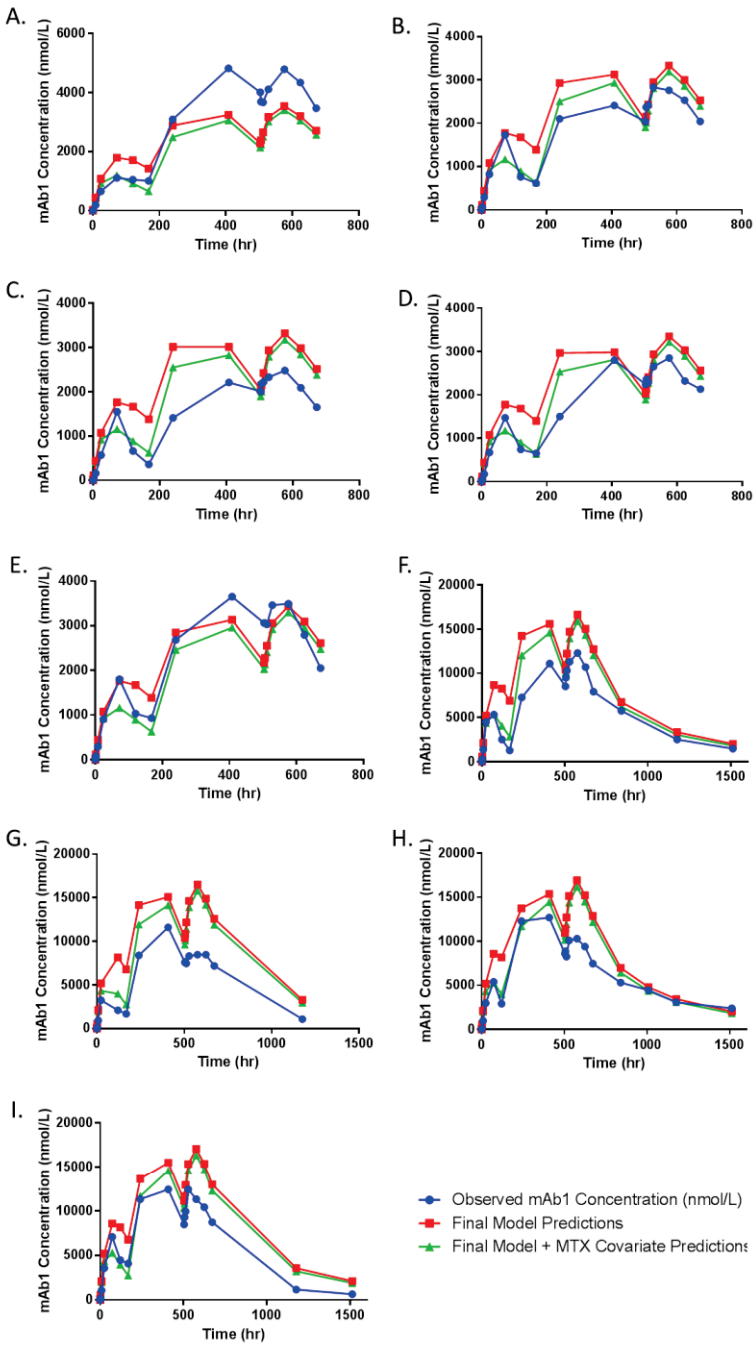

Figure 4-11. Methotrexate's Effect Modeled
Figures displayed below are individual concentration-time profiles for the 50 mg/kg dose and the 300 mg/kg dose groups that received methotrexate. Model fit from final model shown in red, model fit after methotrexate covariate added shown in green and observed data in blue.

The simulations performed with our final model demonstrated the effect ADA has on the serum concentrations of mAb1 over time (**Figure 4-12**). By simulating different percentages of immunogenicity, we can see the effect ADA has on the average concentration-time profile for a study, as well as the overall systemic exposure to the biotherapeutic. In multiple dose toxicity studies, a goal AUC/exposure is required to evaluate the potential toxicity of a medication over time. In the simulation shown in **Figure 4-12**, the goal of the hypothetical multiple dose study was to evaluate any toxicity which could be seen at a high exposure to the mAb, deemed to be an exposure of 5 mmol*h/L over four weeks. In this hypothetical study, 100 animals were necessary to identify any toxicity that might exist. As seen in **Figure 4-12**, a dose of 300 mg/kg will result in an exposure of 9 mmol*h/L in 100% of the animals. On the other hand, if immunogenicity is seen in the study, the number of animals required to reach the goal exposure will need to increase. In the simulations depicted in **Figure 4-12**, a concentration-time profile for animals that did not form ADA or had a 100% incidence of ADA, dosed with 300 mg/kg of mAb1, are shown. Due to the variability in the animals' immune responses, which were captured by our model and are now reflected in the simulation, some of the animals will still reach the goal exposure. This is important to note, as even though 100% of the animals had an immune reaction some will still reach the goal exposure. What our model and simulation can show is the number of animals which will reach the goal exposure in the presents of ADA, which can subsequently inform how many more animals will be necessary to have an appropriately powered toxicity study. In the case of the hypothetical toxicity study outlined above, 100 animals were necessary to identify any toxicity that might exist in the absence an immune reaction. In the presents of an immune reaction in every animal, our simulation showed that 42% of the animals will still reach the goal exposure. Therefore, in order to power the toxicity study appropriately in the presents of ADA, 240 animals will be needed at the 300 mg/kg dose level. As the simulation shows, by modeling and appreciating immunogenicity's effect on the pharmacokinetics of a mAb, we can gain a better understanding of how to design toxicity studies with the necessary power to identify any potential toxicity.

Overall, this study simultaneously modeled the serial concentration-time profiles of a human monoclonal antibody as well as the corresponding ADA signal-to-noise measurements to provide a quantitative and continuous description of ADA's effect on the pharmacokinetics and systemic exposure of mAb1. This study also highlighted the high variability in the time course and intensity of an ADA reaction and the highly variable effect on a biotherapeutic's concentration-time course. The methodology used in this study demonstrates a modeling strategy that can be applied to other therapeutic proteins to assess the effect of immunogenicity on their pharmacokinetics, as well as allowing for the simulation of the variability in exposure introduced by immunogenicity, aiding in the development of appropriately powered toxicology studies and a better evaluation of the PK of biotherapeutics in preclinical settings.

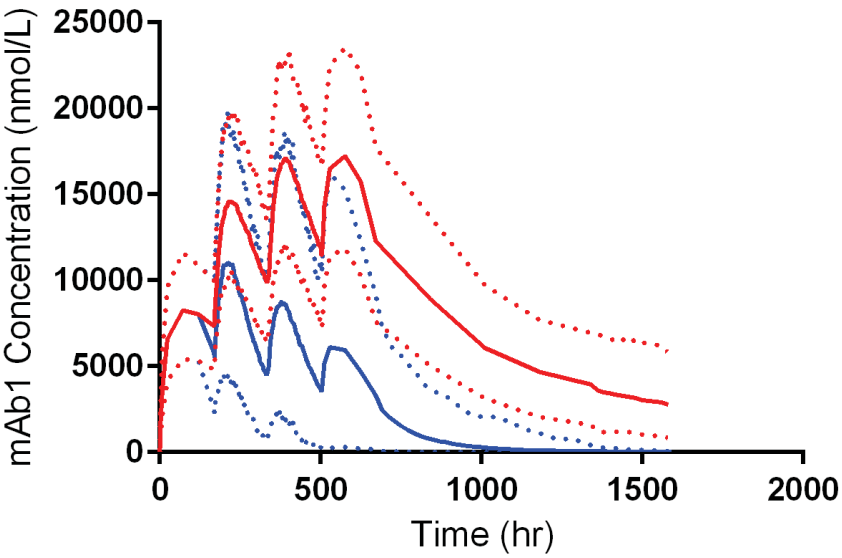

Figure 4-12. Simulation
Simulated data for a 1 month multiple dose study. Shown are concentration-time profiles for two simulations using the same dose (300 mg/kg). The red simulation represents the mean and 95% confidence interval from 2000 simulated individuals dosed with a mAb that is associated with 0% ADA formation across the population. The blue simulation represents the mean and 95% confidence interval from 2000 simulated individuals dosed with a mAb that is associated with a 100% ADA formation across the population.

CHAPTER 5. MRP2 ONTOGENY AND ITS EFFECTS ON PEDIATRIC CEFTRIAXONE EXPOSURE: A NON-LINEAR MIXED EFFECT MODELING APPROACH

Introduction

Understanding the interdependent absorption, distribution, metabolism and elimination processes governing the pharmacokinetics of medications is complex. This complexity is increased by the ontogeny changes in drug metabolizing enzymes and transporters during the maturational process in the pediatric population. The ontogeny of drug metabolizing enzymes and their contribution towards differences seen in drug biotransformation have been widely studied and reviewed in the pediatric population.[158-161] However, studies regarding the ontogeny of drug transporters are still limited. What is known about the development of drug transporters stem mainly from rodent models. Currently, there are very few published studies on the ontogeny of human hepatic drug transporters during the early postnatal into childhood ages.[162]

One such hepatic transporter is MRP2 (ABCC2). Human multi-drug resistance proteins (MRPs) belong to the C sub-family of the ATP-binding cassette (ABC) protein family.[163] This C sub-family consists of 13 members, nine of which are MRP1 through MRP9. MRP2 (ABCC2) is localized in the apical surface, predominantly in the canalicular membrane of hepatocytes, and the major physiological function of this protein is to transport conjugated metabolites into the bile canaliculus in the liver.[163] MRP2 has been associated with the hepatobiliary transport of bile acids and bilirubin, as well as several therapeutic agents used in the pediatric population. Some of the pediatric pharmacotherapies include antibiotics, angiotensin II receptor antagonists, chemotherapeutics, and HIV protease inhibitors, namely valsartan, olmesartan, irinotecan, saquinavir, ritonavir, indinavir, and ceftriaxone.[164, 165] In adults, the deficiency of MRP2 occurs in Dubin-Johnson syndrome.[166] Dubin-Johnson syndrome clinically results in an increase in conjugated bilirubin, which turns the liver black, but is typically benign in nature. The same cannot be said in the case of the transport of medications. If a medication relies upon MRP2 as a significant source of their clearance, a deficiency in MRP2 can lead to potential toxicities as the drug builds up in the patient.

An example of a MRP2 related medication toxicity is seen with ceftriaxone. Ceftriaxone is a third generation cephalosporin antibiotic often used in the pediatric population to treat lower respiratory infections, meningitis and acute otitis media. It has been shown in previous pharmacokinetic studies that approximately 33% of the drug is eliminated unchanged in the bile through MRP2.[167, 168] With a significant amount of the drug's elimination relying on MRP2 transport, problems may be associated with a lack of MRP2 presence and activity. Indeed, there have been several clinical reports of ceftriaxone related toxicities, such as biliary sludging or pseudolithiasis in the pediatric population.[169, 170] Pseudolithiasis is secondary to a high concentration of ceftriaxone in the liver which forms an insoluble salt with calcium in the bile. In cases where high doses of ceftriaxone are given, this risk of ceftriaxone induced cholestasis drastically

increases.[171, 172] The ontogeny of MRP2 is not well understood in humans, and the administration of ceftriaxone at the typically used doses in the pediatric population, particularly in newborns and infants whose drug clearance mechanisms are still developing, may lead to an accumulation of ceftriaxone in the hepatocyte and thus increase the risk of cholestasis.

The aim of this study was to evaluate the effect of MRP2 ontogeny on the pharmacokinetics of a model drug, ceftriaxone, using a model-based approach. To accomplish this task, nonlinear mixed effects modeling was applied to integrate previously generated data on variations in MRP2 expression from neonates to adults, pharmacokinetic data on ceftriaxone in normal and MRP2 deficient rodents, and human pharmacokinetic data in pediatric and adult patient. Once the model was developed and qualified, it was used to model and simulate the effect of various dose levels and levels of MRP2 expression on the concentration-time profile of ceftriaxone. The results of the model provide additional insight into safe and efficacious dosing in pediatric patients with various MRP2 expression levels.

Ceftriaxone was chosen as model drug for this study, not only because of the potential for toxicity in the pediatric population, but also due to its reliance on only two main mechanisms of clearance, which makes it an ideal medication to evaluate ontogeny effects. Ceftriaxone is primarily eliminated by MRP2 located on the canalicular membrane of hepatocytes and through renal excretion.[173] Ceftriaxone is not metabolized to any relevant extent, and this lack of metabolism helped to reduce the number of variables required to take into consideration when modeling MRP2's effect on ceftriaxone in adult and pediatric patients, allowing us to focus on the transporter maturation as the primary determinant.

Methods

The following analyses for the determination of the ontogeny of the relative MRP2 protein expression in pediatric liver specimens and the pharmacokinetic study of ceftriaxone in normal and TR- Wistar rats were performed by Dr. Lisa Tang at the University of Tennessee Health Science Center.[174] The data generated from these experiments form the basis for the model-based analysis of the impact of MRP2 ontogeny on the pharmacokinetics of ceftriaxone in pediatric patients.

Ontogeny of Relative MRP2 Protein Expression

Human pediatric liver tissues were acquired from two main sources – St. Jude Children's Research Hospital (SJCRH, Memphis, TN) and the Medical College of Wisconsin (MCW, Milwaukee, WI). The samples from SJCRH (n = 72) originated from the Liver Tissue Procurement and Distribution System (University of Pittsburgh, Pittsburgh, PA, funded by National Institutes of Health Contract N01-DK-9-2310) and from the Cooperative Human Tissue Network (University of Alabama, Birmingham, AL,

funded by the National Cancer Institute). Samples from MCW (n = 67) originated from the Brain and Tissue Bank for Developmental Disorders, University of Baltimore and University of Miami (National Institute of Child Health and Human Development contract N01-DK-8-3284). All samples were collected from donors less than twelve years of age. The SJCRH samples were obtained from living donors either through biopsy or within one hour of cross-clamping in the case of organ donors. Harvested tissue was immediately flash frozen in transplant solution. Demographic information on the donor population and health status is provided in **Table 5-1**. 72 patients were used for protein analysis from the SJCRH samples. MCW samples were obtained from deceased donors and all tissues were used for MRP2 protein analysis. The postmortem samples from donors with disease processes that could potentially involve liver damage were excluded from the study. Demographic information for the MCW samples is provided in **Table 5-2**. The tissue membrane isolation and Western blotting procedure used for relative MRP2 quantification are summarized in Lisa Tang's dissertation Age-Associated Hepatic Drug Transporter Expression and Its Implications for Pediatric Pharmacotherapy.[174]

Pharmacokinetics of Ceftriaxone in Normal and Mrp2 Deficient Rats

Eight-week old male Wistar (Hsd:WI, n = 7) and Mrp2 deficient TR- (HsdAmc:TR-Abcc2, n = 6) rats received a single intravenous injection of 100 mg/kg ceftriaxone sodium. Serial blood samples were obtained at 10 pre-defined time point for up to 6 hours post dose, and ceftriaxone plasma concentrations were determined high pressure liquid chromatography with UV detection. Excreted ceftriaxone amounts were also determined in urine and feces.

The details on the pharmacokinetic study of ceftriaxone in normal and Mrp2 deficient rats as well as the applied bioanalytical methodology for ceftriaxone quantification are described in Lisa Tang's dissertation Age-Associated Hepatic Drug Transporter Expression and Its Implications for Pediatric Pharmacotherapy.[174]

Collection of Ceftriaxone Human Pharmacokinetics in Children and Adults from Literature Sources

In order to identify ceftriaxone concentration-time profiles reported for adult and pediatric patients of different age reported in the literature that could be used as a reference point for our model-based analysis, an electronic literature search was performed. PUBMED (Medline, using MeSH headings and text words) was searched from the early 1980's (the decade ceftriaxone was being developed) to present; EMBASE (subject headings and text words) was searched from the early 1980's to present. All databases were searched between Sept. 1 and 27, 2016.

Studies were included that recruited patients commencing intravenous ceftriaxone treatment. We included both adult and pediatric studies. A study had to report all of the following measures: drug dose, concentration-time profiles, patient weights and ages.

Table 5-1. Donor Demographics for Human Pediatric Liver Samples Provided by St. Jude Children's Research Hospital (SJCRH)

Demographics	N	Age (yrs) Mean ±SD
Age Group		
A (<0.7 yrs)	9	0.53±0.18
B (0.7 - <3 yrs)	19	1.69±0.45
C (3 - <6 yrs)	12	3.83±0.83
D (6-12 yrs)	22	8.38±2.04
Gender		
Male	29	
Female	22	
Unknown	11	
Race		
Caucasian	35	
Black	7	
Others	6	
Unknown	14	
Disease Status		
Normal	36	
Cirrhosis	10	
Fibrosis	10	
Acute Hepatitis	4	
Necrosis	2	

Data in table used with permission from Lisa Tang and Bernd Meibohm. Tang, L., *Age-Associated Hepatic Drug Transporter Expression and Its Implications for Pediatric Pharmacotherapy*. Vol. Theses and Dissertations (ETD). Paper 260. http://dx.doi.org/10.21007/etd.cghs.2007.0312. . 2007, Memphis, TN: University of Tennessee Health Science Center.

Table 5-2. Donor Demographics for Human Pediatric Liver Samples Provided by Medical College of Wisconsin (MCW)

Demographics	N	Age (yrs) Mean ±SD	PMI (hrs) Mean ±SD
Age Group			
A (<0.7 yrs)	43	0.23±0.15	18.1±8.21
B (0.7 - <3 yrs)	3	2.24±0.32	15.67±2.31
C (3 - <6 yrs)	7	4.22±0.96	17.43±9.43
D (6-12 yrs)	16	9.20±1.55	21±7.28
Gender			
Male	45		
Female	23		
Unknown	0		
Race			
Caucasian	43		
Black	22		
Others	3		
Unknown	1		

Data in table used with permission from Lisa Tang and Bernd Meibohm. Tang, L., *Age-Associated Hepatic Drug Transporter Expression and Its Implications for Pediatric Pharmacotherapy*. Vol. Theses and Dissertations (ETD). Paper 260. http://dx.doi.org/10.21007/etd.cghs.2007.0312. . 2007, Memphis, TN: University of Tennessee Health Science Center.

Data included in several studies contained individual data sets, while other studies only reported average concentration-time profiles times for the individuals being analyzed. In order to prevent the inflation of between-subject variability, we multiplied the average concentration-time profiles based on the number of subjects whose data has been averaged. This approach attempts to balance the different information content between average and individual concentration-time profiles. Though, while fixing the issue of potential inflation of the between-subject variability, the opposite problem could occur, shrinkage of between subject variability. Therefore, in order to compensate and come to a reasonable estimate for between subject variability, we ran the model with the non-duplicated patient averages data set and averaged both of the model runs between subject variability estimates.

Due to the historic context when ceftriaxone was developed and introduced into clinical practice, it is worth noting that much of the ceftriaxone concentration data acquired from the literature was analyzed using the agar diffusion method, as HPLC was not a readily available technique in the early 1980's. Agar diffusion measures the concentration of an antibiotic much like the well-known Kirby-Bauer antibiotic test. The difference being, instead of an antibiotic wafer being applied to bacteria swabbed across a culture plate, plasma from the patient is pipetted into a well within the agar plate uniformly filled with a bacterium susceptible enough to permit a clear-cut zone of inhibition with the lowest serum concentration of the antibiotic.[175] Once the patient's serum is applied to the well, the antibiotic within the sample will diffuse from the well into the agar. This diffusion of the antibiotic into the bacteria filled agar will create a circular zone of killing, which can be measured and compared to the known calibration standards. There are limitations of using the agar diffusion method compared to HPLC to analyze antibiotic concentrations. These limitations are that agar diffusion is not be as accurate or precise as HPLC, as well as having a higher lower limit of quantification compared to HPLC. In addition, HPLC measures total drug concentrations, while the agar diffusion method as a bioassay is limited to unbound, pharmacologically active compound. The limitations of agar diffusion compared to HPLC are highlighted in a study done by Perea et al. investigating voriconazole levels in human plasma.[176] In this study, agar diffusion method was neither as precise as HPLC, with a precision of 12.1% compared to 3.5% for HPLC, nor as accurate as HPLC, with an accuracy of 1.28% compared to 0.81% for HPLC.[176]

Although the agar diffusion method has limitations in the precision, accuracy and LLOQ compared to HPLC when analyzing data, these differences did not have a discernable effect on the data collected using this technique. When comparing dose normalized data in the studies using different methods of measuring ceftriaxone concentration, the areas under the plasma concentration-time curves between the study groups did not differ significantly, as seen in **Figure 5-1**. Therefore, we felt comfortable using data obtained with both methods in our subsequent analysis.

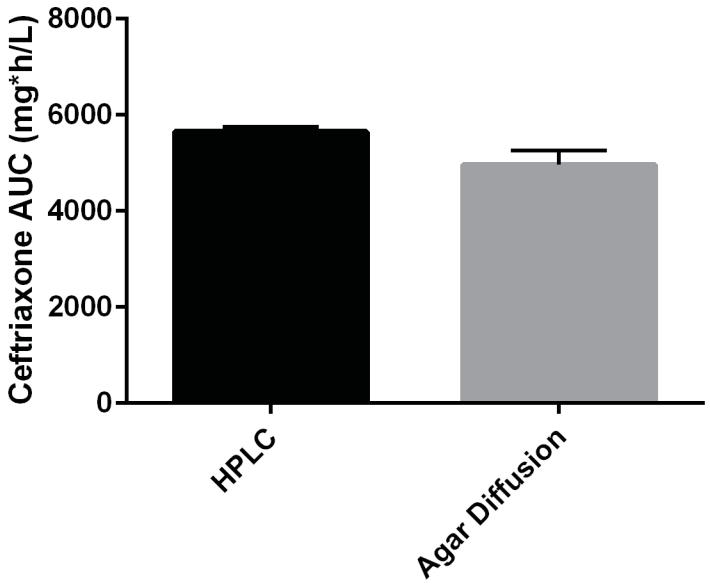

Figure 5-1. Comparison of HPLC Versus Agar Concentration Measurements
Average AUC comparison of ceftriaxone analyzed by HPLC and ceftriaxone analysis done by agar diffusion method. Average AUC were calculated after a single dose of ceftriaxone of a 24 hour period.

Model-Based Integrated Data Analysis to Assess the Impact of MRP2 Ontogeny on Pharmacokinetics of Ceftriaxone

Modeling Approach

Model development was guided by a sequential approach of fitting a model first to the preclinical pharmacokinetic data obtained in the wild-type and Mrp2 deficient rats, followed by the analysis of the pharmacokinetic data obtained for adults, and lastly the analysis of ontogeny data in pediatric populations (**Figure 5-2**). This approach allowed us to effectively elucidate the effect of Mrp2 on the concentration-time profile of ceftriaxone in rats before moving into human data. Once the percent contribution of Mrp2 to the clearance of ceftriaxone was determined in the rat model the same percent contribution was used to inform the human model going forward. Modeling the adult data helped to determine ceftriaxone clearance and volume parameters and their between-patient variability in humans. Subsequently, the ceftriaxone pharmacokinetic parameter estimates in adults, the contribution of Mrp2 to the total clearance of ceftriaxone from the rat study, and the ontogeny data on relative MRP2 expression in the pediatric population were integrated to predict ceftriaxone concentration-time profiles in the pediatric population. The prediction, rather than model fitting, for the ceftriaxone concentration-time profiles in children and comparison with literature-reported data can be viewed as an external validation of the approach to integrate animal pharmacokinetic data, human pharmacokinetic data, and human ontogeny data on MRP2 expression to predict the impact of maturational changes in MRP2 expression on the pharmacokinetics of ceftriaxone in pediatric patients.

Software

The plasma concentration–time profiles of ceftriaxone for each individual animal were simultaneously analyzed by nonlinear mixed effects modeling (NONMEM) (version VII, ICON Development Solutions). The first order conditional estimation (FOCE) method was used for estimation of model parameters.

Pharmacokinetic Structural Models

The pharmacokinetics of ceftriaxone were described using traditional compartmental pharmacokinetic modeling. One- and two-compartment models were tested. Estimated pharmacokinetic parameters were central volume of distribution, peripheral volume of distribution, as well as intercompartmental and elimination clearances. Structural models were compared using Akaike's information criterion (AIC), defined as follows: AIC = −2LL + 2p, where −2LL is the twice the negative log-likelihood of the model and p is the number of model parameters that were estimated.

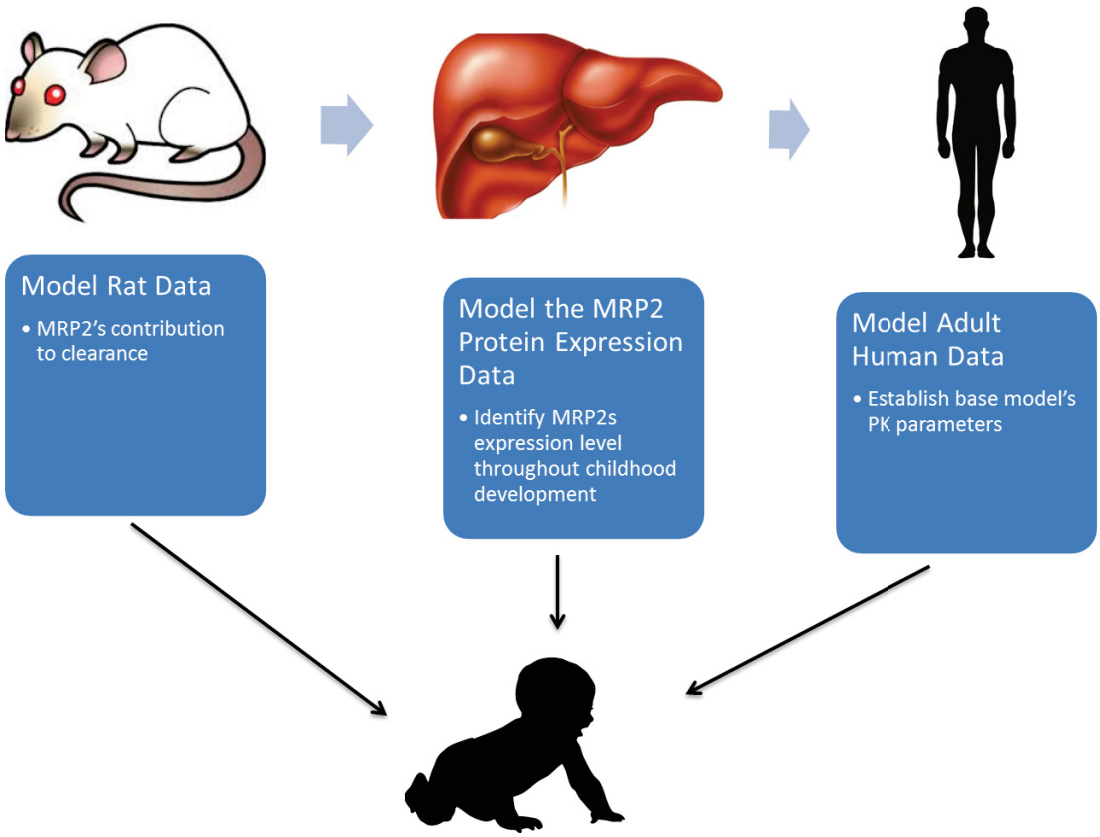

Figure 5-2. Modeling Strategy Used to Elucidate MRP2 Contribution to Pediatric Ceftriaxone Exposure

Interindividual and Error Models

The interindividual variability in pharmacokinetic parameters were described using an exponential model, as follows in **Equation 5-1**:

$$\theta_i = \theta_{TV} \times e^{\eta_i} \quad \textbf{Eq. 5-1}$$

where θ_i is the estimated individual parameter, θ_{TV} is the typical value of the parameter and η_i is the random effect for the i^{th} patient. The values of η_i were assumed to be normally distributed, with a mean of zero and variance ω^2. Correlations between random effects were tested. Additive, proportional and mixed additive– proportional residual error models were tested.

Covariate Analysis

The model building for both preclinical and human models was guided by standard diagnostic plots and plausibility of the parameter estimates. Interindividual, residual and covariate models were compared using −2LL and AIC. The model with the lowest significant −2LL value, assessed by a likelihood ratio $\chi 2$ test, and the lowest AIC, was selected. The individual influence of each covariate on each realistic pharmacokinetic parameter was tested using the likelihood ratio test with $\alpha = 0.05$ (change in OFV≥3.84). The number of selected covariates was low, so no stepwise forward/backward covariate selection was needed. The covariates were kept in the final model if their influence was significant for $\alpha = 0.01$ (change in OFV≥10.83) with an improvement in between subject variability of greater than 10%.

Results

The model-based analysis of the impact of MRP2 ontogeny on the pharmacokinetics of ceftriaxone in pediatric patients used datasets from multiple sources. The MRP2 ontogeny data in humans, as well as the plasma concentration-time profiles of ceftriaxone in wild-type and Mrp2-deficient rats the rat data were previously generated by Dr. Lisa Tang in the laboratory of Dr. Bernd Meibohm at The University of Tennessee College of Pharmacy.[174] The ceftriaxone concentration-time profiles in pediatric and adult populations were obtained from literature sources.

The observed ceftriaxone concentration time-profiles for the pharmacokinetic study in rats, for the adult data collection and the pediatric data collection are shown along with the model predicted concentration-time profiles for each group in **Figure 5-3**. A total of 13 rats were included in the ceftriaxone pharmacokinetic study, six Mrp2 deficient TR- rats and seven wild-type Wistar rats. **Table 5-3** shows the measured systemic exposures (area under the plasma concentration-time curve [59]), and the percentage of the ceftriaxone dose excreted in urine and feces over 24 hours.

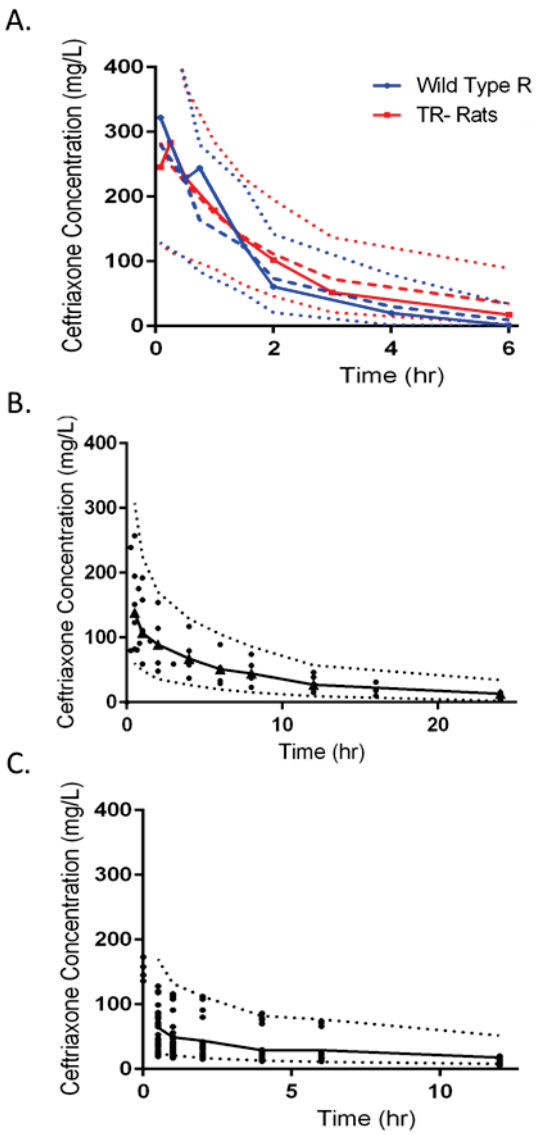

Figure 5-3. Ceftriaxone Concentration-Time Profiles
Ceftriaxone was administered intravenously. The dotted lines represent the 5 and 95% simulated visual predicted check concentrations over time. A). Ceftriaxone concentration-time profiles for both wild type and TR- rats. (Dose 50 mg/kg) The solid lines are the mean observed concentration-time profiles. The dashed lies represent the mean simulated concentration over time. B). Ceftriaxone concentration-time profiles for adults. (Dose 1000-2000 mg) The solid line represents the mean simulated concentration over time. The dark circles represent the observed concentrations. C). Ceftriaxone concentration-time profiles for pediatric population (age range: 2 days-5.8 years) (Dose 50 mg/kg). The solid line represents the mean simulated concentration over time. The dark circles represent the observed concentrations.

Table 5-3. Mean ± SD AUC Renal Elimination and Fecal Elimination in WT Versus TR- Rats

Parameter	Wild-Type Rats	TR- Rats
CL_T (L/hr/kg)	0.279±0.090	0.189±0.050
CL_r (L/hr/kg)	0.076±0.050	0.123±0.050
AUC_{inf} (mg*hr/L)	396±148	570±182
% Urine (24 hrs)	25.5±12.0	64.5±17.0
% Fecal (24 hrs)	18.5±16.0	0.0±0.0

CL_T: Total Clearance
CL_r: Renal Clearance

Data in table used with permission from Lisa Tang and Bernd Meibohm. Tang, L., *Age-Associated Hepatic Drug Transporter Expression and Its Implications for Pediatric Pharmacotherapy*. Vol. Theses and Dissertations (ETD). Paper 260. http://dx.doi.org/10.21007/etd.cghs.2007.0312. . 2007, Memphis, TN: University of Tennessee Health Science Center.

The pharmacokinetics of ceftriaxone was best described using a two-compartment model with intravenous infusion, with an inter-compartmental clearance Q and clearance from the central compartment CL (**Figure 5-4**).

The steps within the modeling strategy used to elucidate MRP2's contribution to pediatric ceftriaxone exposure are outlined in **Figure 5-2**.

Modeling the rat data from Dr. Lisa Tang's study was the first step, and allowed for the estimate of MRP2's contribution to the total clearance of ceftriaxone. By modeling both the wild-type and TR- rats' ceftriaxone concentration data I was able to identify MRP2's contribution to the total clearance, which would be applied to predict pediatric ceftriaxone concentrations.

When modeling the concentration-time profiles in rats, two covariates were found to be significant, as indicated by a drop in objective function value (OFV) of 3.84 or greater. The two covariates were weight and Mrp2 expression. Weight was a continuous covariate, while Mrp2 expression was a binary covariate (present for wild-type Wistar rats, and absent for TR- rats). Weight was used as a continuous covariate, centered on the mean weight of all the animals in the study, for both clearance and the volumes of distribution. The structure of the covariate is seen in **Equation 5-2**:

$$\theta_i = \theta_{TV} \times \left(\frac{WT}{WT_{mean}}\right)^{\theta_c} \quad \textbf{Eq. 5-2}$$

where WT is the weight of the individual animal, WT_{mean} is the mean weight of the animals in the study and θ_c is the allometric scaling parameter. Mrp2 expression was a significant covariate for clearance (CL). The TR- rats naturally do not have Mrp2 expression; hence will not be able to eliminate the ceftriaxone through the biliary duct. Therefore, Mrp2 expression was used as a categorical covariate for MRP2 mediated clearance (CL_{MRP2}) in these animals, and implemented as follows in **Equation 5-3**:

$$CL_{MRP2} = (\theta_{\%})^{MRP2} \times TV_{CL} \quad \textbf{Eq. 5-3}$$

where the parameter estimate for the typical value of clearance (TV_{CL}) is multiplied by the parameter estimate of the percent contribution of MRP2 $(\theta_{\%})^{MRP2}$, with MRP2 representing a switch that indicates whether MRP2 is expressed (Wild-type; *MRP2*=1) or not expressed (TR-; *MRP2*=0). The contribution of MRP2 as a covariate is incorporated into the overall clearance in **Equation 5-4** as follows:

$$CL = [R_{\%} \times TV_{CL}] + [(\theta_{\%})^{MRP2} \times TV_{CL}] + [\{1 - R_{\%CL} - (\theta_{\%})^{MRP2}\} \times TV_{CL}] \quad \textbf{Eq. 5-4}$$

In **Equation 5-4**, the parameter estimate for the typical value of clearance (TV_{CL}) is multiplied by three different clearance percentages, which are subsequently added together to make the overall clearance. The first clearance percentage is multiplied into

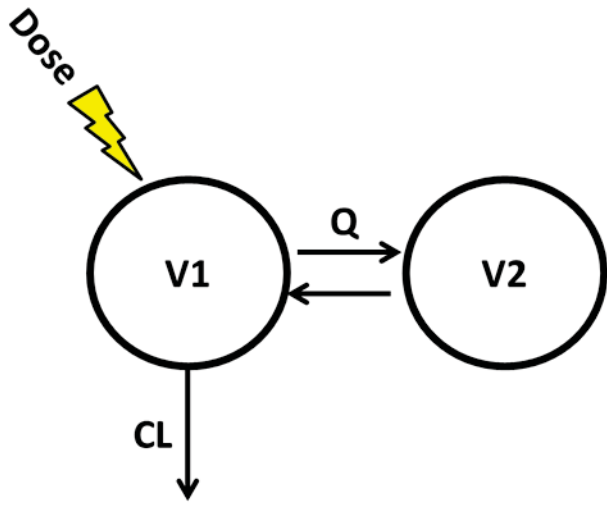

Figure 5-4. Ceftriaxone 2-Compartment Model

the typical value of clearance and represents the percent contribution of renal clearance $R_{\%}$, which was obtained from the urine data collected in the wild-type rats and fixed to 25.5% (**Table 5-3**). The second clearance percentage multiplied into the typical clearance is the percent contribution of MRP2 $(\theta_{\%})^{MRP2}$, which was discussed in the previous paragraph. The last clearance percentage term multiplied into the typical value of clearance is the 'unaccounted' clearance not captured by renal or biliary excretion. In the pharmacokinetic study in rats, both urinary and fecal output were collected and analyzed, but both sources did not account for 100% of the drug elimination, therefore we incorporated a third term as contributor to the typical clearance, allowing for an accurate estimate of MRP2's contribution to ceftriaxone elimination of 59% (**Table 5-4**).

Once the contribution of MRP2 to the total clearance was identified through modeling the rat data, the next step of the methodology was to assess the ontogeny of MRP2 expression in order to identify the level of MRP2 expression through childhood development (**Figure 5-2**). To do this, liver specimens from a total of 72 patients were included in the analysis. The resulting MRP2 expression profile that has previously been reported is shown in **Figure 5-5**.[174] All samples were collected from donors less than twelve years of age. The MRP2 data from this study was then fit to a maturation function (sigmoid hyperbolic model), which has been shown previously to be a versatile and widely applicable method to fit maturational processes in pediatric populations.[177] Hence, we applied this model to fit the MRP2 data to identify the level of MRP2 expression throughout physiologic development. **Equation 5-5** describes the maturational process is as follows:

$$\text{MAT} = \frac{AGE^{HILL}}{(AGE^{HILL}) + (TM_{50}^{HILL})} \qquad \textbf{Eq.5-5}$$

where AGE is the age of the patient, HILL is the hill coefficient which best described the slope of the maturation profile and TM_{50} is the maturation half-time. The result of the fit indicated that the best fit had a hill coefficient of 3.51 and a TM_{50}^{HILL} of 0.586 years old (Model fit seen in **Figure 5-5**). This function will be used moving forward to predict pediatric ceftriaxone concentration.

The last step of the modeling was to use the adult human data to model the ceftriaxone pharmacokinetics, the output of which was fixed to predict pediatric ceftriaxone concentration. For the population pharmacokinetic analysis of ceftriaxone in humans, data collected from literature included 8 adult and 53 pediatric patients. The adult data came from studies performed by Zhou et al., Meyers et al., Gobeaux et al. and from clinical trial data obtained from Hospira New Zealand and Roche.[167, 178-181] The pediatric data was obtained from studies conducted by Toyonaga et al., McCracken et al. and Schaad et al.[182-184] The ages ranged from 1 day to 70 months for the pediatric data included, equivalent to 0.00274 to 5.83 years (**Table 5-5**).

The pharmacokinetics of ceftriaxone in adults was modeled using a two-compartment structural model (**Figure 5-4**), which estimated the parameters clearance

Table 5-4. Population Pharmacokinetic Model Parameters for the Disposition of Ceftriaxone in Wild-Type and MRP2 Deficient Rats

Parameter	Estimate	RSE (%)	BSV (%)
CL (L/hr)	0.069	9.00	28.9
V1 (L)	0.105	148	31.3
V2 (L)	0.045	120	--
Q (L/hr)	0.020	12.0	--
MRP-2 CL (%)	59.0	16.0	--

Allometric scaling coefficients
θ_c=0.75 (CL)
θ_c=1.00 (V1 and V2)

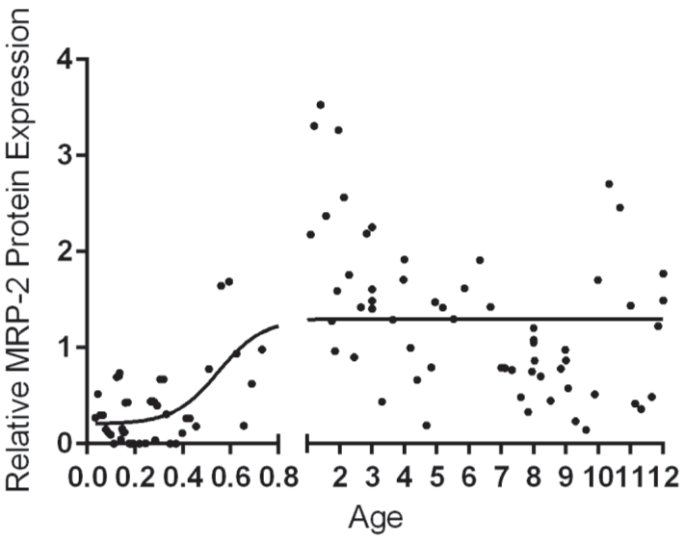

Figure 5-5. Hyperbolic Sigmoidal Equation Fitted to the Relative MRP2 Protein Expression in Human Pediatric Liver Samples

Table 5-5. Pediatric Patient Age Distribution

Age of Patients (yrs)	Number of Patients
0.005-0.500	43
0.510-6.00	10

(CL), intercompartmental clearance (Q), central volume (V1) and peripheral volume (V2) (**Table 5-6**), which would be fixed to predict pediatric ceftriaxone concentration using the same 2-compartment model.

Once the pharmacokinetic parameters were obtained from the rat model (MRP2 clearance contribution), adults model (PK parameters) and maturation function (pediatric ontogeny function fit), each was used to predict pediatric ceftriaxone exposure. Each of the parameters in the 2-compartment model were fixed to the adult parameter estimates, shown in **Table 5-6**. The modeled maturation function (**Figure 5-5**) was incorporated into the two compartment structural model as a covariate for clearance (CL), as seen in **Equation 5-6**. The covariate structure incorporates **Equation 5-5**, which is the maturation function, and multiplies it into the percent contribution of MRP2 ($\theta_{\%}^{MRP2}$) identified in the rat modeling step (59%):

$$CL = \left(\frac{AGE^{HILL}}{(AGE^{HILL})+(TM_{50}^{HILL})} \times \theta_{\%}^{MRP2} \times TV_{CL}\right) + ([1 - \theta_{\%}^{MRP2}] \times TV_{CL}) \qquad \textbf{Eq. 5-6}$$

In this case, the switch that was used in Eq.4 for ceftriaxone pharmacokinetics in rats to turn on and off contribution of MRP2 to clearance was not used here, as the sigmoid hyperbolic model represents the relative expression of MRP2. Of note, MRP2's contribution ($\theta_{\%}^{MRP2}$) was assumed to be the same as in rats. The MRP2 in humans is an orthologue to the one in rats, but despite that, the contribution should remain the same. The second half of the covariate equation ($1 - \theta_{\%}^{MRP2}$) represents the remaining percentage of clearance not mediated by MRP2, which includes the renal excretion as well as other elimination pathways as represented in the model for rats as 'unaccounted' clearance.

After we predicted the pediatric ceftriaxone concentration-time profiles, several other covariates were also tested in our model to help explain additional BSV. One of the covariates was weight. Weight was used as a continuous covariate for clearance, and it was centered on the mean weight of a typical adult (70 kg). The structure of the covariate model for weight was identical to **Equation 5-2**, where WT is the weight of the individual patient, WT_{mean} is the mean weight of a typical adult and θ_c is the allometric scaling parameter. Another covariate identified was age's correlation to the volumes of distribution in the pediatric population. Age was used as a continuous covariate centered on the mean age in adults (36.5 years) as seen in **Equation 5-7**:

$$V = TV_V * \left(\frac{AGE}{AGE_{Avg}}\right)^{\theta_{AGE}} \qquad \textbf{Eq. 5-7}$$

where AGE represents the age of the patient, AGE_{Avg} represents the average adult age and θ_{AGE} represents the parameter estimate of the power change in volume.
The plots of predicted vs. observed measurements, as well as VPC show that the prediction described the data satisfactorily (**Figure 5-6** and **Figure 5-7**). The pharmacokinetic parameters estimated are summarized in **Table 5-7**.

Table 5-6. Population Pharmacokinetic Model Parameters for Ceftriaxone in Humans

Parameter	Estimate	RSE (%)	BSV (%)
CL (L/hr)	1.05	8.00	16.9
V1 (L)	5.33	6.00	16.9
V2 (L)	3.98	4.00	--
Q (L/hr)	2.47	9.00	--

Data obtained from multifocal published reports
Allometric scaling coefficients
θ_c=0.75 (CL)
θ_c=1.00 (V1 and V2)

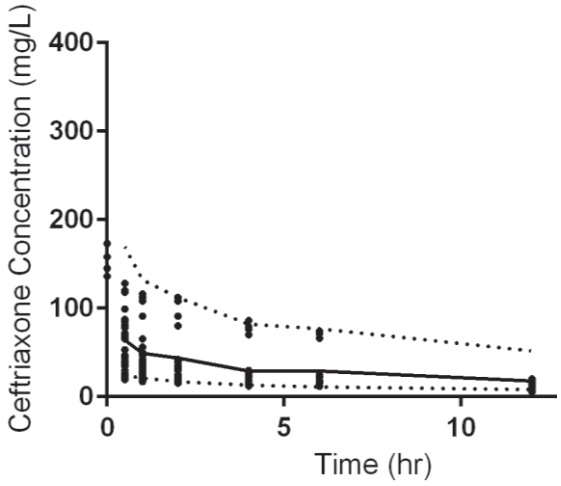

Figure 5-6. Pediatric Ceftriaxone Visual Predictive Check
Ceftriaxone concentration-time profiles for pediatric population (age range: 2 days-5.8 years) (Dose 50 mg/kg). The solid line represents the mean simulated concentration over time. The dark circles represent the observed concentrations. Dotted lines represent the 95% CI for 2000 simulations.

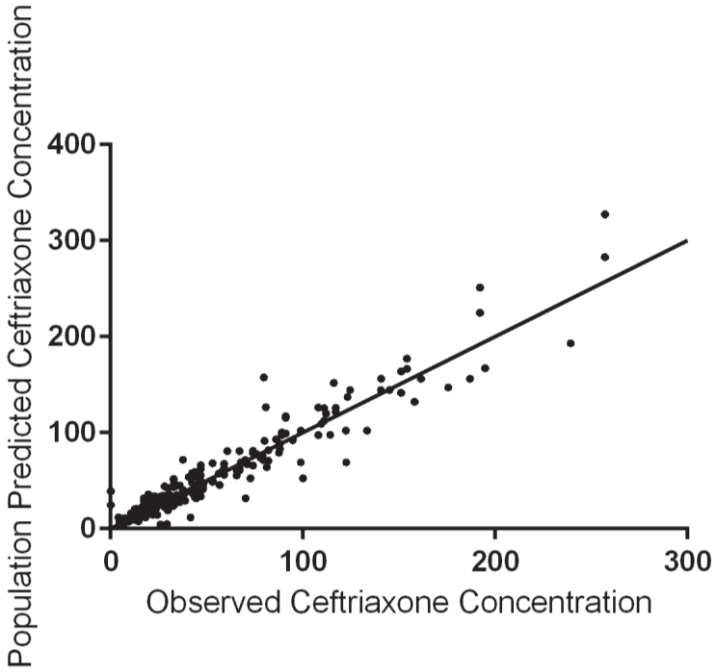

Figure 5-7. Pediatric Population Predicted Ceftriaxone Concentration Versus Observed Ceftriaxone Concentration for Final Model

Table 5-7. Population Pharmacokinetic Model Parameters for the Disposition of Ceftriaxone in Pediatric Patients with an Age Range of (2 Days - 6 Years)

Parameter	Estimate	RSE (%)	BSV (%)
CL (L/hr)	1.05	--	20.4
V1 (L)	5.33	--	33.8
V2 (L)	3.98	--	--
Q (L/hr)	2.47	--	--
Age Effect on Volume	-0.167	--	--
MRP2 CL (%)	31.4	19	--

Allometric scaling coefficients
θ_c=0.75 (CL)
θ_c=1.00 (V1 and V2)

Discussion

We used pharmacokinetic modeling to investigate the effect MRP2 ontogeny has on the concentration-time profile of ceftriaxone in pediatric patients. Structurally similar models have been used by prior studies modeling the pharmacokinetics of ceftriaxone.[185, 186] Our pharmacokinetic model, similar to the previous models, is based on a two-compartment model with intravenous infusion and clearance from the central compartment. In contrast to previous studies, however, our model integrates preclinical and *ex vivo* molecular biology data obtained in several previous studies, as well as data from literature sources, in order to model and simulate ceftriaxone concentration-time profiles across different pediatric age ranges.

In order to identify the contribution of MRP2 to the total clearance of ceftriaxone, Mrp2 deficient TR- and wild-type Wistar rats were given a single intravenous dose of ceftriaxone, and the resulting plasma concentration-time profiles were analyzed and modeled. The ceftriaxone concentration-time profile was best described using a two-compartment model with first-order elimination rate, which is a common structural model used for ceftriaxone in rats.[187] The value of clearance, estimated in the present study as 69 mL/hr, was divided into three components, with each route representing a relative percentage of elimination, as shown in **Equation 5-1**. The relative contribution of each clearance route was defined by the pharmacokinetic study performed in wild-type and Mrp2-deficient rats and the subsequent model-based analysis. The percent of renal elimination was defined through assessment of the fraction of the dose excreted unchanged in the urine and was found to be 25.5% of the total clearance in the wild-type Wistar rats. The subsequent model-based analysis estimated the percent contribution of Mrp2-mediated biliary excretion to the total clearance as 59%. This percentage contribution of Mrp2 estimated by the model agrees with the literature, which states the biliary clearance can contribute from 25-75% to the total clearance of ceftriaxone in rats.[188, 189] Our model also estimated that the third route of elimination had a relative contribution of 15.5%. Adding the third route of relative contribution to the clearance was required in this instance, as the TR- rats had an increase in renal clearance compared to the wild- type rats (0.123 L/hr/kg vs 0.076 L/hr/kg), as well as a total clearance that could not be explained by renal clearance alone, as seen in **Table 5-3**. In an ideal situation one would expect identical renal clearances, and in the case of TR- rats, a renal clearance that explained the total clearance. Instead, the TR- rats had an increase in renal clearance, and a total clearance that was greater than the renal elimination in those animals. This contradictory data may be explained by compensatory mechanisms, such as alternative renal transporters that more than likely exist in the TR- rats which have developed and or become contributors for extraction if substrate concentrations increase in the absence of Mrp2.[163, 190] Therefore, in order to account for additional clearance mechanisms, which may include intestinal transport and metabolism, a third contributor to total clearance was introduced into the covariate equation, as shown in **Equation 5-4**. In this equation, the percent contribution of both Mrp2 and renal excretion were subtracted from 100% and multiplied into the total clearance, in order to account for the clearance that was not captured by the urinary data or the difference in clearance caused by a lack of MRP2 expression.

Once the relative contribution of MRP2 to clearance was established in rats, the next step was to establish a population pharmacokinetic model for adult ceftriaxone concentration-time data. Data from several studies in healthy adult patients given different doses of ceftriaxone through the intravenous route were analyzed and modeled using a two-compartment model with first-order elimination rate. This base model was found to be the most appropriate and is a common structural model used for ceftriaxone in humans.[185, 186] Ceftriaxone's central volume of distribution (V1) and peripheral volume of distribution (V2) were estimated as 5.33 L and 3.98 L, respectively, values that have also been observed in other studies.[191] Intercompartmental clearance (Q) was estimated at 2.47 L/hr. The point estimate for clearance (CL) in the present study was 1.05 L/hr, a value similar to what other studies have found in humans.[179, 191, 192] Due to the good agreement between the results of our population pharmacokinetic model and the available literature reports, we were confident to apply and fix these parameters when modeling and simulating pediatric data.

The last step was to expand the two-compartment structural model to pediatric data on ceftriaxone disposition obtained from clinical studies in the literature. We first fixed the adult parameter estimates in our structural model and attempted to predict the pediatric data by simply scaling parameters based on weight-based allometric scaling, using the typically applied allometric exponents of 0.75 for clearance terms and 1 for volume terms.[193] As shown in **Figure 5-8**, the adult parameters, even when allometrically scaled, over predicted the ceftriaxone concentrations encountered in pediatric patients. When evaluating covariates, we found that age was correlated to the volumes of distribution in the pediatric population. In response to this observation, we expanded the structural model with a covariate for both central volume and peripheral volume, as seen in **Equation 5-7**. In **Equation 5-7**, AGE represents the age of the patient, AGE_{Avg} represents the average adult age and θ_{AGE} represents the parameter estimate of the power change in volume. Age also had an effect on the clearance of ceftriaxone, beyond what was captured by allometric scaling.

In the infants, the clearance of ceftriaxone was over-predicted when only allometric scaling was applied. This observation was not unexpected as the ontogeny of MRP2 was not accounted for by allometric scaling. In order to effectively describe the influence of the ontogeny of MRP2 expression on the clearance of ceftriaxone in this age group, we fit a sigmoid hyperbolic model to the age-dependent relative MRP2 expression data previously generated in Dr. Meibohm laboratory as indicated in **Equation 5-5** and **Figure 5-5**.[174]

We subsequently integrated both, the hyperbolic sigmoidal maturation curve fit and the percent contribution of MRP2 to build and inform our covariate model for clearance as shown in **Equations 5-5** and **5-6**. **Equation 5-5** represents the maturation of MRP2 expression in pediatric patients, and it is multiplied into the percent contribution of MRP2 to clearance ($\theta_{\%}^{MRP2}$) in **Equation 5-6**, which is added to (1- $\theta_{\%}^{MRP2}$) representing the remaining percent contribution to the total clearance by non-MRP2 mediated elimination processes. Within these equations, we fixed the relative contribution of

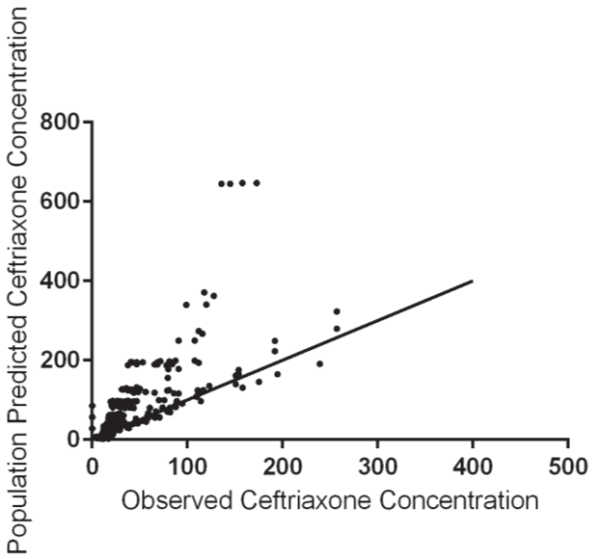

Figure 5-8. Population Predicted Ceftriaxone Concentration Versus Observed Ceftriaxone Concentration for Pediatric and Adult Populations
Observed Ceftriaxone Concentration versus the Model Predicted Ceftriaxone Concentration for Pediatric and Adult Populations. Structural model with only allometric scaling being applied to each parameter (V1, V2, CL and Q).

MRP2 to the estimate obtained from the rat study (59%), along with incorporating the fitted sigmoidal hyperbolic maturation equation. The total clearance remained fixed to the adult value. Integration of the contribution of MRP2 ontogeny to the clearance of ceftriaxone further improved the correlation between model predicted ceftriaxone concentrations and the observed values in the pediatric patient population, as seen in **Figure 5-9**. Unfortunately, the model fit was not adequate. The clearance was under predicted now in the infant population, as indicated by the poor fit of the VPC to the observed data and skewed distribution of individual predictions (ETA) from the population estimate for clearance, shown in **Figures 5-10** and **5-11**. Therefore, the rat data on MRP2 contribution may not be predictive of what happens in infants.

We decided that we could not rely on the rat data. Instead of using the rat data for MRP2 contribution, we estimated MRP2's relative contribution based on the adult and pediatric data, and the hyperbolic sigmoidal maturation model for the ontogeny of MRP2 expression. The same structural model and covariates were applied, and the relative contribution of MRP to the clearance of ceftriaxone was estimated to be 32%, instead of the 59% estimated from the rat data. A 32% contribution of biliary elimination is agreeable with the literature,[191] more accurately predicted the clearance in infants based on the adult data, and lead to the correct ceftriaxone concentration-time profile predictions in infants as indicated by the VPC and the normal distribution of individual predictions (ETA) from the population estimate for clearance.(**Figures 5-6** and **5-12**).

In summary, we used pharmacokinetic modelling to investigate the effect MRP2 ontogeny has on the concentration time profile of ceftriaxone using multiple studies and literature. Our model was able to capture ceftriaxone's pharmacokinetics, and MRP2's contribution to its clearance in adult and pediatric population. This study highlights MRP2's contribution to clearance of ceftriaxone, as well as its ontogeny. The methodology used in this study demonstrates a modeling strategy that can be applied to other transport proteins or drug metabolizing enzymes to assess the potential effect their ontogeny may have on the pharmacokinetics of a medication, aiding in the development of appropriate dosing protocols in the pediatric patient populations.

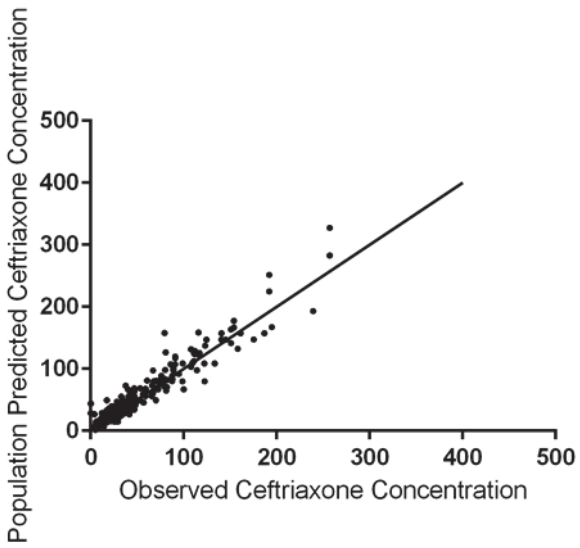

Figure 5-9. Observed Ceftriaxone Concentration Versus the Model Predicted Ceftriaxone Concentration for Pediatric and Adult Populations
Structural model plus the age covariate model for V1 and V2, as well as the maturation covariate model for CL built in. MRP2/Biliary contribution is fixed to 59% of total clearance (Rat predicted percent contribution).

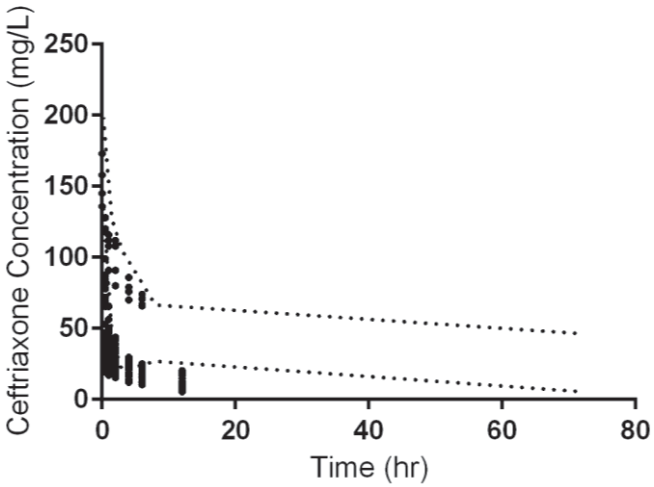

Figure 5-10. Pediatric Predictive Model Visual Predictive Check with 59% MRP2 Contribution to Total Clearance

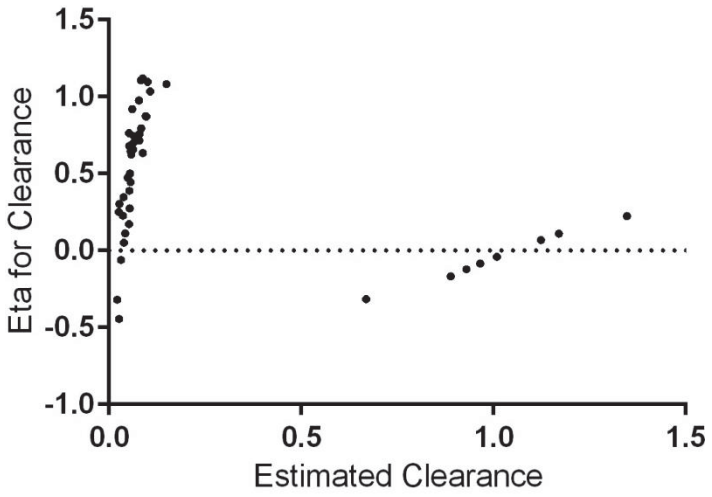

Figure 5-11. Estimated Clearance Versus Difference Between Population and Individual Predicted Clearance in Final Model with the Fixed MRP2 Contribution of 59% (Obtained from the Rat Study)
Model is consistently under-predicting clearance for a large population of individuals.

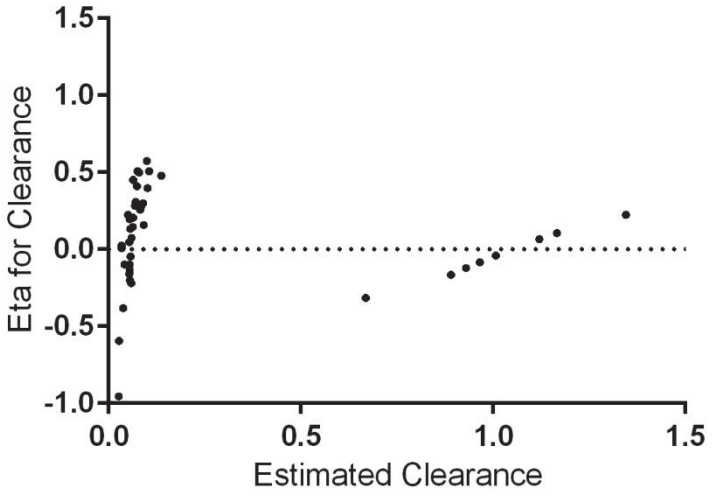

Figure 5-12. Estimated Clearance Versus Difference Between Population and Individual Predicted Clearance in Final Model with Estimated MRP2 Contribution
Clearance estimates are now representative of the true population distribution.

CHAPTER 6. SUMMARY

Advances in the technology and development of monoclonal antibodies (mAbs) have provided vast improvements in modern medicine. The preclinical development of a fully human or humanized mAb can be challenging, as dynamic changes in physiologic processes during pharmacokinetic and toxicological research of mAbs cause variability in drug disposition and elimination processes. The focus of this dissertation is on the variability in pharmacokinetics caused by ADA formation and ontogeny changes in a transport protein. These dynamic and variable changes affect decisions on toxicology assessments and first-in-human dosing in drug development, as well as pediatric dosing of therapeutic drugs. Therefore, new methods of preventing variability in these processes and accounting for the variability were explored in order to better understand the pharmacokinetics of the affected therapeutic drugs. In this dissertation I hypothesized that there are physiologically associated changes in the immune system and age-associated changes in transport protein expression which can lead to significant changes in pharmacokinetic parameters of therapeutic drugs, and that we can control for these dynamic changes through either preventing or limiting them through immunomodulatory therapies and or accounting for them through model-based pharmacometric approaches. This overall goal was accomplished in three examples:: 1.) The development of new immunomodulation treatment modalities, which will limit or prevent ADA formation in preclinical studies, 2.) The development of a pharmacometric PK-ADA modeling strategy that accounts for the effect of ADA formation on the systemic exposure of mAbs, and 3.) The development of a systems pharmacology modeling strategy that accounts for a transport protein's ontogeny and the variable and dynamic effect on a substrate that is a therapeutically used drug. In order to limit or prevent ADA formation towards a mAB in preclinical species, I tested two different immunomodulation strategies. In addition, I investigated the effect of an ADA forming immune response on the pharmacokinetics of a therapeutic mAb using a pharmacometric modeling approach. Lastly, I demonstrated a systems pharmacology modeling approach to assess the potential impact of maturational changes in transport proteins on the pharmacokinetics of the model drug ceftriaxone, a third generation cephalosporin antibiotic.

We confirmed our hypothesis that the use of immune suppressant regimens will mitigate an ADA response to a fully-humanized mAb in preclinical animal studies, and we successfully lowered antibody responses in animals to humanized therapeutics. This reduced the variability in the therapeutic mAb exposure in the systemic circulation. The combination of tacrolimus/sirolimus was able to reduce ADA incidence and magnitude at each studied dose level effectively. Tacrolimus/sirolimus treatment more than halved ADA incidence across all dose levels and the maximum ADA signal-to-noise ratio fell to less than 1% of that of the non-immunomodulated group. Methotrexate elicited at least a 50% drop in ADA incidence in the higher dose groups, although it was not as effective in the lower dose groups. This less efficacious immune suppression by methotrexate at lower dosages could be due to the insufficient frequency of immune suppressant administration, and/or the possibility that insufficient mAb was present in the circulation to induce methotrexate-mediated tolerance. To this end, utilizing additional cycles of

methotrexate along with higher doses of the therapeutic mAb may further mitigate anti-drug immune responses. Additional studies will be essential to streamlining immunomodulatory drug use in preclinical drug development. Studies evaluating different doses and dosing frequencies of the current therapies used in this dissertation, as well as a broader selection of immunosuppressant drugs and techniques could further aid in the selection of an optimal immunosuppressive regimen to help reduce mAb pharmacokinetic variability caused by immune reactivity.

The preclinical pharmacokinetic evaluation of a therapeutic mAb is complicated by immune responses from the animals being tested. A pharmacometric modeling approach was applied to investigate the dynamic and variable effect ADA formation has on the concentration-time profile of a mAb. Our PK/ADA model was based on the assumption that the drug disposition is affected by ADA-mediated clearance. The performed study took simultaneous and serial measurements of both the concentration of mAb, as well as the ADA signal-to-noise level. These measurements informed a PK/ADA model, which was built to model the data and simulate the ADA effect on the mAb. The mAb pharmacokinetic profile was best described using a two-compartment model with first-order elimination rate and a first-order absorption process. The ADA exposure and effect was described by a series of delay compartments which represented the time it took, after the first mAb dose, for ADA to form and eventually move into the central compartment. Once in the central compartment the ADA was able to bind to the mAb and eliminate it as a mAb-ADA complex. The magnitude and increase in clearance caused by the ADA responses are described in the model by the parameters K_{ada} and $k_{complex}$, respectively, while the timing of the ADA response is described by the parameter T_{lag}. K_{ada} represented the molar rate of ADA moving into the delay compartments, and eventually into the central compartment and was dependent on the measured ADA signal-to-noise ratios. The timing of the initiation of ADA response is depicted in the model by estimating T_{lag}, the ADA lag time. $K_{complex}$ was a second-order rate constant that captured the rate at which ADA bound to mAb and was thereby eliminated from the systemic circulation. This parameter was informed by the increase in mAb clearance beyond clearance of the mAb in ADA negative animals. It was this parameter that had the most between subject variability (BSV). The high amount of unexplained BSV on $k_{complex}$ was a weakness of the study design, which was captured by this modeling strategy. For future studies, I would recommend increasing the number of ADA sampling points, with a focus on the second, third and fourth week of dosing. This will help to delineate the change in affinity over time and allow for the estimation of affinity maturation in the ADA reaction. Also capturing additional potential covariates, like HLA subtype, in each of the subjects may help to account for the BSV on $k_{complex}$. Despite the weaknesses, by applying this modeling approach, I was able to capture the pharmacokinetics of the mAb, as well as ADA's effect on the mAb concentration-time profile. The model also allowed the simulation of ADA production in preclinical species receiving multiple doses of a mAb, and the subsequent effect that ADA formation will have on the mAb profile. The methodology used in this study demonstrates a modeling strategy that can be applied to other therapeutic mAbs. This methodology allows the assessment of the effect of immunogenicity on the pharmacokinetics of a therapeutic mAb, as well as allowing for the simulation of the variability in mAb systemic exposure

introduced by immunogenicity, which will aid in the development of appropriately powered toxicology studies and allow for a better evaluation of the pharmacokinetics of novel therapeutic mAbs in the preclinical setting.

Understanding the absorption, distribution, metabolism and elimination of therapeutic drugs is complex. This complexity is increased by the ontogeny-related changes in transport proteins during the maturational process in the pediatric population. A systems pharmacology modelling approach was applied to investigate the dynamic and variable effect the ontogeny of MRP2 has on the clearance of a substrate drug, ceftriaxone, in pediatric subjects. This modeling strategy can also be used to evaluate ontogeny changes in other biochemical transposition proteins, and their effect on the pharmacokinetics of other therapeutically used compounds, small molecule drugs as well a therapeutic proteins such as mAbs. The model developed during my dissertation research applies data obtained in several previous studies, as well as data from literature sources to model and simulate ceftriaxone concentration-time profiles across different age ranges. To identify the contribution of MRP2 to the total clearance of ceftriaxone, wild-type Wistar rats and Mrp2-deficient TR- rats received a single intravenous dose of ceftriaxone, and the resulting plasma concentration-time profiles were measured, analyzed and modeled. I then developed a human population pharmacokinetic model for ceftriaxone and estimated adult human pharmacokinetic parameters using data collected from studies previously published in the literature. Once I had established MRP2's contribution to clearance using the rat study and determined the adult pharmacokinetic model parameters, I fixed the adult parameter estimates in our structural model and allometrically scaled the parameter estimates based on body weight to predict ceftriaxone concentration-time profiles in pediatric patients of different age. When using the allometric approach alone, it leads to an overprediction of the concentration-time profiles of ceftriaxone in the pediatric population. With the allometric scaling approach the volumes of distribution were under predicted and clearance was over predicted. MRP2's ontogeny was not accounted for by allometric scaling, and in order to effectively describe the ontogeny effect of MRP2 in this age range I integrated the ontogeny data for MRP2 protein expression in human liver obtained in a previous study performed in our laboratory to fit a sigmoid hyperbolic model that described the maturation process of MRP2 expression. I used both the MRP2 ontogeny data, which informed the hyperbolic sigmoidal maturation curve fit, and the percent contribution of MRP2 to total ceftriaxone clearance, identified in the rat study, to build and inform our covariate model for the clearance of ceftriaxone. With this strategy, the model fit improved, but the clearance was under predicted in the infant population using the rat MRP2 relative contribution to clearance. It was identified that the rat data, which I used to ascertain MRP2 contribution, may not be predictive of what happens in infants. Therefore, we estimated MRP2's relative contribution to ceftriaxone clearance in our established modeling framework. Another limitation in this study came from the different methodologies applied to analyze ceftriaxone concentration in the studies. The model included data analyzed with agar method and some with HPLC. Although the effect of the methods on the concentration analysis was not significant, variability was still introduced into the parameter estimates because of the different methods used. Despite the increased variability, the model was able to adequately capture the pharmacokinetics of ceftriaxone, and the contribution of

MRP2 to its clearance in the adult and pediatric population. The systems pharmacology modeling methodology used in this study demonstrates a modeling strategy that can be applied to other therapeutic agents, including mAbs, to assess the effect of ontogeny of a biochemical disposition process and the potential effect it may have on the pharmacokinetics of the affected drug, thereby aiding in the development of appropriate dosing protocols in the pediatric population.

In summary, I have successfully determined an immunomodulation strategy that will help prevent ADA formation and the variable pharmacokinetics that are introduced in the presence of ADA. Furthermore, I also applied a pharmacometric modeling strategy to understand and account for the variability in pharmacokinetics caused by an immune reaction. Lastly, I demonstrated a systems pharmacology modeling method to account for ontogeny changes in a transport protein and the subsequent changes in the pharmacokinetics of the substrate. The results of these studies demonstrate that there are physiologic changes associated with the immune system and age-associated changes in biochemical disposition processes which can lead to significant changes in the pharmacokinetic behaviors of therapeutic agents, and that I was able to modulate and account for these dynamic changes through immunomodulatory therapies and through systems pharmacology modeling approaches. Moving forward these strategies can be applied to other therapeutic agents, including mAbs, to understand how dynamic changes that occur in study subjects will affect their pharmacokinetics.

LIST OF REFERENCES

1. Mould, D.R. and B. Meibohm, *Drug Development of Therapeutic Monoclonal Antibodies.* BioDrugs, 2016. **30**(4): p. 275-93.
2. Davis, J.D., et al., *Monoclonal Antibodies: From Structure to Therapeutic Application*, in *Pharmaceutical Biotechnology: Fundamentals and Applications*, D.J.A. Crommelin, R.D. Sindelar, and B. Meibohm, Editors. 2013, Springer: New York. p. 143-78.
3. Vidarsson, G., G. Dekkers, and T. Rispens, *IgG subclasses and allotypes: from structure to effector functions.* Front Immunol, 2014. **5**: p. 520.
4. Dirks, N.L. and B. Meibohm, *Population pharmacokinetics of therapeutic monoclonal antibodies.* Clin Pharmacokinet, 2010. **49**(10): p. 633-59.
5. Kadir, F., et al., *Productiona and Purification of Recombinant Proteins*, in *Pharmaceutical Biotechnology: Fundamentals and Applications*, D.J.A. Crommelin, R.D. Sindelar, and B. Meibohm, Editors. 2013, Springer: New York. p. 47-67.
6. Winter, G. and C. Milstein, *Man-made antibodies.* Nature, 1991. **349**(6307): p. 293-9.
7. Lerner, E.A., *How to make a hybridoma.* Yale J Biol Med, 1981. **54**(5): p. 387-402.
8. Imai, K. and A. Takaoka, *Comparing antibody and small-molecule therapies for cancer.* Nat Rev Cancer, 2006. **6**(9): p. 714-27.
9. Baxter, L.T., et al., *Physiologically based pharmacokinetic model for specific and nonspecific monoclonal antibodies and fragments in normal tissues and human tumor xenografts in nude mice.* Cancer Res, 1994. **54**(6): p. 1517-28.
10. Flessner, M.F., J. Lofthouse, and R. Zakaria el, *In vivo diffusion of immunoglobulin G in muscle: effects of binding, solute exclusion, and lymphatic removal.* Am J Physiol, 1997. **273**(6 Pt 2): p. H2783-93.
11. Covell, D.G., et al., *Pharmacokinetics of monoclonal immunoglobulin G1, F(ab')2, and Fab' in mice.* Cancer Res, 1986. **46**(8): p. 3969-78.
12. Cooper, P.R., et al., *Efflux of monoclonal antibodies from rat brain by neonatal Fc receptor, FcRn.* Brain Res, 2013. **1534**: p. 13-21.
13. Dickinson, B.L., et al., *Bidirectional FcRn-dependent IgG transport in a polarized human intestinal epithelial cell line.* J Clin Invest, 1999. **104**(7): p. 903-11.
14. McCarthy, K.M., Y. Yoong, and N.E. Simister, *Bidirectional transcytosis of IgG by the rat neonatal Fc receptor expressed in a rat kidney cell line: a system to study protein transport across epithelia.* J Cell Sci, 2000. **113 (Pt 7)**: p. 1277-85.
15. Antohe, F., et al., *Expression of functionally active FcRn and the differentiated bidirectional transport of IgG in human placental endothelial cells.* Hum Immunol, 2001. **62**(2): p. 93-105.
16. Claypool, S.M., et al., *Bidirectional transepithelial IgG transport by a strongly polarized basolateral membrane Fcgamma-receptor.* Mol Biol Cell, 2004. **15**(4): p. 1746-59.

17. Molthoff, C.F., et al., *Comparison of the pharmacokinetics, biodistribution and dosimetry of monoclonal antibodies OC125, OV-TL 3, and 139H2 as IgG and F(ab')2 fragments in experimental ovarian cancer.* Br J Cancer, 1992. **65**(5): p. 677-83.
18. Kingwell, K., *Drug delivery: New targets for drug delivery across the BBB.* Nat Rev Drug Discov, 2016. **15**(2): p. 84-5.
19. Kairemo, K.J., et al., *In vivo detection of intervertebral disk injury using a radiolabeled monoclonal antibody against keratan sulfate.* J Nucl Med, 2001. **42**(3): p. 476-82.
20. Danilov, S.M., et al., *Lung uptake of antibodies to endothelial antigens: key determinants of vascular immunotargeting.* Am J Physiol Lung Cell Mol Physiol, 2001. **280**(6): p. L1335-47.
21. Glassman, P.M., L. Abuqayyas, and J.P. Balthasar, *Assessments of antibody biodistribution.* J Clin Pharmacol, 2015. **55 Suppl 3**: p. S29-38.
22. Meibohm, B., *Pharmacokinetics and Pharmacodynamics of Peptide and Protein Therapeutics*, in *Pharmaceutical Biotechnology: Fundamentals and Applications*, D.J.A. Crommelin, R.D. Sindelar, and B. Meibohm, Editors. 2013, Springer: New York. p. 143-78.
23. Wiig, H., et al., *Effect of charge on interstitial distribution of albumin in rat dermis in vitro.* J Physiol, 2003. **550**(Pt 2): p. 505-14.
24. Bell, D.R., P.D. Watson, and E.M. Renkin, *Exclusion of plasma proteins in interstitium of tissues from the dog hind paw.* Am J Physiol, 1980. **239**(4): p. H532-H538.
25. Mullins, R.J. and D.R. Bell, *Changes in interstitial volume and masses of albumin and IgG in rabbit skin and skeletal muscle after saline volume loading.* Circ Res, 1982. **51**(3): p. 305-13.
26. Cao, Y., J.P. Balthasar, and W.J. Jusko, *Second-generation minimal physiologically-based pharmacokinetic model for monoclonal antibodies.* J Pharmacokinet Pharmacodyn, 2013. **40**(5): p. 597-607.
27. Berdeja, J., et al., *Pharmacokinetics and Safety of Elotuzumab Combined With Lenalidomide and Dexamethasone in Patients With Multiple Myeloma and Various Levels of Renal Impairment: Results of a Phase Ib Study.* Clin Lymphoma Myeloma Leuk, 2016. **16**(3): p. 129-38.
28. Waldmann, T.A., W. Strober, and R.P. Mogielnicki, *The renal handling of low molecular weight proteins. II. Disorders of serum protein catabolism in patients with tubular proteinuria, the nephrotic syndrome, or uremia.* J Clin Invest, 1972. **51**(8): p. 2162-74.
29. Waldmann, T.A. and W. Strober, *Metabolism of immunoglobulins.* Prog Allergy, 1969. **13**: p. 1-110.
30. Mager, D.E. and W.J. Jusko, *General pharmacokinetic model for drugs exhibiting target-mediated drug disposition.* J Pharmacokinet Pharmacodyn, 2001. **28**(6): p. 507-32.
31. Gessner, J.E., et al., *The IgG Fc receptor family.* Ann Hematol, 1998. **76**(6): p. 231-48.
32. Nimmerjahn, F. and J.V. Ravetch, *Fcgamma receptors as regulators of immune responses.* Nat Rev Immunol, 2008. **8**(1): p. 34-47.

33. Abuqayyas, L. and J.P. Balthasar, *Application of knockout mouse models to investigate the influence of FcgammaR on the tissue distribution and elimination of 8C2, a murine IgG1 monoclonal antibody.* Int J Pharm, 2012. **439**(1-2): p. 8-16.
34. Gibiansky, L., et al., *Model-based pharmacokinetic analysis of elotuzumab in patients with relapsed/refractory multiple myeloma.* J Pharmacokinet Pharmacodyn, 2016. **43**(3): p. 243-57.
35. Wright, A., et al., *In vivo trafficking and catabolism of IgG1 antibodies with Fc associated carbohydrates of differing structure.* Glycobiology, 2000. **10**(12): p. 1347-55.
36. Brambell, F.W., W.A. Hemmings, and I.G. Morris, *A Theoretical Model of Gamma-Globulin Catabolism.* Nature, 1964. **203**: p. 1352-4.
37. Roopenian, D.C. and S. Akilesh, *FcRn: the neonatal Fc receptor comes of age.* Nat Rev Immunol, 2007. **7**(9): p. 715-725.
38. Kim, J., et al., *Kinetics of FcRn-mediated recycling of IgG and albumin in human: pathophysiology and therapeutic implications using a simplified mechanism-based model.* Clin Immunol, 2007. **122**(2): p. 146-55.
39. Kontermann, R.E., *Strategies for extended serum half-life of protein therapeutics.* Curr Opin Biotechnol, 2011. **22**(6): p. 868-76.
40. Junghans, R.P. and C.L. Anderson, *The protection receptor for IgG catabolism is the beta2-microglobulin-containing neonatal intestinal transport receptor.* Proc Natl Acad Sci U S A, 1996. **93**(11): p. 5512-6.
41. Deng, R., et al., *Pharmacokinetics of humanized monoclonal anti-tumor necrosis factor-{alpha} antibody and its neonatal Fc receptor variants in mice and cynomolgus monkeys.* Drug Metab Dispos, 2010. **38**(4): p. 600-5.
42. Jin, F. and J.P. Balthasar, *Mechanisms of intravenous immunoglobulin action in immune thrombocytopenic purpura.* Hum Immunol, 2005. **66**(4): p. 403-10.
43. Morell, A., W.D. Terry, and T.A. Waldmann, *Metabolic properties of IgG subclasses in man.* J Clin Invest, 1970. **49**(4): p. 673-80.
44. Zhao, L., et al., *The antibody drug absorption following subcutaneous or intramuscular administration and its mathematical description by coupling physiologically based absorption process with the conventional compartment pharmacokinetic model.* J Clin Pharmacol, 2013. **53**(3): p. 314-25.
45. Supersaxo, A., et al., *Recombinant human interferon alpha-2a: delivery to lymphoid tissue by selected modes of application.* Pharm Res, 1988. **5**(8): p. 472-6.
46. McDonald, T.A., et al., *Subcutaneous administration of biotherapeutics: current experience in animal models.* Curr Opin Mol Ther, 2010. **12**(4): p. 461-70.
47. Kota, J., et al., *Lymphatic absorption of subcutaneously administered proteins: influence of different injection sites on the absorption of darbepoetin alfa using a sheep model.* Drug Metab Dispos, 2007. **35**(12): p. 2211-7.
48. Kagan, L., et al., *Subcutaneous absorption of monoclonal antibodies: role of dose, site of injection, and injection volume on rituximab pharmacokinetics in rats.* Pharm Res, 2012. **29**(2): p. 490-9.

49. Reddy, S.T., et al., *A sensitive in vivo model for quantifying interstitial convective transport of injected macromolecules and nanoparticles.* J Appl Physiol (1985), 2006. **101**(4): p. 1162-9.
50. Richter, W.F., S.G. Bhansali, and M.E. Morris, *Mechanistic determinants of biotherapeutics absorption following SC administration.* AAPS J, 2012. **14**(3): p. 559-70.
51. Ober, R.J., et al., *Differences in promiscuity for antibody-FcRn interactions across species: implications for therapeutic antibodies.* Int Immunol, 2001. **13**(12): p. 1551-9.
52. Swartz, M.A., *The physiology of the lymphatic system.* Adv Drug Deliv Rev, 2001. **50**(1-2): p. 3-20.
53. Gibney, M.A., et al., *Skin and subcutaneous adipose layer thickness in adults with diabetes at sites used for insulin injections: implications for needle length recommendations.* Curr Med Res Opin, 2010. **26**(6): p. 1519-30.
54. Olszewski, W., et al., *Flow and composition of leg lymph in normal men during venous stasis, muscular activity and local hyperthermia.* Acta Physiol Scand, 1977. **99**(2): p. 149-55.
55. Keizer, R.J., et al., *Clinical pharmacokinetics of therapeutic monoclonal antibodies.* Clin Pharmacokinet, 2010. **49**(8): p. 493-507.
56. Gill, K.L., et al., *A Bottom-Up Whole-Body Physiologically Based Pharmacokinetic Model to Mechanistically Predict Tissue Distribution and the Rate of Subcutaneous Absorption of Therapeutic Proteins.* AAPS J, 2016. **18**(1): p. 156-70.
57. Boswell, C.A., et al., *Effects of charge on antibody tissue distribution and pharmacokinetics.* Bioconjug Chem, 2010. **21**(12): p. 2153-63.
58. Herve, F., N. Ghinea, and J.M. Scherrmann, *CNS delivery via adsorptive transcytosis.* AAPS J, 2008. **10**(3): p. 455-72.
59. Zheng, Y., et al., *Minipig as a potential translatable model for monoclonal antibody pharmacokinetics after intravenous and subcutaneous administration.* MAbs, 2012. **4**(2): p. 243-55.
60. Kobayashi, H., et al., *The pharmacokinetic characteristics of glycolated humanized anti-Tac Fabs are determined by their isoelectric points.* Cancer Res, 1999. **59**(2): p. 422-30.
61. Khawli, L.A., et al., *Charge variants in IgG1: Isolation, characterization, in vitro binding properties and pharmacokinetics in rats.* MAbs, 2010. **2**(6): p. 613-24.
62. Jiang, X.R., et al., *Advances in the assessment and control of the effector functions of therapeutic antibodies.* Nat Rev Drug Discov, 2011. **10**(2): p. 101-11.
63. Kaneko, Y., F. Nimmerjahn, and J.V. Ravetch, *Anti-inflammatory activity of immunoglobulin G resulting from Fc sialylation.* Science, 2006. **313**(5787): p. 670-3.
64. Junttila, T.T., et al., *Superior in vivo efficacy of afucosylated trastuzumab in the treatment of HER2-amplified breast cancer.* Cancer Res, 2010. **70**(11): p. 4481-9.
65. Yamane-Ohnuki, N. and M. Satoh, *Production of therapeutic antibodies with controlled fucosylation.* MAbs, 2009. **1**(3): p. 230-6.
66. Newkirk, M.M., et al., *Differential clearance of glycoforms of IgG in normal and autoimmune-prone mice.* Clin Exp Immunol, 1996. **106**(2): p. 259-64.

67. Jones, A.J., et al., *Selective clearance of glycoforms of a complex glycoprotein pharmaceutical caused by terminal N-acetylglucosamine is similar in humans and cynomolgus monkeys.* Glycobiology, 2007. **17**(5): p. 529-40.
68. Keck, R., et al., *Characterization of a complex glycoprotein whose variable metabolic clearance in humans is dependent on terminal N-acetylglucosamine content.* Biologicals, 2008. **36**(1): p. 49-60.
69. Yu, M., et al., *Production, characterization, and pharmacokinetic properties of antibodies with N-linked mannose-5 glycans.* MAbs, 2012. **4**(4): p. 475-87.
70. Deng, R., et al., *Monoclonal antibodies: what are the pharmacokinetic and pharmacodynamic considerations for drug development?* Expert Opin Drug Metab Toxicol, 2012. **8**(2): p. 141-60.
71. Sachs, U.J., et al., *A variable number of tandem repeats polymorphism influences the transcriptional activity of the neonatal Fc receptor alpha-chain promoter.* Immunology, 2006. **119**(1): p. 83-9.
72. Billiet, T., et al., *A Genetic Variation in the Neonatal Fc-Receptor Affects Anti-TNF Drug Concentrations in Inflammatory Bowel Disease.* Am J Gastroenterol, 2016. **111**(10): p. 1438-1445.
73. Gouilleux-Gruart, V., et al., *Efficiency of immunoglobulin G replacement therapy in common variable immunodeficiency: correlations with clinical phenotype and polymorphism of the neonatal Fc receptor.* Clin Exp Immunol, 2013. **171**(2): p. 186-94.
74. Musolino, A., et al., *Immunoglobulin G fragment C receptor polymorphisms and clinical efficacy of trastuzumab-based therapy in patients with HER-2/neu-positive metastatic breast cancer.* J Clin Oncol, 2008. **26**(11): p. 1789-96.
75. Trotta, A.M., et al., *Prospective Evaluation of Cetuximab-Mediated Antibody-Dependent Cell Cytotoxicity in Metastatic Colorectal Cancer Patients Predicts Treatment Efficacy.* Cancer Immunol Res, 2016. **4**(4): p. 366-74.
76. Zhang, W., et al., *Fcgamma receptor IIIA polymorphisms and efficacy of rituximab therapy on Chinese diffuse large B-cell lymphoma.* Chin Med J (Engl), 2010. **123**(2): p. 198-202.
77. Nishio, S., et al., *Pharmacokinetic study and Fcgamma receptor gene analysis in two patients with rheumatoid arthritis controlled by low-dose infliximab.* Mod Rheumatol, 2009. **19**(3): p. 329-33.
78. Roxburgh, C.S. and D.C. McMillan, *Cancer and systemic inflammation: treat the tumour and treat the host.* Br J Cancer, 2014. **110**(6): p. 1409-12.
79. Fearon, K.C., et al., *Influence of whole body protein turnover rate on resting energy expenditure in patients with cancer.* Cancer Res, 1988. **48**(9): p. 2590-5.
80. Cosson, V.F., et al., *Population pharmacokinetics and exposure-response analyses of trastuzumab in patients with advanced gastric or gastroesophageal junction cancer.* Cancer Chemother Pharmacol, 2014. **73**(4): p. 737-47.
81. Feagan, B.G., et al., *The challenge of indication extrapolation for infliximab biosimilars.* Biologicals, 2014. **42**(4): p. 177-183.
82. Jarnum, S., *Turnover of plasma proteins.* J Clin Pathol Suppl (Assoc Clin Pathol), 1975. **6**: p. 13-21.

83. Ordas, I., et al., *Anti-TNF monoclonal antibodies in inflammatory bowel disease: pharmacokinetics-based dosing paradigms.* Clin Pharmacol Ther, 2012. **91**(4): p. 635-46.
84. Wang, Y., et al., *Towards greater insights on pharmacokinetics and exposure-response relationships for therapeutic biologics in oncology drug development.* Clin Pharmacol Ther, 2017. **106**: p. in press.
85. Azzopardi, N., et al., *Cetuximab pharmacokinetics influences progression-free survival of metastatic colorectal cancer patients.* Clin Cancer Res, 2011. **17**(19): p. 6329-37.
86. Sethu, S., et al., *Immunogenicity to biologics: mechanisms, prediction and reduction.* Arch Immunol Ther Exp (Warsz), 2012. **60**(5): p. 331-44.
87. Weber, C.A., et al., *T cell epitope: friend or foe? Immunogenicity of biologics in context.* Adv Drug Deliv Rev, 2009. **61**(11): p. 965-76.
88. Schellekens, H., *Immunogenicity of therapeutic proteins: clinical implications and future prospects.* Clin Ther, 2002. **24**(11): p. 1720-40; discussion 1719.
89. Ryman, J., et al., *Immune Suppression During Preclinical Drug Development Mitigates Immunogenicity-Mediated Impact on Therapeutic Exposure.* AAPS J, 2017.
90. Ryff, J.C., *Clinical investigation of the immunogenicity of interferon-alpha 2a.* J Interferon Cytokine Res, 1997. **17 Suppl 1**: p. S29-33.
91. Neuberger, M.S., et al., *Memory in the B-cell compartment: antibody affinity maturation.* Philos Trans R Soc Lond B Biol Sci, 2000. **355**(1395): p. 357-60.
92. Chirmule, N., V. Jawa, and B. Meibohm, *Immunogenicity to therapeutic proteins: impact on PK/PD and efficacy.* AAPS J, 2012. **14**(2): p. 296-302.
93. Huang, Z.Y., et al., *Human platelet FcgammaRIIA and phagocytes in immune-complex clearance.* Mol Immunol, 2011. **48**(4): p. 691-6.
94. Dua, P., E. Hawkins, and P.H. van der Graaf, *A Tutorial on Target-Mediated Drug Disposition (TMDD) Models.* CPT Pharmacometrics Syst Pharmacol, 2015. **4**(6): p. 324-37.
95. Dong, J.Q., et al., *Quantitative prediction of human pharmacokinetics for monoclonal antibodies: retrospective analysis of monkey as a single species for first-in-human prediction.* Clin Pharmacokinet, 2011. **50**(2): p. 131-42.
96. Shah, D.K. and A.M. Betts, *Towards a platform PBPK model to characterize the plasma and tissue disposition of monoclonal antibodies in preclinical species and human.* J Pharmacokinet Pharmacodyn, 2012. **39**(1): p. 67-86.
97. Mould, D.R. and K.R. Sweeney, *The pharmacokinetics and pharmacodynamics of monoclonal antibodies--mechanistic modeling applied to drug development.* Curr Opin Drug Discov Devel, 2007. **10**(1): p. 84-96.
98. Mahmood, I., *Pharmacokinetic allometric scaling of antibodies: application to the first-in-human dose estimation.* J Pharm Sci, 2009. **98**(10): p. 3850-61.
99. De Buck, S.S., et al., *Prediction of human pharmacokinetics using physiologically based modeling: a retrospective analysis of 26 clinically tested drugs.* Drug Metab Dispos, 2007. **35**(10): p. 1766-80.
100. Urva, S.R., V.C. Yang, and J.P. Balthasar, *Physiologically based pharmacokinetic model for T84.66: a monoclonal anti-CEA antibody.* J Pharm Sci, 2010. **99**(3): p. 1582-600.

101. Garg, A. and J.P. Balthasar, *Physiologically-based pharmacokinetic (PBPK) model to predict IgG tissue kinetics in wild-type and FcRn-knockout mice.* J Pharmacokinet Pharmacodyn, 2007. **34**(5): p. 687-709.
102. Cao, Y. and W.J. Jusko, *Applications of minimal physiologically-based pharmacokinetic models.* J Pharmacokinet Pharmacodyn, 2012. **39**(6): p. 711-23.
103. Baxter, L.T. and R.K. Jain, *Transport of fluid and macromolecules in tumors. I. Role of interstitial pressure and convection.* Microvasc Res, 1989. **37**(1): p. 77-104.
104. Thway, T.M., et al., *Impact of anti-drug antibodies in preclinical pharmacokinetic assessment.* AAPS J, 2013. **15**(3): p. 856-63.
105. Rehlaender, B.N. and M.J. Cho, *Antibodies as carrier proteins.* Pharm Res, 1998. **15**(11): p. 1652-6.
106. Chen, X., et al., *A mathematical model of the effect of immunogenicity on therapeutic protein pharmacokinetics.* AAPS J, 2013. **15**(4): p. 1141-54.
107. Edlund, H., et al., *Magnitude of Increased Infliximab Clearance Imposed by Anti-infliximab Antibodies in Crohn's Disease Is Determined by Their Concentration.* AAPS J, 2017. **19**(1): p. 223-233.
108. Perez Ruixo, J.J., P. Ma, and A.T. Chow, *The utility of modeling and simulation approaches to evaluate immunogenicity effect on the therapeutic protein pharmacokinetics.* AAPS J, 2013. **15**(1): p. 172-82.
109. Kakkar, T., et al., *Population PK and IgE pharmacodynamic analysis of a fully human monoclonal antibody against IL4 receptor.* Pharm Res, 2011. **28**(10): p. 2530-42.
110. Mould, D.R. and R.N. Upton, *Basic concepts in population modeling, simulation, and model-based drug development.* CPT Pharmacometrics Syst Pharmacol, 2012. **1**: p. e6.
111. Krishna, M. and S.G. Nadler, *Immunogenicity to Biotherapeutics - The Role of Anti-drug Immune Complexes.* Front Immunol, 2016. **7**: p. 21.
112. Kloks, C., et al., *A fit-for-purpose strategy for the risk-based immunogenicity testing of biotherapeutics: a European industry perspective.* J Immunol Methods, 2015. **417**: p. 1-9.
113. Yin, L., et al., *Therapeutic outcomes, assessments, risk factors and mitigation efforts of immunogenicity of therapeutic protein products.* Cell Immunol, 2015. **295**(2): p. 118-26.
114. EMEA, *Guideline on Immunogenicity Assessment of Biotechnology-Derived Therapeutic Proteins*, E.M. Agency, Editor. 2007: London.
115. EMEA, *Guideline on immunogenicity assessment of monoclonal antibodies intended for in vivo clinical use*, in *EMA/CHMP/BMWP/86289/2010*, E.M. Agency, Editor. 2012: London.
116. FDA, *Guidance for Industry: Immunogencity Assessment for Therapeutic Protein Products*, C. U.S. Department of Health and Human Services, CBER, Editor. 2014: Silver Spring, MD 20993.
117. Jiskoot, W., et al., *Mouse Models for Assessing Protein Immunogenicity: Lessons and Challenges.* J Pharm Sci, 2016. **105**(5): p. 1567-75.

118. van Helden, P.M., et al., *Maintenance and break of immune tolerance against human factor VIII in a new transgenic hemophilic mouse model.* Blood, 2011. **118**(13): p. 3698-707.
119. Brehm, M.A., et al., *Generation of improved humanized mouse models for human infectious diseases.* J Immunol Methods, 2014. **410**: p. 3-17.
120. Valbonesi, M., et al., *Plasma exchange and immune complex diseases: the predictability of immune complexes removal to clinical response.* Vox Sang, 1982. **42**(1): p. 27-32.
121. Joseph, A., et al., *Immune tolerance induction to enzyme-replacement therapy by co-administration of short-term, low-dose methotrexate in a murine Pompe disease model.* Clin Exp Immunol, 2008. **152**(1): p. 138-46.
122. Messinger, Y.H., et al., *Successful immune tolerance induction to enzyme replacement therapy in CRIM-negative infantile Pompe disease.* Genet Med, 2012. **14**(1): p. 135-42.
123. United States., United States. Animal and Plant Health Inspection Service., and United States., *Animal Welfare Act and animal welfare regulations; 9 CFR Parts 1, 2, and 3*. Vol. 54. 2005, Washington, D.C.: U.S. Dept. of Agriculture, Animal and Plant Health Inspection Service. x, 136 p.
124. Clark, J.D., et al., *Special Report: The 1996 Guide for the Care and Use of Laboratory Animals.* ILAR J, 1997. **38**(1): p. 41-48.
125. Fealy, M.J., et al., *Efficacy of rapamycin and FK 506 in prolonging rat hind limb allograft survival.* Ann Surg, 1994. **219**(1): p. 88-93.
126. Sakanoue, M., et al., *Tacrolimus, a specific inhibitor of calcineurin, modifies the locomotor activity of quinpirole, but not that of SKF82958, in male rats.* Eur J Pharmacol, 2002. **438**(1-2): p. 93-7.
127. Bautista, A.C., H. Salimi-Moosavi, and V. Jawa, *Universal immunoassay applied during early development of large molecules to understand impact of immunogenicity on biotherapeutic exposure.* AAPS J, 2012. **14**(4): p. 843-9.
128. Joly, M.S., et al., *Transient low-dose methotrexate generates B regulatory cells that mediate antigen-specific tolerance to alglucosidase alfa.* J Immunol, 2014. **193**(8): p. 3947-58.
129. Joseph, A., et al., *Transient low-dose methotrexate induces tolerance to murine anti-thymocyte globulin and together they promote long-term allograft survival.* J Immunol, 2012. **189**(2): p. 732-43.
130. Wessels, J.A., T.W. Huizinga, and H.J. Guchelaar, *Recent insights in the pharmacological actions of methotrexate in the treatment of rheumatoid arthritis.* Rheumatology (Oxford), 2008. **47**(3): p. 249-55.
131. Kakkis, E., et al., *Successful induction of immune tolerance to enzyme replacement therapy in canine mucopolysaccharidosis I.* Proc Natl Acad Sci U S A, 2004. **101**(3): p. 829-34.
132. Halloran, P., et al., *Mycophenolate mofetil in renal allograft recipients: a pooled efficacy analysis of three randomized, double-blind, clinical studies in prevention of rejection. The International Mycophenolate Mofetil Renal Transplant Study Groups.* Transplantation, 1997. **63**(1): p. 39-47.

133. Blazanovic, K., et al., *Structure-based redesign of lysostaphin yields potent antistaphylococcal enzymes that evade immune cell surveillance.* Mol Ther Methods Clin Dev, 2015. **2**: p. 15021.
134. Zhao, H., et al., *Depletion of T cell epitopes in lysostaphin mitigates anti-drug antibody response and enhances antibacterial efficacy in vivo.* Chem Biol, 2015. **22**(5): p. 629-39.
135. Hassan, R., et al., *Major cancer regressions in mesothelioma after treatment with an anti-mesothelin immunotoxin and immune suppression.* Sci Transl Med, 2013. **5**(208): p. 208ra147.
136. Richter, W.F., H. Gallati, and C.D. Schiller, *Animal pharmacokinetics of the tumor necrosis factor receptor-immunoglobulin fusion protein lenercept and their extrapolation to humans.* Drug Metab Dispos, 1999. **27**(1): p. 21-5.
137. Pascual, M. and J.A. Schifferli, *The binding of immune complexes by the erythrocyte complement receptor 1 (CR1).* Immunopharmacology, 1992. **24**(2): p. 101-6.
138. Walport, M.J. and K.A. Davies, *Complement and immune complexes.* Res Immunol, 1996. **147**(2): p. 103-9.
139. Johansson, A., et al., *Idiotypic-anti-idiotypic complexes and their in vivo metabolism.* Cancer, 2002. **94**(4 Suppl): p. 1306-13.
140. Kosugi, I., et al., *Endocytosis of soluble IgG immune complex and its transport to lysosomes in hepatic sinusoidal endothelial cells.* J Hepatol, 1992. **16**(1-2): p. 106-14.
141. Pastuskovas, C.V., et al., *Effect of immune complex formation on the distribution of a novel antibody to the ovarian tumor antigen CA125.* Drug Metab Dispos, 2010. **38**(12): p. 2309-19.
142. Schifferli, J.A. and R.P. Taylor, *Physiological and pathological aspects of circulating immune complexes.* Kidney Int, 1989. **35**(4): p. 993-1003.
143. Montero-Julian, F.A., et al., *Pharmacokinetic study of anti-interleukin-6 (IL-6) therapy with monoclonal antibodies: enhancement of IL-6 clearance by cocktails of anti-IL-6 antibodies.* Blood, 1995. **85**(4): p. 917-24.
144. EMEA, *Guideline on immunogenicity assessment of monoclonal antibodiesintended for in vivo clinical use*, in *EMA/CHMP/BMWP/86289/2010*. 2012, Europena Medicines Agency: London.
145. Meibohm, B. and H. Derendorf, *Basic concepts of pharmacokinetic/pharmacodynamic (PK/PD) modelling.* Int J Clin Pharmacol Ther, 1997. **35**(10): p. 401-13.
146. Wang-Qing Chen, et al., *Polymorphism of ORM1 Is Associated with the Pharmacokinetics of Telmisartan.* PLOS ONE, 2013.
147. Tarlinton, D.M. and K.G. Smith, *Dissecting affinity maturation: a model explaining selection of antibody-forming cells and memory B cells in the germinal centre.* Immunol Today, 2000. **21**(9): p. 436-41.
148. Krzyzanski, W., *Interpretation of transit compartments pharmacodynamic models as lifespan based indirect response models.* J Pharmacokinet Pharmacodyn, 2011. **38**(2): p. 179-204.

149. Ng, C.M., et al., *Pharmacokinetic-pharmacodynamic-efficacy analysis of efalizumab in patients with moderate to severe psoriasis.* Pharm Res, 2005. **22**(7): p. 1088-100.
150. Lowe, P.J., et al., *Relationship between omalizumab pharmacokinetics, IgE pharmacodynamics and symptoms in patients with severe persistent allergic (IgE-mediated) asthma.* Br J Clin Pharmacol, 2009. **68**(1): p. 61-76.
151. Hayashi, N., et al., *A mechanism-based binding model for the population pharmacokinetics and pharmacodynamics of omalizumab.* Br J Clin Pharmacol, 2007. **63**(5): p. 548-61.
152. Bender, B., et al., *A mechanistic pharmacokinetic model elucidating the disposition of trastuzumab emtansine (T-DM1), an antibody-drug conjugate (ADC) for treatment of metastatic breast cancer.* AAPS J, 2014. **16**(5): p. 994-1008.
153. Bonate, P.L., et al., *Conditional modeling of antibody titers using a zero-inflated poisson random effects model: application to Fabrazyme.* J Pharmacokinet Pharmacodyn, 2009. **36**(5): p. 443-59.
154. Wagner, C.L., et al., *Consequences of immunogenicity to the therapeutic monoclonal antibodies ReoPro and Remicade.* Dev Biol (Basel), 2003. **112**: p. 37-53.
155. Stephens, S., et al., *Comprehensive pharmacokinetics of a humanized antibody and analysis of residual anti-idiotypic responses.* Immunology, 1995. **85**(4): p. 668-74.
156. Takahashi, Y., et al., *In situ studies of the primary immune response to (4-hydroxy-3-nitrophenyl)acetyl. V. Affinity maturation develops in two stages of clonal selection.* J Exp Med, 1998. **187**(6): p. 885-95.
157. Wijngaarden, S., et al., *Down-regulation of activating Fcgamma receptors on monocytes of patients with rheumatoid arthritis upon methotrexate treatment.* Rheumatology (Oxford), 2005. **44**(6): p. 729-34.
158. Hines, R.N., *Ontogeny of human hepatic cytochromes P450.* J Biochem Mol Toxicol, 2007. **21**(4): p. 169-75.
159. Kearns, G.L., et al., *Developmental pharmacology--drug disposition, action, and therapy in infants and children.* N Engl J Med, 2003. **349**(12): p. 1157-67.
160. Leeder, J.S., *Ontogeny of drug-metabolizing enzymes and its influence on the pathogenesis of adverse drug reactions in children.* Current Therapeutic Research, 2001. **62**(12): p. 900-912.
161. Leeder, J.S. and B. Meibohm, *Challenges and Opportunities for Increasing the Knowledge Base Related to Drug Biotransformation and Pharmacokinetics during Growth and Development.* Drug Metab Dispos, 2016. **44**(7): p. 916-23.
162. Brouwer, K.L., et al., *Human Ontogeny of Drug Transporters: Review and Recommendations of the Pediatric Transporter Working Group.* Clin Pharmacol Ther, 2015. **98**(3): p. 266-87.
163. Chen, Z.S. and A.K. Tiwari, *Multidrug resistance proteins (MRPs/ABCCs) in cancer chemotherapy and genetic diseases.* FEBS J, 2011. **278**(18): p. 3226-45.
164. Ho, R.H. and R.B. Kim, *Transporters and drug therapy: implications for drug disposition and disease.* Clin Pharmacol Ther, 2005. **78**(3): p. 260-77.

165. Huisman, M.T., et al., *Multidrug resistance protein 2 (MRP2) transports HIV protease inhibitors, and transport can be enhanced by other drugs.* AIDS, 2002. **16**(17): p. 2295-301.
166. Paulusma, C.C., et al., *A mutation in the human canalicular multispecific organic anion transporter gene causes the Dubin-Johnson syndrome.* Hepatology, 1997. **25**(6): p. 1539-42.
167. Roche, *Rocephin(R) (ceftriaxone) [product information]*. 2004, Nutely, New Jersey: Roche Laboratories.
168. Suzuki, H. and Y. Sugiyama, *Transporters for bile acids and organic anions.* Pharm Biotechnol, 1999. **12**: p. 387-439.
169. Bor, O., et al., *Ceftriaxone-associated biliary sludge and pseudocholelithiasis during childhood: a prospective study.* Pediatr Int, 2004. **46**(3): p. 322-4.
170. de Moor, R.A., A.C. Egberts, and C.H. Schroder, *Ceftriaxone-associated nephrolithiasis and biliary pseudolithiasis.* Eur J Pediatr, 1999. **158**(12): p. 975-7.
171. Papadopoulou, F., et al., *Incidence of ceftriaxone-associated gallbladder pseudolithiasis.* Acta Paediatr, 1999. **88**(12): p. 1352-5.
172. Xia, Y., et al., *Concentrative biliary secretion of ceftriaxone. Inhibition of lipid secretion and precipitation of calcium ceftriaxone in bile.* Gastroenterology, 1990. **99**(2): p. 454-65.
173. Mizuno, N., et al., *Impact of drug transporter studies on drug discovery and development.* Pharmacol Rev, 2003. **55**(3): p. 425-61.
174. Tang, L., *Age-Associated Hepatic Drug Transporter Expression and Its Implications for Pediatric Pharmacotherapy*. Vol. Theses and Dissertations (ETD). Paper 260. http://dx.doi.org/10.21007/etd.cghs.2007.0312. . 2007, Memphis, TN: University of Tennessee Health Science Center.
175. Bennett, J.V., et al., *Simplified, accurate method for antibiotic assay of clinical specimens.* Appl Microbiol, 1966. **14**(2): p. 170-7.
176. Perea, S., et al., *Comparison of high-performance liquid chromatographic and microbiological methods for determination of voriconazole levels in plasma.* Antimicrob Agents Chemother, 2000. **44**(5): p. 1209-13.
177. Anderson, B.J. and N.H. Holford, *Tips and traps analyzing pediatric PK data.* Paediatr Anaesth, 2011. **21**(3): p. 222-37.
178. Zhou, H.H., et al., *Single-dose pharmacokinetics of ceftriaxone in healthy Chinese adults.* Antimicrob Agents Chemother, 1985. **27**(2): p. 192-6.
179. Meyers, B.R., et al., *Crossover study of the pharmacokinetics of ceftriaxone administered intravenously or intramuscularly to healthy volunteers.* Antimicrob Agents Chemother, 1983. **24**(5): p. 812-4.
180. Gobeaux, D., et al., *Ceftriaxone diffusion from blood to aqueous humour in man.* Br J Ophthalmol, 1989. **73**(7): p. 574-5.
181. Hospira, *Ceftriaxone Data Sheet*, H.N. Limited, Editor. 2014: Auckland, New Zealand.
182. Toyonaga, Y., M. Sugita, and M. Hori, *[Pharmacokinetic and clinical evaluation of ceftriaxone in neonates and premature infants].* Jpn J Antibiot, 1988. **41**(3): p. 244-61.
183. McCracken, G.H., Jr., et al., *Ceftriaxone pharmacokinetics in newborn infants.* Antimicrob Agents Chemother, 1983. **23**(2): p. 341-3.

184. Schaad, U.B. and K. Stoeckel, *Single-dose pharmacokinetics of ceftriaxone in infants and young children.* Antimicrob Agents Chemother, 1982. **21**(2): p. 248-53.
185. Garot, D., et al., *Population pharmacokinetics of ceftriaxone in critically ill septic patients: a reappraisal.* Br J Clin Pharmacol, 2011. **72**(5): p. 758-67.
186. Iida, S., et al., *The pharmacokinetics of ceftriaxone based on population pharmacokinetics and the prediction of efficacy in Japanese adults.* Eur J Drug Metab Pharmacokinet, 2009. **34**(2): p. 107-15.
187. Kovar, A., T. Dalla Costa, and H. Derendorf, *Comparison of plasma and free tissue levels of ceftriaxone in rats by microdialysis.* J Pharm Sci, 1997. **86**(1): p. 52-6.
188. Wright, W.E. and V.D. Line, *Biliary excretion of cephalosporins in rats: influence of molecular weight.* Antimicrob Agents Chemother, 1980. **17**(5): p. 842-6.
189. Baietto, L., et al., *A 30-years review on pharmacokinetics of antibiotics: is the right time for pharmacogenetics?* Curr Drug Metab, 2014. **15**(6): p. 581-98.
190. Chen, C., G.E. Hennig, and J.E. Manautou, *Hepatobiliary excretion of acetaminophen glutathione conjugate and its derivatives in transport-deficient (TR-) hyperbilirubinemic rats.* Drug Metab Dispos, 2003. **31**(6): p. 798-804.
191. Patel, I.H., et al., *Pharmacokinetics of ceftriaxone in humans.* Antimicrob Agents Chemother, 1981. **20**(5): p. 634-41.
192. Seddon, M., et al., *Pharmacokinetics of Ro 13-9904, a broad-spectrum cephalosporin.* Antimicrob Agents Chemother, 1980. **18**(2): p. 240-2.
193. Meibohm, B., et al., *Population pharmacokinetic studies in pediatrics: issues in design and analysis.* AAPS J, 2005. **7**(2): p. E475-87.
194. Bradford, M.M., *A rapid and sensitive method for the quantitation of microgram quantities of protein utilizing the principle of protein-dye binding.* Anal Biochem, 1976. **72**: p. 248-54.
195. Rasband, W.S. *ImageJ*. 1997 [cited 2016 October 16].
196. Granich, G.G. and D.J. Krogstad, *Ion pair high-performance liquid chromatographic assay for ceftriaxone.* Antimicrob Agents Chemother, 1987. **31**(3): p. 385-8.
197. Kohlhepp, S.J., D.N. Gilbert, and J.E. Leggett, *Influence of assay methodology on the measurement of free serum ceftriaxone concentrations.* Antimicrob Agents Chemother, 1998. **42**(9): p. 2259-61.
198. Trautman, K.H.a.P.H., *Determination of the cephalosporin Ro 13-9904 in plasma, urine, and bile by means of ion-pair reversed phase chromatography.* Journal of High Resolution Chromatography Chromatography Communications, 1981(4): p. 54-59.
199. Kwon, K.I. and D.W. Bourne, *Effect of caffeine on ceftriaxone disposition and plasma protein binding in the rat.* J Pharmacokinet Biopharm, 1986. **14**(4): p. 397-408.
200. Davis et.al., *Pharmaceutical Biotechnology*. 4th ed, ed. D.J.A. Crommelin, Sindelar, Robert D., Meibohm, Bernd. 2013, Verlag New York: Springer. XXI, 544.

VITA

Josiah Thomas Ryman was born in 1985 in Goshen, Indiana, USA. In 2007, he received his Bachelors of Science degree from the University of Tennessee at Knoxville with a major focus in biochemistry and molecular biology. In 2012, he received his Doctorate of Pharmacy degree from the University of Tennessee Health Science Center. Shortly thereafter in 2012, he began his graduate studies under the tutelage of Dr. Bernd Meibohm, Professor in the Department of Pharmaceutical Sciences at the University of Tennessee Health Science Center. He received the Doctor of Philosophy degree in Pharmaceutical Sciences in the spring of 2017.